Scattering lasers

an exploration of the smallest lasers possible

Scattering lasers

an exploration of the smallest lasers possible

ACADEMISCH PROEFSCHRIFT

ter verkrijging van de graad van doctor
aan de Universiteit van Amsterdam
op gezag van de Rector Magnificus
prof. mr. P. F. van der Heijden
ten overstaan van een door het college voor promoties
ingestelde commissie, in het openbaar te verdedigen
in de Aula der Universiteit
op woensdag 14 februari 2007, te 14.00 uur

door

Tom Savels

geboren te Blankenberge, België

Promotiecommissie:

Promotor	Prof. Dr. A. Lagendijk
Co-promotor	Dr. A.P. Mosk
Overige leden	Prof. Dr. R. Blatt
	Prof. Dr. G. Shlyapnikov
	Prof. Dr. J.T.M. Walraven
	Prof. Dr. H.B. van Linden van den Heuvell
	Prof. Dr. W.L. Vos

Faculteit der Natuurwetenschappen, Wiskunde en Informatica

The work described in this thesis is part of the research program of the "Stichting Fundamenteel Onderzoek der Materie (FOM)", which is financially supported by the "Nederlandse Organisatie voor Wetenschappelijk Onderzoek (NWO)".

This work was carried out at the
Complex Photonic Systems Group,
Faculty of Science and Technology and MESA$^+$ Research Institute,
University of Twente, P.O. Box 217, 7500AE Enschede, The Netherlands,

and at the
FOM Institute for Atomic and Molecular Physics
Kruislaan 407, 1098SJ Amsterdam, The Netherlands,
where a limited number of copies of this thesis is available.

Druk: Printpartners Ipskamp, Enschede, The Netherlands (2007).
ISBN: 978-90-77209-13-4

to Kathrine and Fernand
the most loving parents a boy could possibly wish for

Paranimfen: J.R. Savels en K.J. Huyghe

Whenever you find yourself at the side of the majority it is time to pause and reflect.
— Mark Twain —

Dankwoord

Dit proefschrift duidt het einde aan van een voor mij bijzondere periode. Bij het afsluiten van deze periode zou ik een aantal mensen de erkenning willen geven die ze volgens mij zeker verdienen.

Ad, ik ben je uiterst en oprecht erkentelijk voor de grote hoeveelheid aan inzichten die je me in de afgelopen drieëneenhalf jaar hebt meegegeven. Je hebt me niet alleen op wetenschappelijk vlak grote vrijheid gegund, maar me daarenboven op niet-wetenschappelijk vlak veel bijgeleerd. Je hebt een bijzondere begeleidingsfilosofie, die heel inspirerend kan werken.

Allard, ik heb je tijdens het eerste jaar van mijn promotie vaak lastig gevallen met mijn nieuwsgierigheid en ongeduldig karakter, maar je nam steeds de tijd om me een helpende hand toe te reiken. Je grondigheid tijdens het lezen van manuscripten en enthousiast opperen van ideeën tijdens discussies werkt erg aanstekelijk.

Ik had het grote geluk om tijdens de eerste anderhalf jaar van mijn promotie de kamer exclusief te delen met twee achtereenvolgende postdocs. Martijn en Peter, jullie hebben me ontzettend snel vooruit geholpen tijdens die initiële periode. Ik ervoer jullie aanwezigheid en raad als een absolute luxe.

De groep Complex Photonic Systems waarin ik mijn promotie begon vertoonde een voor mij verbazingwekkend grote mate aan cohesie en dynamica. Het bijzondere karakter van onze groep is niet in het minst te wijten aan Willem Vos, naast kritisch wetenschappelijk klankbord een grote stimulator van samenhang binnen de groep.

De werksfeer binnen een groep wordt voor een groot deel bepaald door de groepsleden zelf; ik zou iedereen die de afgelopen periode in de groep actief was willen bedanken voor het open en enthousiaste klimaat.

Halverwege mijn promotie zijn we met een deel van de groep van Enschede naar Amsterdam verhuisd. Dit proces was niet altijd even gemakkelijk, zowel op persoonlijk als op professioneel vlak. Ik zou op het Amolf Piet, Wouter en Lars willen bedanken voor hun hulpvaardigheid en souplesse tijdens die periode.

Tijmen, ik heb ontzettend veel plezier beleefd aan onze kook-, drink-, barbecue-, tennis-, zwem- en filmavonden. Ik ben blij dat ik de verhuiservaring met jou kon delen. Ivan, bedankt voor je raad en hulp tijdens mijn worstelpartijen met Latex bij het genereren van dit proefschrift.

Op persoonlijk vlak waren de afgelopen jaren vrij rumoerig. Tine, mijn promotieperiode is niet verlopen zoals we beiden hadden ingeschat. Het leven verloopt niet altijd even probleemloos en rooskleurig, en dat was voor ons beiden moeilijk. Weet dat je een ontzettend grote steun was voor mij. Je hebt een grote opoffering gemaakt door met me mee te gaan naar Nederland; zonder jou was ik nooit aan mijn promotie begonnen. Al klinkt het misschien wat bitterzoet, je hebt een speciale plek in dit dankwoord.

Veel mensen in mijn vrienden- en kennissenkring vroegen zich meermaals af wat ik in hemelsnaam had verloren in het "verre" Nederland. Ik kan jullie uit de grond van mijn hart vertellen dat wat het ook was, ik het nu gevonden heb. In het bijzonder wil ik Piet, Wim, Folke, Hanne en Peter bedanken voor de emails, telefoontjes en lange avonden op café.

In Nederland heb ik een aantal inspirerende mensen ontmoet die me nauw aan het hart liggen. Cobi en Jan, jullie zijn voor mij een bron van steun en raad. Bedankt om er te zijn.

Kurt, mijn gedicht is af. Ik ben ontzettend blij dat je samen met Jo de last van paranimf-zijn op je hebt willen nemen. Ik kan me geen beter duo indenken om mijn promotiefeest aan toe te vertrouwen. Je kijk op de wereld inspireert me telkens weer — je bent een fantastische vriend.

Jootje, *what can I say*? Je bent een broer uit de duizend. Als er één iemand is die me mijn promotie af en toe liet relativeren, ben het jij wel. Ik heb je niet zo vaak gezien de afgelopen jaren, maar je was er wel. Sofietje, ik wil je hartelijk bedanken voor je ondersteuning tijdens de voorbereiding van mijn promotie.

Ik heb dit proefschrift opgedragen aan mijn ouders. Ook voor jullie waren de afgelopen jaren wat hobbelig. Waar ik ook verzeilde en met wie dat ook was, jullie zijn me altijd onvoorwaardelijk blijven steunen. Er zijn vast boeken geschreven die veel beter bij jullie passen, maar dit boekje krijgen jullie van mij.

Ten slotte is er één iemand die een speciale plek heeft veroverd in mijn leven. Lieve Karen, ik heb lang nagedacht over de woorden die ik hier voor jou zou schrijven, maar ze zeggen geen van allen wat ik echt bedoel. De tijd die je voor me vrijmaakt, het begrip dat je kan opbrengen en de energie waarmee we samen door het leven dansen doen me versteld staan. Je bent niet enkel mijn vriendin en beste vriend — je hebt me laten openbloeien. Kom, samen kunnen we de wereld aan!

Tom

Contents

CHAPTER 1

Introduction: optical gain in atomic systems

1.1 Optical gain and laser oscillation

In a laser, light is generated by a combination of light amplification by stimulated emission and optical feedback [54, 79, 111]. The practical implementation of both functional laser parts — optical gain and optical feedback — comes in many varieties. For example, laser oscillation has been shown to be possible using solid-state gain media [78] or gaseous media [117], while implementations of laser cavities include, among many others, ring-type cavities [102], chaotic cavities [89] and photonic-crystal cavities [70, 116].

In its simplest form, optical feedback in a laser is implemented through a Fabry-Pérot resonator, as shown in Figure 1.1. External pumping of a gain medium in the resonator leads to amplification of the intracavity laser light. One of the resonator mirrors transmits part of the light, thereby allowing for the emission of an output laser beam with (typically) a high degree of spatial and spectral coherence.

Remarkably, despite the abundance of excellent textbooks on laser dynamics, it is rather challenging to find an actual definition of the word "laser" [128]. Quite obviously, the expansion of the acronym — light amplification by stimulated emission of radiation — is not defining in itself, since it fails to express in what sense the characteristics of laser light differ from those of other light sources. For example, the stimulated emission rate may exceed the spontaneous emission rate even below the laser threshold, yet the term "laser" is often reserved to denote operation above threshold.

In this thesis, we will present a study of the fundamental building blocks of

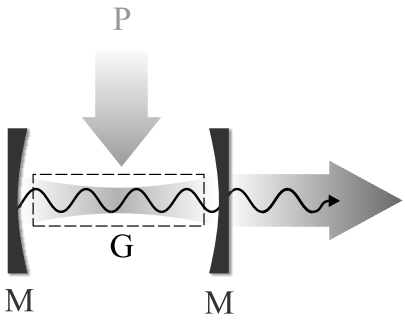

Figure 1.1: A conventional laser consists of a gain medium (G) inside a Fabry-Pérot cavity. The gain medium is pumped by an external pumping mechanism (P). The cavity is made up of two mirrors (M) which confine the light and provide feedback. One of the cavity modes is shown; light in this mode resonates in the cavity and is amplified through stimulated emission.

laser systems. In this respect, we are facing the question of presenting a workable definition of a laser. Defining a laser is no easy feat, given that different scientific communities focus on laser operation in different systems and regimes. Nevertheless, we believe it is rewarding to start from a workable laser definition since this clarifies semantic issues right from the beginning and allows us to focus on the physics of the systems we present. In this thesis, we adopt the following definition:

> *A single-mode laser is a system which combines gain and feedback, such that one field mode (the laser mode) is characterized by a gain-induced increase of its spectral weight at the cost of all other system modes. The amplitude of all system modes decays to an external bath and is replenished by the gain source. The implementation of the source of gain which feeds the system is arbitrary but different from the laser mode itself.*

Some general remarks are at order with respect to the above definition. First, gain-induced competition between different system modes is a well-known laser dynamic behavior [112]; in that sense, our definition follows naturally from standard laser descriptions. Secondly, we excluded the notion of stimulated emission from our definition, because we aim at a definition in terms of experimentally observable quantities: in general, stimulated emission and spontaneous emission appear as indistinguishable components of the light emitted by a laser, rendering a definition in terms of stimulated emission rather impractical. (We acknowledge that in many standard laser descriptions the difference between both emission types is indeed very clear, but this distinction vanishes in more complicated systems such as the ones described in this thesis). Thirdly, no reference is made to the concept of a laser threshold, because the threshold concept is well-defined only in the thermody-

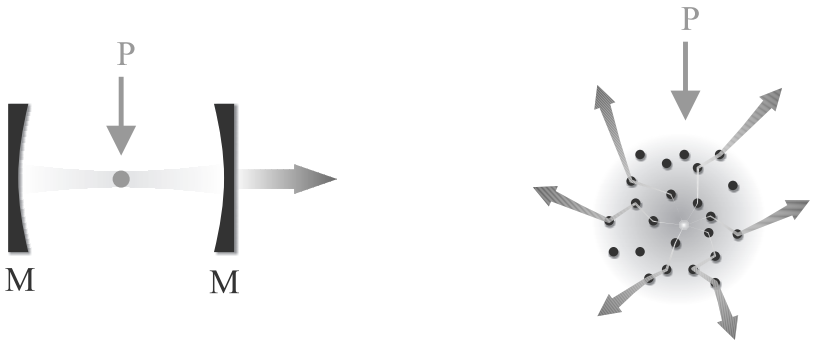

(a) (b)

Figure 1.2: (a) A one-atom (single-ion) laser consists of single atom (ion) inside a cavity. The atom (ion) is pumped while the cavity provides feedback. (b) A random laser consists of a gain medium containing random scatterers. The gain medium is pumped by an external pumping mechanism (P), while the optical feedback is provided by multiple scattering of light.

namic limit [99] and therefore of limited use in the microscopic systems of interest. In other words, while the spectral width and power of the emitted light may vary nonlinearly (as they do in conventional lasers) and a threshold might be associated with their behavior "by eye", no fundamental quantitative criterion for the existence of a laser threshold exists in microscopic systems. Finally, we excluded any notion on second-order coherence in the above definition. As is well-known from, e.g., bad-cavity lasers [29, 49, 130], the second-order correlations of laser light may behave drastically differently from the correlations in conventional lasers (especially in the low photon number limit); defining a laser based on second-order correlations therefore seems impractical, if not meaningless. Our definition of a single-mode laser is, though debatable, a workable definition in terms of experimentally observable quantities; we will henceforth disregard laser-related semantic issues and focus on the physics of the systems at hand.

1.2 Microscopic building blocks of a laser

In order to study the basic physics of the processes involved in laser oscillation, there has been an intensive search for laser operation in fundamental systems [67]. The resulting drive toward miniaturization has led to, among others, the realization of vertical-cavity semiconductor lasers [28], dye-microsphere lasers [119], microring and microdisc semiconductor lasers [84], microsphere lasers [46, 123] and photonic-bandgap lasers [58]. As laser systems are made smaller, a purely macroscopic description becomes inadequate and microscopic considerations should be taken into account [130]. An interesting example of lasers which require a (partially) micro-

scopic treatment is the class of one-atom lasers, schematically depicted in Figure 1.2 (a). In one-atom (or single-ion) lasers [9, 80], the gain medium is reduced to a fundamental level, while macroscopic mirrors provide feedback. Another, contrasting example is the class of random lasers [21, 68, 73, 122], shown in Figure 1.2 (b). In random lasers, the optical feedback is provided by scattering from microscopic particles, while the gain medium remains macroscopic. Obviously, neither the feedback mechanism nor the gain medium can be reduced to less than one atom.

In this thesis, we explore the most fundamental system displaying both gain and feedback: a single pumped atom, surrounded by one or more passive atoms providing optical feedback by scattering. The atoms are positioned in free space in the absence of a cavity. The absence of a macroscopic cavity and its modes differentiates our model from models in which atoms interact via a single field mode such as, e.g., atoms in a single-atom maser [83]. Our few-atom system can be described fully microscopically, without introducing any phenomenological parameters or paraxial approximations. Hence, the presented results are based solely on the scattering properties of the atomic building blocks and their description. We show that this system, though very simple, shows surprisingly strong spectral gain narrowing and mode redistribution, indicating an approach to laser oscillation. In addition, the observed gain-induced phenomena are more pronounced as the number of atoms increases, in correspondence with the intuitive $N \to \infty$ limit. Due to their remarkable behavior, we will refer to few-atom systems with gain as "scattering lasers".

The dynamics of the scattering lasers we consider are governed by the collective behavior of the passive atoms acting as a cavity and the pumped atom providing gain. The interplay of gain and feedback distinguishes the cooperativity in our systems from the type of collective atomic behavior found in literature. For example, descriptions of the decay of atomic ensembles with an initial dipole moment (referred to as *superradiant* systems [1, 5, 33, 35, 50, 98]) or without an initial dipole moment (referred to as *superfluorescent* systems [16, 32, 51, 52, 115]) are inherently transient, in contrast to the steady-state behavior we will focus on. In addition, the spectral width of a superradiant pulse broadens quadratically with the number of atoms, as opposed to the spectral narrowing we will present. We stress that atomic ensembles with laser-like behavior have been reported in literature, but these systems are either ensembles in the very large atom-number limit [34], systems describing amplified spontaneous emission [6–8, 25, 77, 93, 94] or atomic systems in a (macroscopic) cavity [53]. In relation to the aforementioned studies of atomic ensembles we will show that, remarkably, pronounced mode competition is possible in few-atom systems even in the absence of a cavity.

1.3 Overview of this thesis

We start in chapter 2 by describing the optical scattering properties of a single pumped atom. A master equation approach will lead to a description of an atom with gain in terms of its polarizability. The influence of the pump field can be characterized by a single dimensionless parameter, expressing both a broadening of the atomic transition and a decrease of the atom's polarizability. In addition, we

will show that the presence of gain not only causes the atom to scatter partially inelastically, but also changes the atom's dispersion and dissipation [104].

In chapter 3 we use the results of chapter 2 to describe N atoms with gain in the framework of multiple scattering of light. Remarkably, the presence of gain allows for the existence of a threshold for atom numbers as low as $N = 2$. In other words, we demonstrate that a two-atom system with gain exhibits discontinuous threshold behavior within a semiclassical multiple-scattering formalism.

Although the threshold prediction of chapter 3 is quite surprising, the applied multiple-scattering approach is approximative since multiple scattering of off-resonant light is disregarded. In chapter 4 we calculate a first-order estimation of the atomic saturation induced by off-resonant light. We will demonstrate such saturation to be significant and to suppress the manifestation of a threshold.

In chapter 5, we proceed beyond the above first-order approximation and present a quantum-mechanical study of N-atom systems with gain, including off-resonant interactions in all scattering orders. A Master equation approach will reveal that few-atoms with gain exhibit pronounced mode competition, providing the atoms are in each other's near-field.

Finally, we will argue that the physical properties of an N-atom system in the presence of gain are determined by the system's photon storage capacity. Since the storage capacity in an N-atom system is limited by the number of atoms, few-atom systems are computationally challenging. In chapter 6, we circumvent this computational restriction by eliminating the saturation of the passive atoms, thus leading to even more pronounced mode competition effects. In relation to the threshold prediction of chapter 3, we show that as the applied pump intensity increases, the microscopic systems under consideration exhibit a smooth crossover from a regime dominated by spontaneous emission to a regime where pronounced laser effects are apparent.

CHAPTER 2

A quantum optical approach to multiple scattering of light

We present an extension of the T-matrix approach to scattering of light by three- and four-level systems, using a description based on a Master equation. The presented formalism allows us to determine the light-scattering properties of an atomic point scatterer based on its internal energy-level structure. More particularly, we calculate the T-matrix of an optically pumped atom, providing an exact and analytical expression describing the influence of a pump field on the light-scattering properties of an atomic system. Finally, we demonstrate the generality of the presented formalism by considering a few practical atomic systems with their associated T-matrix.

2.1 Introduction

In the description of the interaction of atomic ensembles with light, the atoms are often treated in the electric-dipole approximation, and are therefore effectively considered to be point dipoles. The advantages of the point-dipole formalism are twofold. First, the delta-function potential associated with point scatterers allows for significant mathematical simplifications compared to finite-size scatterers [31]. Secondly, the point-scatterer formalism allows for a transparent description of many multiple-scattering phenomena, mimicking most of the associated relevant physics [66]. The light-scattering properties of point dipoles can be expressed by means of their T-matrix $\overleftrightarrow{T}$, which is related to their dynamic (dipole-dipole) polarizability $\overleftrightarrow{\alpha}$. If one describes the internal structure of the atoms as an effective two-level system [4] or a damped harmonic oscillator, one finds the well-known Lorentzian expression for

the linear dynamic polarizability [75] for frequencies near the resonance frequency, valid for intensities well below saturation.

In this chapter, we present an extension of the point-dipole T-matrix formalism to three- and four-level atoms. In practice, the "atoms" could be implemented as any type of sub-wavelength quantum objects, for example: trapped atoms, quantum dots [45, 47], trapped ions [18, 39, 72] or dye molecules. Few-level atoms have been subject to a lot of theoretical research in the past, especially in the context of lasing without inversion [55, 82, 96, 106, 124]. However, in this chapter we focus on a rather different route: our aim is to develop a connection between the internal resonance structure of a sub-wavelength quantum object — such as an atom — and its light-scattering properties in terms of a classical T-matrix. This approach allows us to present a transparent formulation of a point dipole with gain, based on clear physical grounds. The introduction of a pump in the point-dipole model is highly attractive because it allows, within the framework of the T-matrix formalism, for a description of optically amplifying atomic systems [9, 48, 80, 83].

We demonstrate how to derive the T-matrix of an atomic scatterer by considering the example of an optically pumped three-level system. In section 2.2, we derive and solve the system's Master equation. The evolution of all atomic populations and internal coherences can then be deduced. In particular, we will focus on the system's steady-state regime. In section 2.3, we will connect the reduced density matrix of the system with its dynamic polarizability, which will lead to the T-matrix of a point dipole with gain, based on a three-level pumping scheme. We show in section 2.4 that the optical properties of such an optically pumped dipole can be straightforwardly deduced from its T-matrix; we elaborate on the effect of gain on the atom's dispersion and dissipation behavior in more detail. Finally, we demonstrate the general applicability of the presented formalism by considering a few standard quantum optical systems and their corresponding T-matrix in section 2.5. More particularly, we derive the T-matrix of an atomic "V" system and a "Λ" system as opposed to a standard two-level system. Furthermore, we derive the T-matrix of a point dipole with gain based on a four-level pumping scheme as opposed to a three-level scheme; we point out that the choice of pumping implementation has important implications on the resulting light-scattering properties.

2.2 Master equation of a three-level atom with gain

We start by considering a three-level atom abc, shown in Figure 2.1. The atom has three relevant energy levels: the ground state a, a highly excited state b and the upper state of the relevant $c \rightarrow a$ transition c. Decay between the energy levels levels a, b and c occurs according to the decay rates Γ_{bc} and Γ_{ca}. The $b \rightarrow c$ transition either has a non-radiative nature, or its transition frequency is far detuned compared to the other relevant frequencies in the system. We are interested in the simplest possible scheme that allows for incoherent pumping. Therefore, we will make the following simplifying assumptions. We assume that spontaneous emission

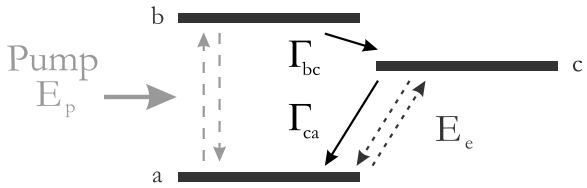

Figure 2.1: The three-level system *abc*. Decay from b to c and from c to a occurs at a rate Γ_{bc} and Γ_{ca}, respectively. Decay from b to a is neglected. The left dashed arrows express the interaction with the pump. The right dashed arrows depict the interaction with the external probe field.

from level b to level a can be neglected compared to other decay processes, hence $\Gamma_{ba} \approx 0$. Furthermore, the life time Γ_{bc}^{-1} of level b is chosen to be small compared to the life time Γ_{ca}^{-1}. Both previous restrictions on the decay rates do not affect our final results in any qualitative way, and are only introduced for mathematical simplicity. Two incident electromagnetic fields $\boldsymbol{E}_e$ and $\boldsymbol{E}_p$ interact with *abc*. The field $\boldsymbol{E}_p$ serves as a pump to establish population inversion in the two-level system *ac*. The external probe field $\boldsymbol{E}_e$ allows for the calculation of the dynamic polarizability of the *ac* system in a one-way response theory approach.

We are interested in the steady-state behavior of the system *abc*. We will now derive the Master equation of the system, using the standard procedure presented in [30]. The total Hamiltonian of the system *abc*, the electromagnetic fields and interactions can be written in the electric-dipole approximation as

$$\hat{H} \equiv \hat{H}_A + \hat{H}_P + \hat{H}_R + \hat{V}_{AR} + \hat{V}_{AE} + \hat{V}_{AP}. \tag{2.1}$$

The atomic Hamiltonian $\hat{H}_A$ is given by $\hat{H}_{ab} + \hat{H}_c$, with

$$\hat{H}_{ab} \equiv \hbar\omega_{ba}\hat{S}_{ab}^{+}\hat{S}_{ab}^{-}, \qquad \hat{H}_c \equiv \hbar\omega_{ca}\hat{S}_{ac}^{+}\hat{S}_{ac}^{-}, \tag{2.2}$$

with $\hat{S}_{ij}^{+}$, $\hat{S}_{ij}^{-}$ the ij dipole raising and lowering operators respectively, defined as

$$\hat{S}_{ij}^{+} \equiv |j\rangle\langle i|, \qquad \hat{S}_{ij}^{-} \equiv |i\rangle\langle j|, \qquad i,j = a,b,c. \tag{2.3}$$

The Hamiltonian of the pump field is given by

$$\hat{H}_P \quad \equiv \quad \hbar\omega_p\Big(\hat{a}_p^{\dagger}\hat{a}_p + \tfrac{1}{2}\Big), \tag{2.4}$$

where the operators $\hat{a}_p$ and $\hat{a}_p^{\dagger}$ respectively annihilate and create a pump photon with frequency ω_p. The system *abc* is coupled via the interaction $\hat{V}_{AR}$

$$\hat{V}_{AR} \equiv -\hat{\boldsymbol{d}} \cdot \sum_{\boldsymbol{k}\lambda} \boldsymbol{\epsilon}_{\boldsymbol{k}\lambda} \Big(\frac{\hbar\omega_{\boldsymbol{k}\lambda}}{2\varepsilon_0 V} \Big)^{1/2} \Big(\hat{a}_{\boldsymbol{k}\lambda} + \hat{a}^\dagger_{\boldsymbol{k}\lambda} \Big), \tag{2.5}$$

to the three-dimensional multimode electromagnetic field with Hamiltonian

$$\hat{H}_R \equiv \sum_{\boldsymbol{k}\lambda} \hbar\omega_{\boldsymbol{k}\lambda} \Big(\hat{a}^\dagger_{\boldsymbol{k}\lambda} \hat{a}_{\boldsymbol{k}\lambda} + \tfrac{1}{2} \Big), \tag{2.6}$$

where the subscripts $\boldsymbol{k}$ and λ respectively denote the wave vector and polarization state of each field mode. The dipole operator is defined as

$$\hat{\boldsymbol{d}}(t) \equiv \boldsymbol{d}_{ac} \left(\hat{S}^+_{ac}(t) + \hat{S}^-_{ac}(t) \right), \tag{2.7}$$

with $\boldsymbol{d}_{ac}$ the ac transition dipole moment. The operators $\hat{a}_{\boldsymbol{k}\lambda}$ and $\hat{a}^\dagger_{\boldsymbol{k}\lambda}$ respectively annihilate and create a photon with polarization $\boldsymbol{\epsilon}_{\boldsymbol{k}\lambda}$ in the multimode field, and $V = L^3$ is the quantization volume. The external field $\boldsymbol{E}_e$ has a frequency ω, and interacts with the system abc by

$$\hat{V}_{AE} \equiv \frac{1}{2}\hbar\Omega_e \Big(\hat{S}^+_{ac} e^{-i\omega t} + \hat{S}^-_{ac} e^{i\omega t} \Big), \tag{2.8}$$

where the interaction strength is given by the Rabi frequency $\Omega_e \equiv -\boldsymbol{d}_{ac} \cdot \boldsymbol{E}_e/\hbar$.

The interaction Hamiltonian $\hat{V}_{AP}$, finally, denotes the coupling of the atom to the pump:

$$\hat{V}_{AP} \equiv g \Big(\hat{S}^+_{ab} + \hat{S}^-_{ab} \Big) \Big(\hat{a}_p + \hat{a}^\dagger_p \Big), \tag{2.9}$$

with g expressing the coupling strength between the pump field and the system [30]. The pump field shifts the energies of the levels a and b. This shift, which can be significant for large pump intensities, can be taken into account (see, e.g., [23]) by considering the *dressed states* or eigenstates of the Hamiltonian $\hat{H}_D \equiv \hat{H}_{ab} + \hat{H}_P + \hat{V}_{AP}$, given by:

$$|1(N)\rangle \equiv \sin(\theta)|a, N+1\rangle + \cos(\theta)|b, N\rangle, \tag{2.10a}$$
$$|2(N)\rangle \equiv \cos(\theta)|a, N+1\rangle - \sin(\theta)|b, N\rangle, \tag{2.10b}$$

graphically represented in Figure 2.2. Since the energy of level c is unaffected by

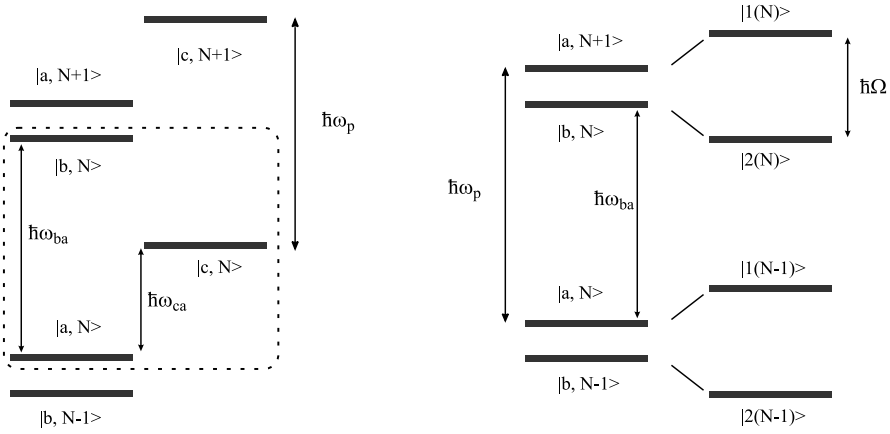

(a) The three-level system abc.

(b) The dressed states $|1(N)\rangle$ and $|2(N)\rangle$.

Figure 2.2: In Figure (a), levels $|a, N\rangle$, $|b, N\rangle$ and $|c, N\rangle$ are shown for different number of pump photons N. The energy differences between energy levels are also indicated. The dashed box denotes the abc system with N pump photons. In Figure (b), the dressed states $|1(N)\rangle$ and $|2(N)\rangle$ are schematically shown. The energy difference between both states is given by $\hbar\Omega$, with $\hbar^2\Omega^2 = \hbar^2(\delta_p^2 + \Omega_p^2)$.

the pump, we use the notation $|c(N)\rangle \equiv |c, N\rangle$. The number of pump photons is then given by N, and

$$\tan 2\theta \equiv -\frac{\Omega_p}{\delta_p}, \qquad 0 \leq 2\theta < \pi, \tag{2.11}$$

where we used

$$\hbar\Omega_p \equiv -\boldsymbol{d}_{ab} \cdot \boldsymbol{E}_p, \qquad \delta_p \equiv \omega_p - \omega_{ba}, \tag{2.12}$$

with $\boldsymbol{d}_{ab}$ the ab transition dipole moment. We assume for now that the distribution of pump photons is relatively narrow around a large average value ($\langle N\rangle \gg \Delta N \gg 1$), for which $2g\sqrt{\langle N\rangle} = \hbar\Omega_p$ holds (see, e.g., [30]); this assumption is well justified if, e.g., the pump field is in a coherent state with large average photon number.

The dynamics of the system can be expressed in terms of the Master equation for the reduced density matrix $\hat{\sigma}$. As we will show in chapter 5, the Master equation is in the Born-Markov approximation, written in the Lindblad form, given by

[74, 97, 107]

$$\begin{aligned}\frac{d}{dt}\hat{\sigma} &= \hat{\mathcal{L}}\hat{\sigma} \\ &\equiv \hat{\mathcal{L}}_{nd}\hat{\sigma} + \hat{\mathcal{L}}_{d}\hat{\sigma}.\end{aligned} \tag{2.13}$$

The non-dissipative part of the Lindblad operator can be written as

$$\hat{\mathcal{L}}_{nd}\hat{\sigma} \equiv -\frac{i}{\hbar}[\hat{H}_D + \hat{H}_c + \hat{V}_{AE}, \hat{\sigma}], \tag{2.14}$$

while the dissipative part is given by

$$\begin{aligned}\hat{\mathcal{L}}_{d}\hat{\sigma} \equiv &-\frac{\Gamma_{ca}}{2}\left(\hat{S}^{+}_{ac}\hat{S}^{-}_{ac}\hat{\sigma} + \hat{\sigma}\hat{S}^{+}_{ac}\hat{S}^{-}_{ac}\right) + \Gamma_{ca}\hat{S}^{-}_{ac}\hat{\sigma}\hat{S}^{+}_{ac} \\ &-\frac{\Gamma_{bc}}{2}\left(\hat{S}^{+}_{bc}\hat{S}^{-}_{bc}\hat{\sigma} + \hat{\sigma}\hat{S}^{+}_{bc}\hat{S}^{-}_{bc}\right) + \Gamma_{bc}\hat{S}^{-}_{bc}\hat{\sigma}\hat{S}^{+}_{bc}.\end{aligned} \tag{2.15}$$

We will elaborate in more detail in chapter 5 on the assumptions that lead to the above Master equation. The explicit evolution equations for all reduced density matrix elements are found by expanding equation (2.13) in the basis $\{|1(N)\rangle, |2(N')\rangle, |c, N''\rangle\}$, where N, N' and N'' are not necessarily equal. However, we will show in the next section that only an expansion in the basis $\{|1(N)\rangle, |2(N)\rangle, |c, N+1\rangle\}$ is required to determine the system's T-matrix, and we will therefore restrict ourselves to this particular basis. If we introduce the following notations for typographical simplicity

$$\sigma^{N,M}_{i,j} \equiv \langle i(N)|\hat{\sigma}|j(M)\rangle, \tag{2.16a}$$

$$E^{N}_{i} \equiv \langle i(N)|\hat{H}_D + \hat{H}_c|i(N)\rangle, \qquad i,j \in \{1,2,c\}, \tag{2.16b}$$

we can focus on the evolution equations obtained by an expansion of (2.13). First, the evolution of the population of the dressed state $|1(N)\rangle$ is given by

$$\begin{aligned}\dot{\sigma}^{N,N}_{1,1} = &-i\frac{\Omega_e}{2}\sin(\theta)\left(e^{i\omega t}\sigma^{N+1,N}_{c,1} - e^{-i\omega t}\sigma^{N,N+1}_{1,c}\right) + \Gamma_{ca}\sin^2(\theta)\sigma^{N+1,N+1}_{c,c} \\ &-\Gamma_{bc}\cos^2(\theta)\sigma^{N,N}_{1,1} + \frac{\Gamma_{bc}}{2}\sin(\theta)\cos(\theta)\left(\sigma^{N,N}_{1,2} + \sigma^{N,N}_{2,1}\right),\end{aligned} \tag{2.17}$$

with similar expressions for the populations $\sigma^{N,N}_{2,2}$ and $\sigma^{N,N}_{c,c}$. Secondly, coherences

such as $\sigma_{1,2}^{N,N}$ evolve as

$$\begin{aligned}\dot{\sigma}_{1,2}^{N,N} = &-i\frac{\Omega_e}{2}\Big(e^{i\omega t}\sin(\theta)\sigma_{c,2}^{N+1,N} - e^{-i\omega t}\cos(\theta)\sigma_{1,c}^{N,N+1}\Big) \\ &+ \Gamma_{ca}\sin(\theta)\cos(\theta)\sigma_{c,c}^{N+1,N+1} - \frac{i}{\hbar}\Big(E_1^N - E_2^N\Big)\sigma_{1,2}^{N,N} \\ &- \frac{\Gamma_{bc}}{2}\Big(\sigma_{1,2}^{N,N} - \sin(\theta)\cos(\theta)\sigma_{2,2}^{N,N} - \sin(\theta)\cos(\theta)\sigma_{1,1}^{N,N}\Big),\end{aligned} \tag{2.18}$$

with analogous expressions for all other coherences, derived in Appendix A. Expanding the Master equation allows us to describe the dynamics of our system, and in particular to look at its steady-state behavior. If we examine the Master equation more closely, then two types of evolutions can be distinguished. First, the coherences are driven by the external probe field; therefore their evolution can be separated in a quickly oscillating component (evolving typically at the probe frequency) and a slowly decaying envelope (evolving typically at Γ_{ca}^{-1}). Hence, a time-independent regime or *steady-state* for $\hat{\sigma}(t)$ can only be obtained for the envelope of the coherences (this separation of time scales is often referred to as the Rotating Wave Approximation [107]). Secondly, the other matrix elements (the populations), do not exhibit such quick oscillatory behavior and decay to their steady-state value without any persistent oscillations. The steady-state value of the level populations π_i, $i \in \{a, b, c\}$, for example, is given in the small external probe field limit by

$$\pi_c^{st} \equiv \sum_N \sigma_{c,c}^{N,N} = \frac{\Gamma_{bc}}{\Gamma_{ca}}\pi_b^{st} = \frac{W}{1 + W(1 + 2\frac{\Gamma_{ca}}{\Gamma_{bc}})} = 1 - \pi_b^{st} - \pi_a^{st}, \tag{2.19}$$

where we defined the dimensionless pumping intensity

$$W \equiv \frac{\Omega_p^2}{\Gamma_{bc}\Gamma_{ca}}, \qquad 0 \leq W < +\infty, \tag{2.20}$$

such that population inversion occurs in the *ac* system for $W \geq 1$. Now we can describe the dynamics of the system, we focus on the connection between the steady-state solution of the Master equation and the scattering properties of the system for incident light near the $c \rightarrow a$ resonance.

2.3 Derivation of the T-matrix of a dipole with gain

The Master equation allows us to express expectation values of atomic operators in terms of reduced density matrix elements [79]. We will elaborate in more detail on expectation values of atomic operators in chapter 5; at this point, we focus on the

expectation value of the operator $\hat{\boldsymbol{d}}$ associated with the ac dipole transition

$$\left\langle \hat{\boldsymbol{d}} \right\rangle \equiv \left\langle \hat{\boldsymbol{d}}_- \right\rangle + \left\langle \hat{\boldsymbol{d}}_+ \right\rangle = \boldsymbol{d}_{ac}\big(Tr(\hat{\sigma}\hat{S}^-_{ac}) + Tr(\hat{\sigma}\hat{S}^+_{ac})\big), \tag{2.21}$$

with

$$\begin{aligned} Tr(\hat{\sigma}\hat{S}^-_{ac}) &\equiv \sum_N \sum_{i=1,2,c} \langle i(N)|\hat{\sigma}\hat{S}^-_{ac}|i(N)\rangle \\ &= \sum_N \big(\sigma_{c,1}^{N,N-1}\sin(\theta) + \sigma_{c,2}^{N,N-1}\cos(\theta)\big), \end{aligned} \tag{2.22}$$

from which we can see that indeed only the reduced density matrix elements given by an expansion of (2.13) in the basis $\{|1(N)\rangle,\ |2(N)\rangle,\ |c, N+1\rangle\}$ appear in the expression for the average dipole moment. Furthermore, if we assume the pump frequency to be on resonance of the ab transition, we can deduce that in steady-state (defining $\omega_{ca} - \omega \equiv \delta$):

$$\left\langle \hat{\boldsymbol{d}}_- \right\rangle = -\boldsymbol{d}_{ac}e^{-i\omega t}\frac{1-W}{1+W}\frac{\Omega_e}{2\delta - i\Gamma_{ca}(1+W) + \frac{2\Omega_e^2}{2\delta + i\Gamma_{ca}(1+W)}}. \tag{2.23}$$

The (time-)averaged atomic ac dipole operator is related to the dynamic polarizability $\overleftrightarrow{\alpha}$ of the ac system by (see, e.g., [75])

$$\left\langle \hat{\boldsymbol{d}} \right\rangle \equiv \varepsilon_0 \mathrm{Re}\Big[\overleftrightarrow{\alpha}(\omega)\cdot \boldsymbol{E}_e e^{-i\omega t}\Big]. \tag{2.24}$$

Both equivalent expressions (2.21) and (2.24) allow us to connect the polarizability $\overleftrightarrow{\alpha}$ with the reduced density matrix, yielding

$$\overleftrightarrow{\alpha}(\omega)\cdot\boldsymbol{E}_e = -\frac{1}{\hbar\varepsilon_0}\boldsymbol{d}_{ac}(\boldsymbol{d}_{ac}\cdot\boldsymbol{E}_e)\frac{1-W}{1+W}\frac{1}{-\delta + i\frac{\Gamma_{ca}}{2}(1+W) - \frac{\Omega_e^2}{2\delta + i\Gamma_{ca}(1+W)}}, \tag{2.25}$$

which yields for small external probe fields

$$\overleftrightarrow{\alpha}(\omega) = -\overleftrightarrow{\alpha_0}\frac{1-W}{1+W}\frac{1}{2}\frac{\omega_{ca}}{\omega - \omega_{ca} + i\frac{\Gamma_{ca}}{2}(1+W)}. \tag{2.26}$$

The static polarizability is given by

$$\overleftrightarrow{\alpha_0} \equiv \alpha_0 \boldsymbol{\mu}_{ac}\otimes\boldsymbol{\mu}_{ac}, \qquad \alpha_0 \equiv \frac{2|\boldsymbol{d}_{ac}|^2}{\omega_{ca}\hbar\varepsilon_0}, \tag{2.27}$$

where "$\otimes$" denotes the tensor product of two vectors, and $\boldsymbol{\mu}_{ac}$ is the unit vector parallel to $\boldsymbol{d}_{ac}$.

(A small comment is at order here: although we currently focus on the derivation of the polarizability $\overleftrightarrow{\alpha}$, only the combination $\overleftrightarrow{\alpha} \cdot \boldsymbol{E}_e$ appears in a multiple-scattering formalism, as we will show in chapter 3; the separation of the polarization $\overleftrightarrow{\alpha} \cdot \boldsymbol{E}_e$ in $\overleftrightarrow{\alpha}$ and $\boldsymbol{E}_e$ is at this point only introduced for notational simplicity.)

It is important to note that the same expression (2.25) is obtained if the dressing of the levels a and b is omitted (and the optical Bloch equations, discussed in chapter 4, are used instead of the Master equation). The incoherent pumping mechanism only appears in the polarizability as a parameter W, without causing any detuning effects.

The scattering properties of a point dipole — or, more generally, any scattering object — can be expressed by its T-matrix. As mentioned in the introduction, the T-matrix of a scatterer is closely connected to its dynamic polarizability. For a point dipole located at $\boldsymbol{r} = 0$, both scattering quantities are related by

$$\begin{aligned} \langle \boldsymbol{r} | \overleftrightarrow{\hat{T}}(\omega) | \boldsymbol{r}' \rangle &= -\Big(\frac{\omega_{ca}}{c}\Big)^2 \overleftrightarrow{\alpha}(\omega) \delta(\boldsymbol{r}) \delta(\boldsymbol{r} - \boldsymbol{r}') \\ &= t(\omega) \boldsymbol{\mu}_{ac} \otimes \boldsymbol{\mu}_{ac} \delta(\boldsymbol{r}) \delta(\boldsymbol{r} - \boldsymbol{r}'), \end{aligned} \tag{2.28}$$

with as matrix element $t(\omega)$:

$$t(\omega) \equiv \alpha_0 \Big(\frac{\omega_{ca}}{c}\Big)^2 \frac{1 - W}{1 + W} \frac{1}{2} \frac{\omega_{ca}}{\omega - \omega_{ca} + i\frac{\Gamma_{ca}}{2}(1 + W) - \frac{\Omega_e^2}{2\omega_{ca} - 2\omega + i\Gamma_{ca}(1+W)}}, \tag{2.29}$$

which is nonlinear in the in the pump intensity (through W) and the incident probe field (through Ω_e). Both delta functions appearing in (2.28) express the local character of the scatterer; the anisotropy of the T-matrix is clearly due to the preferential orientation induced by the transition dipole moment. In the absence of pumping ($W = 0$) and for small external probe fields, we recover the expression for the linear dynamic polarizability of a two-level atom, which satisfies the optical theorem [66, 87] expressing energy conservation:

$$-\mathrm{Im}\Big[\frac{t(\omega)}{\omega_{ca}/c}\Big]\Big|_{\substack{W=0 \\ \Omega_e \to 0}} = \frac{|t(\omega)|^2}{6\pi}\Big|_{\substack{W=0 \\ \Omega_e \to 0}}. \tag{2.30}$$

For the optical theorem to hold, the static polarizability must satisfy

$$\alpha_0 = \frac{6\pi}{(\omega_{ca}/c)^3} \frac{\Gamma_{ca}}{\omega_{ca}}, \tag{2.31}$$

which, if substituted in (2.29), yields the final expression for the T-matrix element of a point dipole with gain for arbitrary pump and external probe field intensity. In the limit for small external probe fields, (2.29) then reduces to

$$t(\omega) = \frac{3\pi}{\omega_{ca}/c}\frac{1-W}{1+W}\frac{\Gamma_{ca}}{\left(\omega - \omega_{ca} + i\frac{\Gamma_{ca}}{2}(1+W)\right)}. \tag{2.32}$$

Expressions (2.28) and (2.32) (or more generally, (2.29)) are the key results of this section. In the next section, we will elaborate on their properties and physical consequences.

2.4 Properties of the T-matrix of a dipole with gain

The T-matrix (2.28) fully expresses the scattering properties of a point dipole with gain and satisfies the Kramers-Kronig relations [10], as is shown in Appendix B.

The pump field influences the T-matrix in a clear physical way. The most obvious effect of the pump is to induce changes of the (time-)averaged populations of the levels a and c, which leads to the multiplication of the dynamic polarizability with a factor $(1-W)/(1+W)$. Remarkably, the multiplication factor becomes negative if population inversion is present in the ac system ($W > 1$), expressing the fact that not only the imaginary, but also the real part of the dynamic polarizability is drastically changed by pumping. In other words, not only does absorption change into gain, but the dispersion relation also changes, as is shown in Figure 2.3. Besides changing the sign of the dynamic polarizability, the gain also effectively broadens the a level by a factor $(1+W)$, which is equivalent with a decrease of the Q factor $Q \equiv \omega_{ca}/\Gamma_{ca}$ of the $c \rightarrow a$ resonance. The latter effect is often referred to as *power broadening*.

It is intuitively clear that the optical theorem does not hold any longer as a nonzero pump field is applied. We will now show that this is indeed the case. If an external probe field with polarization vector $\boldsymbol{\epsilon}$ is incident on the point dipole we consider here, then the dipole scattering cross-section $\sigma_{sca}(\omega)$ and extinction cross-section $\sigma_{ext}(\omega)$ are given by

$$\sigma_{sca}(\omega) = +\frac{(\boldsymbol{\mu}_{ac}\cdot\boldsymbol{\epsilon})^2}{6\pi}|t(\omega)|^2, \tag{2.33a}$$

$$\sigma_{ext}(\omega) = -\frac{(\boldsymbol{\mu}_{ac}\cdot\boldsymbol{\epsilon})^2}{\omega/c}\mathrm{Im}\Big[t(\omega)\Big]. \tag{2.33b}$$

Both cross-sections depend (through $t(\omega)$) on the applied pumping intensity. The albedo a (not to be confused with the energy level a) of the ac system is defined

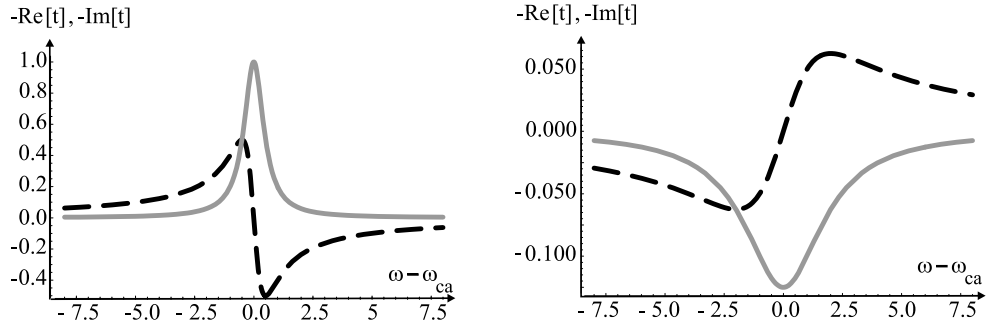

(a) $W = 0$ (b) $W = 3$

Figure 2.3: Comparison of the absorption (solid line) and the dispersion (dashed line) of the two-level *ac* system described in this chapter. The absorption is given by the imaginary part of the T-matrix and the dispersion by the real part of the T-matrix. Both quantities are shown as a function of the detuning $\omega - \omega_{ca}$ (in units of Γ_{ca}) (a) without a pump ($W = 0$) (b) for a pumping intensity in the population inversion regime ($W = 3$). The graphs are scaled such that $-\mathrm{Im}[t(\omega_{ca})] = 6\pi c/\omega_{ca}$ in Figure (a).

as the ratio of the elastic scattering cross-section and the extinction cross-section, which can be written for small incident probe fields as

$$a \equiv \frac{\sigma_{sca}(\omega)}{\sigma_{ext}(\omega)} = \frac{1 - W}{(1 + W)^2}, \tag{2.34}$$

where $(1 - a)$ is the fraction of the incident probe field which is taken away from the incident beam but not transformed into scattered light. If the optical theorem is satisfied, the albedo is one, as can be seen from expressions (2.30), (2.33) and (2.34). Therefore, if the optical theorem does not hold any longer, we expect a to be smaller than unity. (One might intuitively expect the presence of gain to result in an albedo larger than one, but expression (2.34) proves this intuition to be incorrect). To show that indeed $|a| \leq 1$, we plot the albedo (2.34) in Figure 2.4 as a function of the reduced pumping parameter W. As soon as the dipole has internal population inversion ($W > 1$), the albedo becomes negative, which indicates that the point dipole then has a negative extinction cross-section, as we expect. Obviously, the scattering cross-section is — by definition — always positive and the effect of the pump field is manifested purely as a decreasing of the scattered field for increasing pump. Furthermore, the extinction cross-section is, in absolute value, always larger than the scattering cross-section for nonzero pump. In other words, some of the incident probe field is taken away from the incident beam, but not scattered elastically. The presence of inelastic scattering is no surprise, since the total intensity emitted by the dipole is proportional to the population of the upper state c, whereas the coherent intensity emitted by the dipole is proportional

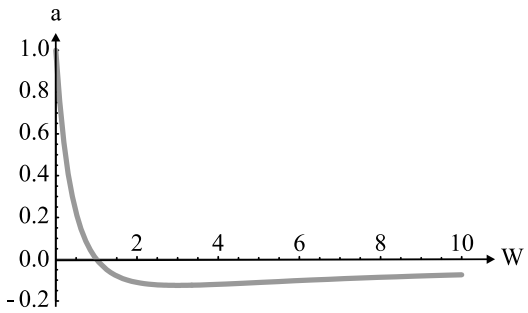

Figure 2.4: The albedo a of the ac system. A value of $a = 1$ denotes that the atom scatters elastically at the $a \rightarrow c$ transition while $a < 1$ reveals the scattering to be partially inelastic. The albedo is shown as a function of the pumping parameter W.

to the amount of coherence between a and c (see, e.g., [30]). Both intensities are only equal (all scattering is then elastic) in the absence of a pump field and in the small external probe field limit. As soon as a pump field is applied, or for larger external probe fields [27, 85], some of the light is scattered inelastically.

Finally, we see from expressions (2.33) that the optical theorem is also satisfied for the nontrivial values $W = 1$ and $W \rightarrow +\infty$. The latter two pumping values correspond to pumping intensities for which the T-matrix vanishes (therefore the optical theorem holds), but the reason why is clearly different for both cases: for $W = 1$, populations are, on average, equally distributed among levels a and c, preventing the building up of an average scattered field; for $W \rightarrow +\infty$, on the other hand, the line width broadening of the $c \rightarrow a$ transition induced by the pump field inhibits scattering. We stress that the absence of light scattering for $W = 1$ has to be interpreted in a statistical sense: the T-matrix is deduced from a (statistical) density matrix, denoting that for $W = 1$, the field scattered by the atom vanishes *on average*. In addition, the above transparency is caused by a fully incoherent pumping scheme, contrary to, e.g., electromagnetically induced transparency [56].

2.5 Extensions

In the previous sections, we have used a three-level atomic system as an example to demonstrate how to derive the light-scattering properties of an atom, based on its internal energy-level structure. The quantity which connects the atom's (classical) T-matrix and its (quantum mechanical) resonance structure is the system's transition dipole moment (2.21). The foregoing derivation of the T-matrix is very general and can be applied to a multitude of atomic systems. To demonstrate this general applicability, we focus in this section on the T-matrix derivation of three

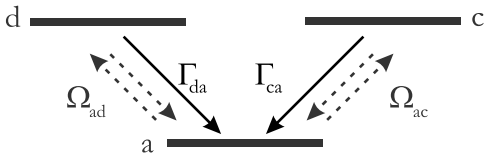

Figure 2.5: A three-level system V-type system adc. An electric field is incident on the system. This field induces transitions between a and c through the Rabi frequency Ω_{ac}, and transitions between a and d through the Rabi frequency Ω_{ad}.

standard quantum optical systems.

2.5.1 The T-matrix of a V system

An extensively studied nontrivial quantum optical system is a V-type system, as shown in Figure 2.5. A ground state a can be excited to two possible excited states c and d. Transitions between the ground state and the excited states are dipole-allowed with transition dipole moments $\boldsymbol{d}_{ac} \equiv |\boldsymbol{d}_{ac}|\,\boldsymbol{\mu}_{ac}$ and $\boldsymbol{d}_{ad} \equiv |\boldsymbol{d}_{ad}|\,\boldsymbol{\mu}_{ad}$. For simplicity, we assume both excited states to have equal energy ($\hbar\omega_d = \hbar\omega_c$) and life time ($\Gamma_{ca}^{-1} = \Gamma_{da}^{-1}$). The transition dipole moments of the $a \to c$ and $a \to d$ transitions are taken to be perpendicular: $\boldsymbol{\mu}_{ac} \cdot \boldsymbol{\mu}_{ad} = 0$. A physical implementation leading to such orthogonal transitions is, e.g., an atomic $|s\rangle \to |p_x\rangle$ and $|s\rangle \to |p_y\rangle$ transition (the $|s\rangle \to |p_z\rangle$ transition is assumed to be irrelevant in this particular example). Direct transitions between d and c are considered forbidden. An incident field $\boldsymbol{E}_e$ with frequency ω interacts with the system; the interaction is quantified by the Rabi frequencies $\Omega_{ac} \equiv -\boldsymbol{d}_{ac} \cdot \boldsymbol{E}_e/\hbar$ and $\Omega_{ad} \equiv -\boldsymbol{d}_{ad} \cdot \boldsymbol{E}_e/\hbar$.

The V system adc can be described by a density matrix $\hat{\sigma}$, of which the evolution is governed by a Master equation of the Lindblad type, similarly to (2.13). The derivation of the resulting Master equation is analogous to the derivation shown above; the resulting T-matrix is

$$\begin{aligned}\overleftrightarrow{\hat{T}}_V(\omega) &= -\left(\frac{\omega_{ca}}{c}\right)^2 \delta(\boldsymbol{r})\hat{\mathbb{1}} \otimes \overleftrightarrow{\alpha}_V(\omega) \\ &\equiv t_V(\omega)\delta(\boldsymbol{r})\hat{\mathbb{1}} \otimes \Big(\boldsymbol{\mu}_{ac} \otimes \boldsymbol{\mu}_{ac} + \boldsymbol{\mu}_{ad} \otimes \boldsymbol{\mu}_{ad}\Big),\end{aligned} \tag{2.35}$$

with

$$t_V(\omega) \equiv \frac{3\pi}{\omega_{ca}/c} \frac{\Gamma_{ca}}{\left(\omega - \omega_{ca} + i\frac{\Gamma_{ca}}{2} + \frac{\Omega_{ac}^2 + \Omega_{ad}^2}{2(\omega - \omega_{ca}) - i\Gamma_{ca}}\right)}, \tag{2.36}$$

where $\hat{\mathbb{1}}$ is a unit operator with matrix elements $\langle \boldsymbol{r}|\hat{\mathbb{1}}|\boldsymbol{r}'\rangle = \delta(\boldsymbol{r} - \boldsymbol{r}')$. The delta function in (2.35) expresses that the atom is positioned at $\boldsymbol{r} = \boldsymbol{0}$. The physical

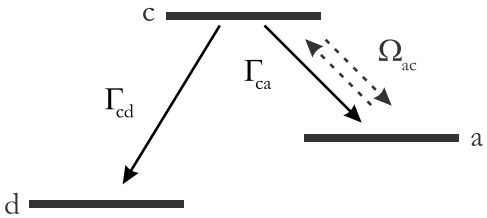

Figure 2.6: A three-level system Λ-type system *adc*. An electric field is incident on the system. This field induces transitions between a and c through the Rabi frequency Ω_{ac}.

meaning of expressions (2.35) and (2.36) can be intuitively understood: exciting the V system can occur via two transitions with orthogonal associated transition dipole moments. The existence of two excitation channels is translated into the saturation behavior and tensor character of the system's T-matrix. The saturation behavior of the V system is quantified by $(\Omega_{ac}^2 + \Omega_{ad}^2)$, indicating that the excitations induced by the external field $\boldsymbol{E}_e$ are evenly distributed over both excitation channels. The special tensor character of the T-matrix (2.35) indicates that in a V system a dipole moment can be excited in two available spatial directions $\boldsymbol{\mu}_{ac}$ and $\boldsymbol{\mu}_{ad}$. In contrast, inducing a dipole moment in a (two-level) point dipole can only occur in one spatial direction, leading to the uniaxial tensor character of (2.28). The observation that the nature and number of available transitions affects the tensor character of the atom's T-matrix leads to the interesting consequence that the simplest atomic level diagram leading to an isotropic scatterer consists of four levels: one ground level and three excitation channels with mutually orthogonal transition dipole moments, as is the case for, e.g., a spinless hydrogen atom [76].

2.5.2 The T-matrix of a Λ system

The second level scheme we consider is a three-level Λ system as shown in Figure 2.6. Two dipole transitions $a \rightarrow c$ and $d \rightarrow c$ share a common excited level c. The associated transition dipole moments are $\boldsymbol{d}_{ac} \equiv |\boldsymbol{d}_{ac}|\, \boldsymbol{\mu}_{ac}$ and $\boldsymbol{d}_{dc} \equiv |\boldsymbol{d}_{dc}|\, \boldsymbol{\mu}_{dc}$. Transitions between a and d are considered forbidden. We assume the frequency of the $d \rightarrow c$ transition to be far detuned from the $a \rightarrow c$ transition. An incident field $\boldsymbol{E}_e$ with frequency ω interacts with the system. The frequency ω is near-resonant with the $a \rightarrow c$ resonance. The interaction of the incident field with the Λ system is quantified by the Rabi frequency $\Omega_{ac} \equiv -\boldsymbol{d}_{ac} \cdot \boldsymbol{E}_e/\hbar$.

In a similar fashion as was described in the previous V-type example, we can associate a density matrix and corresponding Master equation with the Λ system *adc*. The derivation of the Master equation is analogous to the derivation shown above, leading to the system's T-matrix. Surprisingly, the resulting T-matrix is always zero

$$\overleftrightarrow{\hat{T}}_{\Lambda}(\omega) = \overleftrightarrow{0}, \tag{2.37}$$

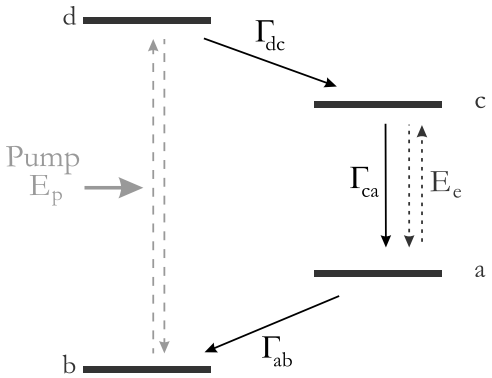

Figure 2.7: A four-level system *acdb*. An electric field $\boldsymbol{E}_e$ is incident on the system, near the $a \rightarrow c$ resonance. A pump field $\boldsymbol{E}_p$ interacts with the system through the $b \rightarrow d$ transition. The life times of levels d, c and a is given by Γ_{dc}^{-1}, Γ_{ca}^{-1} and Γ_{ab}^{-1} respectively. Decay from d to b is assumed to be slow compared to other processes, hence $\Gamma_{db} \approx 0$. The left dashed arrows express the interaction with the pump. The right dashed arrows depict the interaction with the external probe field.

indicating that the Λ system *adc* does not lead to an average scattered field for incident fields at the $a \rightarrow c$ transition. The vanishing of an average scattered field is due to the fact that in steady-state, all population is trapped in the d level, thereby inhibiting any population transfer between levels a and c. In literature, the non-trivial dynamics of the above Λ system have been studied extensively; for example, irradiation of a Λ system with two external fields has led to a demonstration of laser oscillation without inversion [55, 82, 96, 106, 124].

2.5.3 The T-matrix of a four-level system

As a third and final example of a derivation of a T-matrix based on microscopic considerations, we consider a four-level system *acdb* with gain, as shown in Figure 2.7. The transition involved in the scattering process of an incident probe field is the $c \rightarrow a$ transition with associated transition dipole moment $\boldsymbol{d}_{ac} \equiv |\boldsymbol{d}_{ac}|\boldsymbol{\mu}_{ac}$. An incident field $\boldsymbol{E}_e$ interacts through the Rabi frequency $\Omega_{ac} \equiv -\boldsymbol{d}_{ac} \cdot \boldsymbol{E}_e/\hbar$ with the *ac* system. Gain is incorporated in the system by indirectly pumping population from a to c via two other levels b and d. This pumping is implemented by a pump field $\boldsymbol{E}_p$, resonant with the $b \rightarrow d$ transition. The interaction of the pump field and the atom is quantified by the Rabi frequency $\Omega_{bd} = -\boldsymbol{d}_{bd} \cdot \boldsymbol{E}_p/\hbar$, with $\boldsymbol{d}_{bd}$ the $b \rightarrow d$ transition dipole moment. The essential difference between the four-level pumping scheme *acdb* shown here and the three-level scheme considered above (in Figure 2.1) is that in the latter, the scattering transition and the pumping transition share a common (ground) level. In that case, power broadening affects the scattering properties of a pumped three-level system, as discussed in section 2.4.

The four-level scheme of Figure 2.7 eliminates power broadening by separating the pump transition $b \rightarrow d$ and the scattering transition $c \rightarrow a$.

A description of the four-level system *acdb* in terms of its density matrix $\hat{\sigma}$ leads to the T-matrix of the $a \rightarrow c$ scattering transition, yielding

$$\begin{aligned} \overleftrightarrow{\hat{T}}_{4l}(\omega) &= -\Big(\frac{\omega_{ca}}{c}\Big)^2 \delta(\boldsymbol{r}) \hat{\mathbb{1}} \otimes \overleftrightarrow{\alpha}_{4l}(\omega) \\ &\equiv t_{4l}(\omega)\delta(\boldsymbol{r})\hat{\mathbb{1}} \otimes \Big(\boldsymbol{\mu}_{ac} \otimes \boldsymbol{\mu}_{ac}\Big), \end{aligned} \tag{2.38}$$

in the linear regime, with

$$t_{4l}(\omega) \equiv \alpha_0 \Big(\frac{\omega_{ca}}{c}\Big)^2 \frac{1}{2} \Phi(\Omega_{bd}) \frac{\omega_{ca}}{\Big(\omega - \omega_{ca} + i\frac{\Gamma_{ca}+\Gamma_{ab}}{2}\Big)}, \tag{2.39}$$

with the static polarizability α_0 given by (2.27). The pump field enters the expression for the T-matrix through the dimensionless intensity

$$\Phi(\Omega_{bd}) \equiv \frac{(\Gamma_{ca} - \Gamma_{ab})\,\Omega_{bd}^2}{\Omega_{bd}^2\left(\Gamma_{ab} + \Gamma_{ca} + 2\Gamma_{ab}\Gamma_{ca}\Gamma_{dc}^{-1}\right) + \Gamma_{ab}\Gamma_{ca}\Gamma_{dc}}. \tag{2.40}$$

Interesting differences are apparent between T-matrices (2.38) and (2.28), reflecting that the choice of pumping scheme influences the resulting scattering properties. First, we observe that the last factor of (2.39) is independent of the pump. As mentioned above, the nature of this term indicates that the four-level pumping scheme does not exhibit power broadening, in contrast to a three-level pumping scheme. Secondly, the Q factor of the $a \rightarrow c$ scattering transition is given by $Q \equiv \omega_{ca}/(\Gamma_{ca} + \Gamma_{ab})$ which differs from the "bare" value ω_{ca}/Γ_{ca} due to leakage from the a level to the lower-lying b-level. Thirdly, in the absence of a pump field, no scattering occurs at the $a \rightarrow c$ transition, since $\lim_{\Omega_{bd}\rightarrow 0} t_{4l}(\omega) = 0$. This possibility of transparency of the four-level system *acdb* for scattering at the $a \rightarrow c$ transition is intuitively trivial, since in the the absence of a pumping field, all population remains trapped in the b state, unaffected by any field with frequency near the $c \rightarrow a$ transition. Finally, and perhaps most strikingly, the sign of the T-matrix is determined only by the decay rates Γ_{ca} and Γ_{ab}. In other words, whether the population in the ac subsystem is inverted or not is independent of the applied pump field intensity. This observation can be qualitatively expressed in terms of level populations, by calculating the population difference between levels a and c, yielding:

$$\langle a|\hat{\sigma}|a\rangle - \langle c|\hat{\sigma}|c\rangle = \Phi(\Omega_{bd}), \tag{2.41}$$

confirming that the presence of population inversion in the ac system is fully determined by the sign of $(\Gamma_{ca} - \Gamma_{ab})$. Physically, this indicates that if population leaks away from the a level less quickly than it flows towards that level, the population of the a level will build up and exceed the population of the c level in steady-state, regardless of the applied pump field intensity [111].

2.6 Summary

The aim of this chapter was to express the light-scattering properties of an atomic system in terms of its internal energy level structure. As an important application, we determined the T-matrix of a pumped point dipole, modelled as a three-level system. The resulting T-matrix (2.32) (or more generally, (2.29)) is surprisingly intuitive. The influence of the pump field can be characterized by a single dimensionless parameter W, expressing both a decrease of the Q factor and a decrease of the T-matrix. Physically, the presence of gain not only causes the dipole to scatter partially inelastically, but also induces important changes in its dispersion and dissipation.

To stress the generality of the above derivation, we derived the T-matrix of a passive atomic V system and a passive atomic Λ system, and showed that their scattering properties can be straightforwardly determined. Finally, we deduced the T-matrix of a pumped point dipole with the gain implemented through a four-level scheme. We pointed out that the choice of pumping scheme has major implications on the resulting scattering properties. Particularly striking is that the sign of the extinction cross-section (hence the presence of gain) is independent of the applied pump field intensity in a four-level scheme.

In conclusion, the general scattering properties of an atomic system depend strongly on the atomic level structure and, in the case of gain, the applied pump field intensity. This dependence could lead to interesting experimental work on, e.g., coherent backscattering [64, 121, 127]. For example, the width of the coherent backscattering cone is closely related to the albedo of the scatterers in the multiple scattering medium considered. We have shown in this chapter that the albedo is strongly correlated with the microscopic structure and applied pump field intensity. The possibility of incorporating these effects in a classical T-matrix is promising for future theoretical and experimental research on coherent backscattering in systems with a nontrivial microscopic structure.

CHAPTER 3

Few-atom systems with gain: a classical light-scattering approach

We study the light-scattering properties of a system of N atoms in free space using a single-frequency multiple light-scattering formalism. More particularly, we investigate the possibility of threshold behavior in the system if one of the atoms is optically pumped. The system of N atoms with gain is studied in two phases. First, we consider the passive N-atom system and define its quality factor Q. We show that the Q factor in general depends on the polarization and propagation direction of the incident field which probes the system. Secondly, we show that optically pumping one of the atoms allows for the appearance of a well-defined threshold within the presented formalism. Remarkably, a threshold exists for atom numbers as small as $N = 2$. Finally, we discuss the influence of the approximative nature of the applied formalism on the physical reality of the presented results.

3.1 Introduction

In chapter 1, we introduced N-atom systems with gain as the simplest microscopic systems which incorporate both optical gain and optical feedback. The attraction of these atomic systems lies in the absence of any phenomenological parameters or paraxial approximations in their description. The microscopic character of these N-atom systems ensures that the system characteristics depend solely on the scattering properties of the atomic building blocks and their specific description. In

this chapter, we describe the atoms within the framework of single-frequency multiple scattering of light. The advantage of this approach lies within the formalism's transparency and simplicity when applied to the system under consideration here. Furthermore, the computational scaling with the number of atoms of this method is favorable compared to the quantum mechanical density matrix method which will be discussed in chapter 5.

We start our description in section 3.2 with a general introduction to multiple scattering of light by an N-atom system. The T-matrix concept introduced in the previous chapter will be shown to be the essential building block in the description of multiple scattering; the T-matrices we derived can be straightforwardly used to describe the atomic system we consider here. The atoms are studied in two phases. We first focus in section 3.3 on the passive atomic system. In the absence of gain, we can quantify the ability of a collection of N atoms to act as a cavity for light. The quality of such an N-atom cavity is expressed by its quality factor Q. We show that the Q factor is a property not only of the cavity, but also of the incident field by which it is probed. We then proceed by optically pumping one of the atoms. The concept of gain is introduced by considering the proper T-matrices, as proposed in the previous chapter. In section 3.4 we show that the implementation of gain within the framework of a single-frequency multiple-scattering theory allows for the appearance of a threshold of an N-atom system. We show that, surprisingly, a threshold exists within the current framework for numbers of atoms down to $N = 2$. Finally, in section 3.5 we comment on the approximative nature of a single-frequency formalism describing pumped atomic systems; we elaborate in more detail on the physical reality of the obtained results.

3.2 Multiple scattering of light by N atoms

3.2.1 General introduction

The physical problem we focus on is the description of the scattering of an incident electric field $\boldsymbol{E}_e(\omega, \boldsymbol{r})$ by a collection of N atoms. The interference of the incident field and the field scattered by the atoms gives rise to the buildup of a total field $\boldsymbol{E}(\omega, \boldsymbol{r})$. The problem at hand is the determination of this total field $\boldsymbol{E}(\omega, \boldsymbol{r})$ in terms of the incident field and atomic parameters.

In the absence of any atoms (or, more generally, scatterers), the total field is identical to the incident field, and obeys the Helmholtz wave equation for electromagnetic fields in vacuum, given by

$$\left[\left(\frac{\omega}{c}\right)^2 \overleftrightarrow{I} - \boldsymbol{\nabla} \times \boldsymbol{\nabla} \times\right] \boldsymbol{E}_e(\omega, \boldsymbol{r}) = 0, \tag{3.1}$$

where $\overleftrightarrow{I}$ is the 3×3 unit tensor in polarization space. Here and in the following, the frequency ω is understood to contain an infinitesimally small positive imaginary part, ensuring causality.

It will be convenient to regard equation (3.1) as the real-space representation of an abstract tensor operator acting on the vector field $|\boldsymbol{E}_e(\omega)\rangle$. In abstract notation, equation (3.1) becomes

$$\overleftrightarrow{\hat{\mathcal{L}}}(\omega)|\boldsymbol{E}_e(\omega)\rangle = 0. \tag{3.2}$$

(We note that the abstract tensor operator $\overleftrightarrow{\hat{\mathcal{L}}}$ is not to be confused with the Lindblad operator of chapter 2.) The main advantage of using abstracted equations lies within the simplicity of the resulting identities obtained and their independence of a specific representation. The above abstraction reveals the similarity between the current system and wave equations in quantum mechanics: the vector field $|\boldsymbol{E}_e(\omega)\rangle$ is analogous to a quantum mechanical state $|\psi_0\rangle$, whereas the real-space representation $\boldsymbol{E}_e(\omega,\boldsymbol{r}) \equiv \langle \boldsymbol{r}|\boldsymbol{E}_e(\omega)\rangle$ corresponds to a wave function $\psi_0(\boldsymbol{r})$. (We stress, however, that in this chapter all electromagnetic fields are considered to be classical quantities; the presented abstract notation is therefore not to be confused with the "bra-ket" notation used in second quantization.)

We can associate a Green function [118] with wave equation (3.1); the resulting free-space dyadic Green function $\overleftrightarrow{G}_0$ obeys

$$\left[\left(\frac{\omega}{c}\right)^2 \overleftrightarrow{I} - \boldsymbol{\nabla}\times\boldsymbol{\nabla}\times\right] \overleftrightarrow{G}_0(\omega,\boldsymbol{r},\boldsymbol{r}') = \delta^3(\boldsymbol{r}-\boldsymbol{r}')\overleftrightarrow{I}. \tag{3.3}$$

In abstract notation, (3.3) becomes

$$\overleftrightarrow{\hat{\mathcal{L}}}(\omega)\overleftrightarrow{\hat{G}}_0(\omega) = \overleftrightarrow{\hat{\mathbb{1}}}, \tag{3.4}$$

where $\overleftrightarrow{\hat{\mathbb{1}}}$ is the identity operator with matrix elements $\langle \boldsymbol{r}|\overleftrightarrow{\hat{\mathbb{1}}}|\boldsymbol{r}'\rangle = \delta^3(\boldsymbol{r}-\boldsymbol{r}')\overleftrightarrow{I}$.

In the presence of scatterers, the wave equation (3.1) needs to be modified. If the scatterers are characterized by a dimensionless permittivity $\overleftrightarrow{\varepsilon}(\omega,\boldsymbol{r})$, the resulting wave equation for the field $\boldsymbol{E}(\omega,\boldsymbol{r})$ becomes

$$\left[\left(\frac{\omega}{c}\right)^2 \overleftrightarrow{I} - \boldsymbol{\nabla}\times\boldsymbol{\nabla}\times\right] \boldsymbol{E}(\omega,\boldsymbol{r}) = -\left[\left(\overleftrightarrow{\varepsilon}(\omega,\boldsymbol{r}) - \overleftrightarrow{I}\right)\left(\frac{\omega}{c}\right)^2\right] \boldsymbol{E}(\omega,\boldsymbol{r}). \tag{3.5}$$

We can associate a light potential $\overleftrightarrow{V}(\omega,\boldsymbol{r})$ with the scattering system by defining

$$\overleftrightarrow{V}(\omega,\boldsymbol{r}) \equiv -\left(\overleftrightarrow{\varepsilon}(\omega,\boldsymbol{r}) - \overleftrightarrow{I}\right)\left(\frac{\omega}{c}\right)^2, \tag{3.6}$$

which allows us to rewrite (3.5) as

$$\overleftrightarrow{\mathcal{L}}(\omega)|\boldsymbol{E}(\omega)\rangle = \overleftrightarrow{V}(\omega)|\boldsymbol{E}(\omega)\rangle. \tag{3.7}$$

Equations (3.2), (3.4) and (3.7) show that the incident field $|\boldsymbol{E}_e(\omega)\rangle$ and the total field $|\boldsymbol{E}(\omega)\rangle$ are related by the Lippmann-Schwinger equation

$$|\boldsymbol{E}(\omega)\rangle = |\boldsymbol{E}_e(\omega)\rangle + \overleftrightarrow{G}_0(\omega)\overleftrightarrow{V}(\omega)|\boldsymbol{E}(\omega)\rangle. \tag{3.8}$$

The Lipmann-Schwinger equation (3.8) allows for the total field to be written as a series

$$\begin{aligned}|\boldsymbol{E}(\omega)\rangle = |\boldsymbol{E}_e(\omega)\rangle &+ \overleftrightarrow{G}_0(\omega)\overleftrightarrow{V}(\omega)|\boldsymbol{E}_e(\omega)\rangle \\ &+ \overleftrightarrow{G}_0(\omega)\overleftrightarrow{V}(\omega)\overleftrightarrow{G}_0(\omega)\overleftrightarrow{V}(\omega)|\boldsymbol{E}_e(\omega)\rangle + \ldots\end{aligned} \tag{3.9}$$

in terms of the optical potential. If only the first term in the expansion (3.9) is retained, we find the well-known *Born approximation* for the total field. If, on the other hand, all terms in the expansion are taken into account, the above summation (3.9) leads to

$$|\boldsymbol{E}(\omega)\rangle = |\boldsymbol{E}_e(\omega)\rangle + \overleftrightarrow{G}_0(\omega)\overleftrightarrow{T}(\omega)|\boldsymbol{E}_e(\omega)\rangle, \tag{3.10}$$

where the T-matrix $\overleftrightarrow{T}(\omega)$ is formally defined as

$$\overleftrightarrow{T}(\omega) \equiv \overleftrightarrow{V}(\omega)\left[\overleftrightarrow{\mathbb{1}} - \overleftrightarrow{G}_0(\omega)\overleftrightarrow{V}(\omega)\right]^{-1}. \tag{3.11}$$

The presence of the scatterers changes the wave equation (3.2) into equation (3.7). Consequently, the presence of scatterers changes the associated Green function as well. The Green function associated with the wave equation (3.7) obeys

$$\left[\overleftrightarrow{\mathcal{L}}(\omega) - \overleftrightarrow{V}(\omega)\right]\overleftrightarrow{G}(\omega) = \overleftrightarrow{\mathbb{1}}, \tag{3.12}$$

with as formal solution

$$\overleftrightarrow{G}(\omega) = \overleftrightarrow{G}_0(\omega) + \overleftrightarrow{G}_0(\omega)\overleftrightarrow{V}(\omega)\overleftrightarrow{G}(\omega), \tag{3.13}$$

or, equivalently,

$$\overleftrightarrow{\hat{G}}(\omega) = \overleftrightarrow{\hat{G}}_0(\omega) + \overleftrightarrow{\hat{G}}_0(\omega)\overleftrightarrow{\hat{T}}(\omega)\overleftrightarrow{\hat{G}}_0(\omega). \tag{3.14}$$

Expressions (3.13) and (3.14) can be readily deduced from (3.4), (3.11) and (3.12). In terms of light propagation, equation (3.14) describes how light emitted by a (point) source propagates, in contrast to the propagation of an incident field as described by (3.10). Expression (3.14) shows that the Green function of the system in the presence of scatterers can be written in terms of the free-space Green function and a T-matrix describing all scattering events. In other words, once the system's T-matrix is known, the scattering problem can be solved explicitly.

3.2.2 Derivation of the N-atom T-matrix

All expressions derived sofar are independent of the number of scatterers and the (non)local character of each scatterer. We now focus on the current case of interest, and proceed to derive the T-matrix of an N-atom system. This T-matrix will allow us, through equation (3.10), to derive an expression for the total field $\boldsymbol{E}(\omega, \boldsymbol{r})$ in terms of the incident field and atomic parameters only.

The total potential of N atoms can be written as the sum of single-atom potentials

$$\overleftrightarrow{\hat{V}}(\omega) = \sum_{i=1}^{N} \overleftrightarrow{\hat{V}}_i(\omega). \tag{3.15}$$

The formal definition (3.11) then allows us to express the total N-atom T-matrix in terms of single-atom potentials as

$$\overleftrightarrow{\hat{T}}(\omega) = \sum_{i=1}^{N} \overleftrightarrow{\hat{V}}_i(\omega) + \sum_{i,j=1}^{N} \overleftrightarrow{\hat{V}}_i(\omega)\overleftrightarrow{\hat{G}}_0(\omega)\overleftrightarrow{\hat{V}}_j(\omega) + \dots. \tag{3.16}$$

The total T-matrix can also be expanded in terms of single-atom T-matrices. If we formally denote the T-matrix of atom i as

$$\overleftrightarrow{\hat{T}}_i(\omega) \equiv \overleftrightarrow{\hat{V}}_i(\omega)\left[\overleftrightarrow{\hat{\mathbb{1}}} - \overleftrightarrow{\hat{G}}_0(\omega)\overleftrightarrow{\hat{V}}_i(\omega)\right]^{-1}, \tag{3.17}$$

we can rewrite (3.16) as

$$\overleftrightarrow{\hat{T}}(\omega) = \sum_{i=1}^{N} \overleftrightarrow{\hat{T}}_i(\omega) + \sum_{i=1}^{N} \sum_{j=1, j\neq i}^{N} \overleftrightarrow{\hat{T}}_i(\omega) \overleftrightarrow{\hat{G}}_0(\omega) \overleftrightarrow{\hat{T}}_j(\omega) + \dots . \tag{3.18}$$

The above expansion can be straightforwardly checked by inserting the expansion of the single-atom T-matrices (3.17) in terms of single-atom potentials in (3.18), yielding (3.16). The T-matrix (3.18) is expressed in terms of single-atom T-matrices only. As shown in chapter 2, the explicit expression for T-matrix of a single atom depends on the atom's internal structure. In what follows, we consider atoms of the three-level type *abc*, as shown in Figure 2.1. Correspondingly, expression (2.28) shows that the resulting single-atom T-matrix can be written as

$$\overleftrightarrow{\hat{T}}_i(\omega) = t_i(\omega) \boldsymbol{\mu}_{ac}^{(i)} \otimes \boldsymbol{\mu}_{ac}^{(i)} \delta(\boldsymbol{r} - \boldsymbol{r}_i) \hat{\mathbb{1}}, \tag{3.19}$$

with $\boldsymbol{r}_i$ the position vector of atom i and $\boldsymbol{\mu}_{ac}^{(i)}$ its transition dipole moment. We can retrieve the potential associated with a single atom by inserting (3.19) in (3.17), yielding

$$\overleftrightarrow{\hat{V}}_i(\omega) = -(\omega/c)^2 \alpha_i^B \boldsymbol{\mu}_{ac}^{(i)} \otimes \boldsymbol{\mu}_{ac}^{(i)} \delta(\boldsymbol{r} - \boldsymbol{r}_i) \hat{\mathbb{1}}, \tag{3.20}$$

where α_i^B is the bare polarizability [31] of atom i, given by

$$\alpha_i^B = -\frac{t_i(\omega)}{(\omega/c)^2} \frac{1}{1 + t_i(\omega) \boldsymbol{\mu}_{ac}^{(i)} \cdot \overleftrightarrow{G}_0(\omega, \boldsymbol{r}_i, \boldsymbol{r}_i) \cdot \boldsymbol{\mu}_{ac}^{(i)}}. \tag{3.21}$$

The bare polarizability is a measure for the strength of the coupling between the atom and the electromagnetic field in single-scattering events, as can be seen from expression (3.16). Additionally, the bare polarizability can be interpreted in terms of the atomic transition dipole moment: the dipole moment $\boldsymbol{d}_{ac}^{(i)}$ induced in atom i by an external field $\boldsymbol{E}_e$ is, according to (2.24), given by

$$\boldsymbol{d}_{ac}^{(i)} = \varepsilon_0 (\omega/c)^{-2} \boldsymbol{\mu}_{ac}^{(i)} \mathrm{Re}\left[t(\omega) \boldsymbol{\mu}_{ac}^{(i)} \cdot \boldsymbol{E}_e \right], \tag{3.22}$$

which can be equivalently written in terms of the bare polarizability as

$$\boldsymbol{d}_{ac}^{(i)} = \varepsilon_0 \boldsymbol{\mu}_{ac}^{(i)} \mathrm{Re}\left[\alpha_i^B \boldsymbol{\mu}_{ac}^{(i)} \cdot \boldsymbol{E} \right], \tag{3.23}$$

where $\boldsymbol{E}$ is the electric field including depolarization effects.

Using expressions (3.19), we can expand the total T-matrix (3.18) as

$$\begin{aligned}\langle \boldsymbol{r}|\overleftrightarrow{\hat{T}}(\omega)|\boldsymbol{r}'\rangle =& \sum_{i=1}^{N} t_i(\omega)\boldsymbol{\mu}_{ac}^{(i)}\otimes\boldsymbol{\mu}_{ac}^{(i)}\delta(\boldsymbol{r}-\boldsymbol{r}_i)\delta(\boldsymbol{r}'-\boldsymbol{r}_i)\\ &+\sum_{\substack{i,j=1\\ i\neq j}}^{N} t_i(\omega)t_j(\omega)\boldsymbol{\mu}_{ac}^{(i)}\otimes\boldsymbol{\mu}_{ac}^{(j)}\left[\boldsymbol{\mu}_{ac}^{(i)}\cdot\overleftrightarrow{G}_0(\omega,\boldsymbol{r}_i,\boldsymbol{r}_j)\cdot\boldsymbol{\mu}_{ac}^{(j)}\right]\times\\ &\quad\delta(\boldsymbol{r}-\boldsymbol{r}_i)\delta(\boldsymbol{r}'-\boldsymbol{r}_j)\\ &+\dots. \end{aligned} \tag{3.24}$$

We now proceed to rewrite (3.24) such that we can perform the infinite summation explicitly. We introduce the $N\times N$ matrices $D(\omega,\{\boldsymbol{r}\})$ and $M(\omega)$ as

$$D_{ij}(\omega,\{\boldsymbol{r}\})\equiv D_{ij}(\omega,\boldsymbol{r}_1,\dots,\boldsymbol{r}_N)\equiv(1-\delta_{ij})\left[\boldsymbol{\mu}_{ac}^{(i)}\cdot\overleftrightarrow{G}_0(\omega,\boldsymbol{r}_i,\boldsymbol{r}_j)\cdot\boldsymbol{\mu}_{ac}^{(j)}\right], \tag{3.25a}$$

$$M_{ij}(\omega)\equiv\delta_{ij}t_i(\omega), \tag{3.25b}$$

where δ_{ij} is the Kronecker delta. Definitions (3.25) allow us to rewrite (3.24) as

$$\begin{aligned}\langle \boldsymbol{r}|\overleftrightarrow{\hat{T}}(\omega)|\boldsymbol{r}'\rangle =& \sum_{i,j=1}^{N}\boldsymbol{\mu}_{ac}^{(i)}\otimes\boldsymbol{\mu}_{ac}^{(j)}\delta(\boldsymbol{r}-\boldsymbol{r}_i)\delta(\boldsymbol{r}'-\boldsymbol{r}_j)t_i(\omega)\times\\ &\left(\delta_{ij}+\left[M(\omega)D(\omega,\{\boldsymbol{r}\})\right]_{ij}+\left[\left(M(\omega)D(\omega,\{\boldsymbol{r}\})\right)^2\right]_{ij}\dots\right). \end{aligned} \tag{3.26}$$

We see that consecutive terms in the expansion (3.26) contain consecutive powers of the matrix product $M(\omega)D(\omega,\{\boldsymbol{r}\})$. This matrix structure enables us to sum the series expansion exactly, resulting in

$$\langle \boldsymbol{r}|\overleftrightarrow{\hat{T}}(\omega)|\boldsymbol{r}'\rangle =\sum_{i,j=1}^{N}\boldsymbol{\mu}_{ac}^{(i)}\otimes\boldsymbol{\mu}_{ac}^{(j)}\delta(\boldsymbol{r}-\boldsymbol{r}_i)\delta(\boldsymbol{r}'-\boldsymbol{r}_j)t_i(\omega)\Lambda_{ij}(\omega), \tag{3.27}$$

where the $N\times N$ matrix $\Lambda(\omega)$ is given by

$$\Lambda(\omega)\equiv\left(I^{(N)}-M(\omega)D(\omega,\{\boldsymbol{r}\})\right)^{-1}, \tag{3.28}$$

with $I^{(N)}$ the $N \times N$ unit matrix. The problem of finding the system's total T-matrix has been reduced to the much simpler problem of inverting the $N \times N$ matrix $\Lambda(\omega)^{-1}$. Expression (3.27) is the key result of this section: the exact total T-matrix of an N-atom system is expressed as a function of the free-space Green function and atomic parameters only. Using equation (3.10), we can now straightforwardly describe how an incident field $\boldsymbol{E}_e(\omega, \boldsymbol{r})$ is scattered by the N-atom system. In the next section, we show how this knowledge enables us to quantify the quality of the N atoms to act as a cavity for light.

3.3 The Q factor of an N-atom system

3.3.1 Definition of the Q factor

The aim of this chapter is to describe the interaction of a pumped atom with surrounding passive atoms using the scattering formalism described above. If the optical feedback provided by the passive atoms is significant, the light emitted by the gain atom will be sufficiently confined in order for stimulated emission to be possible. The parameter which quantifies the ability of a collection of passive atoms to temporally confine light is their collective Q factor. We now proceed to define an expression for Q.

In the case of a single isolated passive two-level atom, the scattering cross-section on resonance for an incident field $\boldsymbol{E}_e(\omega, \boldsymbol{r}) = \boldsymbol{\epsilon}_k e^{i\boldsymbol{k}\cdot\boldsymbol{r}}$ with $|\boldsymbol{k}| = \omega/c$ is given by (2.33):

$$\sigma_{sca}(\omega_{ca}, \mathbf{1}_k, \boldsymbol{\epsilon}_k) = \frac{3}{2}\frac{\lambda_{ca}^2}{\pi}(\boldsymbol{\mu}_{ac} \cdot \boldsymbol{\epsilon}_k)^2, \tag{3.29}$$

with $\lambda_{ca} = 2\pi c/\omega_{ca}$. We explicitly included the wave vector and polarization of the incident field in (3.29) to stress that, in general, the scattering cross section depends on both incident field properties. The optical cross-section (3.29) is, for the optical frequencies of interest and $\boldsymbol{\mu}_{ac} \parallel \boldsymbol{\epsilon}_k$, very large compared to the atom's geometrical cross-section which is of the order πa_0^2, with the atom's Bohr radius given by [75]

$$a_0 \equiv 4\pi\varepsilon_0\hbar^2/m_e e^2 \approx 5.10^{-11}\text{m}, \tag{3.30}$$

where m_e is the electron's mass and e its charge. The large optical cross-section (3.29) on resonance of a single atom hints at the feasibility of using N atoms as a cavity.

If an incident field is scattered by a system of N atoms, the incident light will experience retardation effects [88]. In other words, it takes a certain time to accumulate and discharge energy in the atoms. The time associated with this delay is

the system's dwell time τ_d, defined as [66]

$$\tau_d(\omega, \mathbf{1}_k, \boldsymbol{\epsilon}_k, S) \equiv \frac{w(\omega, \mathbf{1}_k, \boldsymbol{\epsilon}_k, S)}{\sigma_{sca}(\omega, \mathbf{1}_k, \boldsymbol{\epsilon}_k)c}, \tag{3.31}$$

with $w(\omega, \mathbf{1}_k, \boldsymbol{\epsilon}_k, S)$ the increase in electromagnetic energy inside the volume S due to the presence of scatterers

$$w(\omega, \mathbf{1}_k, \boldsymbol{\epsilon}_k, S) \equiv \int_S \boldsymbol{dr} \left[\boldsymbol{E}^*_{\mathbf{1}_k, \boldsymbol{\epsilon}_k}(\omega, \boldsymbol{r}) \cdot \overleftrightarrow{\varepsilon}(\omega, \boldsymbol{r}) \cdot \boldsymbol{E}_{\mathbf{1}_k, \boldsymbol{\epsilon}_k}(\omega, \boldsymbol{r}) - 1 \right], \tag{3.32}$$

where $\boldsymbol{E}_{\mathbf{1}_k, \boldsymbol{\epsilon}_k}(\omega, \boldsymbol{r})$ is the electric field resulting from the scattering of the aforementioned incident field with wave vector $\omega/c\mathbf{1}_k$ and polarization $\boldsymbol{\epsilon}_k$. The units in (3.31) are chosen such that the energy density of a plane wave in vacuum is normalized to unity ($\boldsymbol{\epsilon}_k \cdot \boldsymbol{\epsilon}_k = 1$); in the absence of any scatterers, $w(\omega, \mathbf{1}_k, \boldsymbol{\epsilon}_k, S)$ then reduces to 0. The cross-section $\sigma_{sca}(\omega, \mathbf{1}_k, \boldsymbol{\epsilon}_k)$ is in general defined as

$$\sigma_{sca}(\omega, \mathbf{1}_k, \boldsymbol{\epsilon}_k) \equiv -\frac{1}{\omega/c} \mathrm{Im} \left[\langle \boldsymbol{k}, \boldsymbol{\epsilon}_k | \overleftrightarrow{T}(\omega) | \boldsymbol{k}, \boldsymbol{\epsilon}_k \rangle \right], \tag{3.33}$$

which can be rewritten, using (3.27), as

$$\sigma_{sca}(\omega, \mathbf{1}_k, \boldsymbol{\epsilon}_k) = -\frac{1}{\omega/c} \sum_{i,j=1}^{N} \left(\boldsymbol{\epsilon}_k \cdot \boldsymbol{\mu}^{(i)}_{ac} \right) \left(\boldsymbol{\epsilon}_k \cdot \boldsymbol{\mu}^{(j)}_{ac} \right) \mathrm{Im} \left[t_i(\omega) \Lambda_{ij}(\omega) e^{i\boldsymbol{k} \cdot (\boldsymbol{r}_i - \boldsymbol{r}_j)} \right], \tag{3.34}$$

for N-atom systems. Similar to the cross section (3.33), the dwell time (3.31) generally depends on the frequency ω, the wave vector $\boldsymbol{k} \equiv |\boldsymbol{k}|\mathbf{1}_k$ and polarization $\boldsymbol{\epsilon}_k$ of the incident field. From a physical point a view, definition (3.31) shows that the delay due to scattering experienced by an incident probe is given by the ratio of the energy stored in the system and the current that carries energy away. The dwell time has the dimensions of a time; we can define a dimensionless dwell time or Q *factor* as

$$Q(\omega, \mathbf{1}_k, \boldsymbol{\epsilon}_k, S) \equiv \omega \tau_d(\omega, \mathbf{1}_k, \boldsymbol{\epsilon}_k, S), \tag{3.35}$$

which, through τ_d, also depends on the incident field and the volume S surrounding the cavity. The explicit dependence of Q on the incident field is usually omitted in literature, often because the system has a well-defined symmetry axis along which it is assumed the incident field propagates. However, since we aim at a general description of N-atom systems, we explicitly retain the dependence of Q on the wave

vector of the incident field in (3.35). In addition, we note that the dependence of Q on the incident field and frequency illustrates the general character of definition (3.35) compared to the concept of a quality factor as introduced in standard response theory (where Q is defined as the ratio of the spectral width of a resonance and its center frequency).

The Q factor (3.35) is a dimensionless measure for the quality of an N-atom system to act as a cavity for light. As an illustrative example, we determine Q for a single atom positioned at $\boldsymbol{r} = \boldsymbol{0}$. Expression (3.35) depends on the bounding volume S; a natural choice for S in the case of a single atom is a sphere with center $\boldsymbol{r} = \boldsymbol{0}$ with an infinitesimally small radius. We then obtain, using (3.10), (3.21), (3.29) and (3.31)-(3.35):

$$\lim_{S\to 0} Q(\omega, \mathbf{1}_k, \boldsymbol{\epsilon}_k, S) = \frac{6\pi}{\alpha^B}\frac{c^3}{\omega^3}, \tag{3.36}$$

where α^B is the atom's bare polarizability (3.21). Remarkably, the Q factor of a single two-level atom does not depend on the wave vector or polarization of the incident field: while the energy stored in the atom and the rate at which the atom radiates may vary with the incident field, the ratio of both quantities remains constant and is given by (3.36).

3.3.2 Connection between Q and the local density of states

The Q factor (3.35) defined above is a measure for the time light spends in the scattering system of interest. We focus on scattering systems consisting of a collection of atoms, but the above definition is applicable to a wide range of cavities. In the definition of Q, we considered the cavity to be probed by an incident field. In many experimental situations, however, one is interested in the interaction of the cavity and a localized emitter. For example, as an experimental realization of such system we consider an excited quantum dot positioned in a photonic crystal cavity [116]. The interaction of an emitter with the surrounding cavity is quantified by the local density of states [36] at the emitter's position. We now proceed to show that the local density of states in a cavity is intimately connected to the cavity's Q factor defined above.

The local density of states $\rho(\omega, \boldsymbol{r})$ can be written as the angle-averaged energy density at position $\boldsymbol{r}$ [66]:

$$\rho(\omega, \boldsymbol{r}) \equiv \frac{\omega^2}{\pi^2 c^3}\left\langle \boldsymbol{E}^*_{\mathbf{1}_k,\boldsymbol{\epsilon}_k}(\omega, \boldsymbol{r}) \cdot \overleftrightarrow{\varepsilon}(\omega, \boldsymbol{r}) \cdot \boldsymbol{E}_{\mathbf{1}_k,\boldsymbol{\epsilon}_k}(\omega, \boldsymbol{r})\right\rangle_{4\pi}, \tag{3.37}$$

or, explicitly,

$$\rho(\omega, \boldsymbol{r}) = \frac{\omega^2}{\pi^2 c^3}\frac{1}{4\pi}\sum_{\boldsymbol{\epsilon}_k}\int_{4\pi} d\Omega_k \boldsymbol{E}^*_{\mathbf{1}_k,\boldsymbol{\epsilon}_k}(\omega, \boldsymbol{r}) \cdot \overleftrightarrow{\varepsilon}(\omega, \boldsymbol{r}) \cdot \boldsymbol{E}_{\mathbf{1}_k,\boldsymbol{\epsilon}_k}(\omega, \boldsymbol{r}), \tag{3.38}$$

where we used the standard notation $\boldsymbol{dk} = k^2 dk d\Omega_k$. In the absence of any scatterers, we obtain the free-space value

$$\rho_0(\omega, \boldsymbol{r}) = \frac{\omega^2}{\pi^2 c^3} \equiv \rho_0(\omega). \tag{3.39}$$

Combining expressions (3.31), (3.35) and (3.38) yields the interesting result

$$\int_S \boldsymbol{dr} \left[\frac{\rho(\omega, \boldsymbol{r})}{\rho_0(\omega)} - 1 \right] = \frac{1}{\omega/c} \left\langle Q(\omega, \mathbf{1}_k, \boldsymbol{\epsilon}_k, S) \sigma_{sca}(\omega, \mathbf{1}_k, \boldsymbol{\epsilon}_k) \right\rangle_{4\pi}, \tag{3.40}$$

expressing that the increase in local density of states with respect to its free-space value, averaged over the volume of the cavity, equals the angle-averaged Q factor providing the latter is weighed with the cross-section. A direct consequence of expression (3.40) is that altering the Q factor of a cavity for a set of incident-field directions has nontrivial implications on the local density of states in the cavity. Experimentally, this implies that the coupling of an emitter and the cavity by which it is surrounded can in general not be optimized by a simple optimization of the cavity's Q factor for one (or a few) incident-field directions.

3.3.3 Practical applicability of Q in N-atom systems

The Q factor (3.35) is a useful dimensionless quantity which can predict the quality of many practical types of cavities in terms of their ability to trap light. Unfortunately, the usefulness of the Q factor in the description of N-atom systems in the presence of gain is rather limited if the dimensions of the atomic system are of the order of the wavelength λ_{ca}. The reasons behind this limitation are twofold. First, the presence of an extra (gain) atom in the vicinity of an N-atom system with an associated Q factor $Q(N)$ generally distorts the N-atom system (especially if the atoms are identical, which is the case we focus on). The dipole-dipole coupling between the atoms causes the system of $(N+1)$ atoms to behave drastically differently from the N atoms that originally made up the cavity. Consequently, the Q factor of the N atoms $Q(N)$ contains little to no information about the $(N+1)$-atom system. In other words, if we follow the definitions of [111] and define the "cold cavity" as "the cavity in the absence of gain material" and the "hot cavity" as "the cavity in the presence of gain material", we find that no straightforward relation exists between the properties of the cold (N-atom) cavity and the hot ($(N+1)$-atom) cavity, even in the absence of gain. Obviously, the distortion of $Q(N)$ due to the addition of an extra atom decreases as N increases but for the small values of N of interest the distortion is significant. The second cause which limits the value of definition (3.35) in the description of N-atom systems with gain, is the effect of saturation and mode mixing induced by the gain atom. If one considers the cavity to consist of $(N+1)$ atoms — N passive atoms and an extra gain atom — the aforementioned

dipole-dipole induced distortion of the Q factor vanishes and a well-defined Q factor is associated with the system. However, even then the usefulness of such Q factor associated with the $(N+1)$-atom system is restricted: as we will show in chapter 5, the introduction of gain alters the eigenmodes of the system, analogous to, e.g., the occurrence of frequency-pulling in macroscopic lasers. However, the information contained in the passive-cavity Q sheds little light on the system behavior in the presence of gain, since the gain-induced changes in an N-atom system can in general not be treated perturbatively.

We can summarize this section by concluding that we defined a general expression for the Q factor of a scattering system. The Q factor is a measure for the time an incident probe beam spends inside the system, and is intimately related to the local density of states through expression (3.40). In the N-atom systems we focus on, the concept of a quality factor has limited use in the presence of gain; we therefore focus back on the general concepts of light scattering and proceed to describe gain within the single-frequency multiple-scattering formalism of section 3.2.

3.4 Gain and the emergence of a threshold

We retake the situation considered in section 3.2 and consider a system of N atoms, irradiated by an incident probe field $\boldsymbol{E}_e(\omega, \boldsymbol{r})$. In particular, we focus on the case $N = 2$ since this is the smallest value of N which allows for optical feedback (note that the case $N = 1$ has been extensively elaborated on in the previous chapter). The question we wish to address here is whether the presence of gain allows for the existence of bound modes; in other words, we look for the conditions under which gain causes the buildup of a nonzero electric field in the limit of a vanishing incident probe field.

The total field $\boldsymbol{E}(\omega, \boldsymbol{r})$ in the absence of an incident field is given by the Lippmann-Schwinger relation (3.8)

$$|\boldsymbol{E}(\omega)\rangle = \overleftrightarrow{\hat{G}}_0(\omega)\overleftrightarrow{\hat{V}}(\omega)|\boldsymbol{E}(\omega)\rangle, \tag{3.41}$$

which can be rewritten, using definition (3.11), as

$$\overleftrightarrow{\hat{V}}(\omega)\overleftrightarrow{\hat{T}}^{-1}(\omega)|\boldsymbol{E}(\omega)\rangle = 0. \tag{3.42}$$

The potential $\overleftrightarrow{\hat{V}}(\omega)$ has no zeros associated with it, as can be deduced from (3.15) and (3.20). Equation (3.42) therefore implies that the bound modes of the system correspond to the poles of the T-matrix. From the T-matrix definition (3.27), we then observe that a bound mode exist if the threshold condition

$$\det\left[\Lambda(\omega)^{-1}\right] = 0 \tag{3.43}$$

is fulfilled. The set of equations (3.42) and (3.43) allows for the determination of the nonzero total field $\boldsymbol{E}(\omega, \boldsymbol{r})$ in the limit of vanishing incident field. The requirements for the threshold condition (3.43) to be satisfied are in general nontrivial; we now focus on the conditions under which (3.43) is fulfilled for $N = 2$. Written explicitly, we can rewrite (3.43) as

$$t_1(\omega)t_2(\omega)\left[\boldsymbol{\mu}_{ac}^{(1)} \cdot \overleftrightarrow{G}_0(\omega, \boldsymbol{r}_1, \boldsymbol{r}_2) \cdot \boldsymbol{\mu}_{ac}^{(2)}\right]^2 = 1 \tag{3.44}$$

The Green function in coordinate space can be written as [31]

$$\overleftrightarrow{G}_0(\omega, \boldsymbol{r}, \boldsymbol{r}') = -\left(\overleftrightarrow{I} + \frac{1}{k^2}\boldsymbol{\nabla} \otimes \boldsymbol{\nabla}\right)\frac{e^{ik|\boldsymbol{r}-\boldsymbol{r}'|}}{4\pi\,|\boldsymbol{r}-\boldsymbol{r}'|} \equiv \overleftrightarrow{G}_0(\omega, \boldsymbol{r}-\boldsymbol{r}'), \tag{3.45}$$

with the standard notations $k = \omega/c$ and $\boldsymbol{\nabla} \otimes \boldsymbol{\nabla} \equiv \boldsymbol{\nabla}^2\overleftrightarrow{I} + \boldsymbol{\nabla} \times \boldsymbol{\nabla}\times$. By performing the partial derivatives in (3.44) explicitly, we can further evaluate the Green function as

$$\overleftrightarrow{G}_0(\omega, \boldsymbol{r}) = -\frac{e^{ikr}}{4\pi r}\left[P(ikr)\overleftrightarrow{I} + \frac{1}{r^2}Q(ikr)\boldsymbol{r} \otimes \boldsymbol{r}\right] + \frac{\delta(\boldsymbol{r})}{3k^2}\overleftrightarrow{I}, \tag{3.46}$$

with $r \equiv |\boldsymbol{r}|$ and

$$P(z) \equiv (1 - \frac{1}{z} + \frac{1}{z^2}), \quad Q(z) \equiv \left(-1 + \frac{3}{z} - \frac{3}{z^2}\right). \tag{3.47}$$

Condition (3.44) can be written in terms of $\{t_i(\omega), \boldsymbol{r}_i, \boldsymbol{\mu}_{ac}^{(i)} | i = 1, 2\}$ and hence depends on the specific choice of the T-matrix elements $t_1(\omega)$ and $t_2(\omega)$. As mentioned above, we focus on atoms of the three-level type *abc*, shown in Figure 2.1. The corresponding T-matrix elements are given by expression (2.29). Since we chose the atoms to have an identical internal structure, they can only differ by the orientation of their transition dipole moment and the rate at which they are pumped.

If none of the atoms is pumped, condition (3.44) can never be fulfilled. The physical motivation for this mathematical impossibility lies within the need for energy conservation: if no external probe field is present and no pump field is applied, no total field can build up.

If only one of the atoms is pumped, the T-matrix of the pumped atom changes sign, as was demonstrated in the previous chapter. This effect of the pump field on the T-matrix of the gain atom has the remarkable consequence that condition (3.44) can be satisfied. In other words, if one atom is pumped in the two-atom system under consideration, equation (3.44) represents a real-valued curve

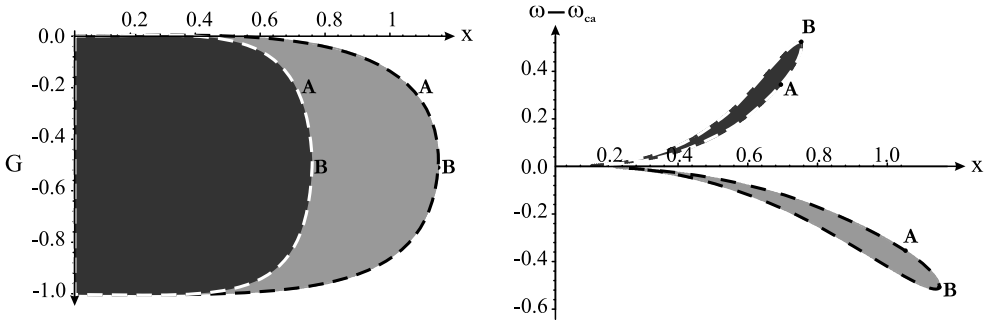

(a) (b)

Figure 3.1: A graphical representation of condition (3.44) for $\boldsymbol{\mu}_{ac}^{(1)} \parallel \boldsymbol{\mu}_{ac}^{(2)}$. The resulting curve connects the detuning $\omega - \omega_{ca}$ (in units of $\Gamma_{ca}/2$), the separation $x \equiv r_{12}\omega_{ca}/c$ between the atoms and the pump field intensity $G \equiv (1-W)/(1+W)$. The curve is projected onto the (a) (x, G) plane and the (b) $(x, \omega - \omega_{ca})$ plane. The white dashed curve represents the case $\boldsymbol{\mu}_{ac}^{(1)}, \boldsymbol{\mu}_{ac}^{(2)} \perp \boldsymbol{r}_1 - \boldsymbol{r}_2$. The black dashed curve represents the case $\boldsymbol{\mu}_{ac}^{(1)}, \boldsymbol{\mu}_{ac}^{(2)} \parallel \boldsymbol{r}_1 - \boldsymbol{r}_2$. The letters "A" and "B" each denote points in the projected planes which correspond to one set of parameters on the curve. The shaded areas represent the regime where the T-matrix formalism predicts the buildup of an electric field in the absence of an incident field.

in the $(\omega, W, \boldsymbol{r}_{12}, \boldsymbol{\mu}_{ac}^{(1)}, \boldsymbol{\mu}_{ac}^{(2)})$ parameter space, where W is the dimensionless pump intensity defined in (2.20) and where we used the standard shorthand notation $r_{12} \equiv |\boldsymbol{r}_{12}| \equiv |\boldsymbol{r}_1 - \boldsymbol{r}_2|$. As an illustrative example, Figure 3.1 shows a graphical representation of the above curve for the case of parallel dipole moments $\boldsymbol{\mu}_{ac}^{(1)} \parallel \boldsymbol{\mu}_{ac}^{(2)}$. This curve connects the detuning $(\omega - \omega_{ca})$, the atomic separation $x \equiv r_{12}\omega_{ca}/c$ and the pump parameter

$$G \equiv (1-W)/(1+W), \quad -1 < G \leq 1. \tag{3.48}$$

Figure 3.1 illustrates that, quite extraordinarily, the single-frequency multiple light-scattering formalism presented above allows for the existence of a threshold in a two-atom system with gain. The threshold condition defines a critical atomic separation and a critical pumping intensity. The existence of these critical values confirms the physical intuition that a threshold can only exist if the feedback is large enough (imposing a maximum value on the atomic separation) and the gain is sufficient (imposing a minimum value on the applied pump intensity). Figure 3.1 further illustrates that condition (3.44) cannot be satisfied for arbitrarily large values of the applied pump power; this behavior at large values of W is a direct consequence of the power broadening effect discussed in section 2.4.

Finally, we conclude this discussion by considering a system of two equally pumped atoms. In that case, the pump will change the sign of the T-matrix el-

ements of both atoms. Consequently, the threshold condition (3.44) can no longer be fulfilled. In other words, a two-atom system with gain does not allow for a threshold if both atoms are equally pumped. The physical motivation behind this observation lies within the role of the passive atom (which is absent in this particular case). In the two-atom system under consideration (or, in general, in any N-atom system with gain), the passive subsystem acts as a cavity for the light emitted by the gain atom. The passive atom is able to store and re-emit the excitations produced by the gain atom which in turn can generate stimulated emission; this storage process is not possible if both atoms are pumped. We will elaborate in more detail on the role of the passive atoms in terms of excitation storage in chapters 5 and 6.

The above discussion can be easily extended to the case $N > 2$ by evaluating the threshold condition (3.44). The details of the resulting threshold depend on N, but we find as a general trend an increase of N leads to an increase of the critical average interatomic distance; this behavior can be attributed to the larger optical feedback in systems with larger atom numbers.

As a closing comment, we briefly elaborate on the physical reality of the above results. The formalism used sofar is based on single-frequency multiple scattering of light. The existence of a threshold within the presented framework for atom numbers as small as $N = 2$ is a nice illustration of the highly nontrivial behavior of atomic systems with gain. However, the threshold predictions presented above are approximative due to the single-frequency character of the applied scattering formalism. In the next section, we elaborate on the approximative nature of the above framework and discuss the validity of the presented results.

3.5 The effect of incoherent radiation

We reconsider the two-atom system with gain discussed above, consisting of two identical atoms of which one is pumped. If the passive atom were absent, the dipole radiation emitted by the system would correspond to a Lorentz spectrum with spectral width $\Gamma_{ca}(1 + W)$, as discussed in section 2.4. In other words, the gain atom emits radiation not only at its resonance frequency ω_{ca}, but in a broad frequency range around ω_{ca}. If a passive atom is positioned in the vicinity of the gain atom, the radiation emitted by the latter will interact with the first. The interaction of the passive atom with off-resonant light can be quantified by the atom's cross-section (2.33) and obeys a Lorentzian distribution with a spectral width Γ_{ca}. Hence, while the emission spectrum of a single gain atom is Lorentzian with a width $\Gamma_{ca}(1+W)$, the absorption spectrum of a single passive atom is Lorentzian with a width Γ_{ca}. The spectral overlap of both Lorentzians is, except for very large values of W, significant; therefore, one intuitively expects the contribution of off-resonant light in the interaction of both atoms to be important and quantitatively alter the results presented above. In the next chapter, we will prove this intuition to be correct, and show that the interaction of both atoms can be quantified by the *overlap integral* of both aforementioned spectra.

3.6 Summary

The aim of this chapter was to study the light-scattering properties of a system of N atoms in free space with gain. The atoms are described within the framework of a single-frequency multiple light-scattering formalism.

In the absence of an external pump mechanism, we can associate a well-defined Q factor with the system; the Q factor is a measure for the quality of the atomic system to act as a cavity for light. Interestingly, we demonstrated the Q factor to be closely connected to the local density of states.

If one of the atoms is pumped, the system exhibits threshold behavior for atom numbers as small as $N = 2$. We can associate a critical average atomic separation and a critical pumping intensity with the system; the presence of these critical values can be interpreted in terms of optical feedback. Furthermore, we showed that power broadening imposes a restriction on the maximum value of the applied pump intensity if the system exhibits a threshold. In addition, we demonstrated that the threshold behavior vanishes if both atoms are pumped, which we interpreted in terms of the system's storage capacity.

Finally, we commented on the approximative nature of the single-frequency character of the applied formalism which leads to the possibility of a threshold. In the next chapters, we proceed beyond the limitations of this single-frequency formalism and include off-resonant interactions. We will show that the N-atom systems under consideration never exhibit a discontinuous threshold; however, a detailed study will reveal that the conclusions drawn above are indicative of the system's crossover from a regime governed by spontaneous emission to a regime where stimulated emission is essential. The qualitative validity of the predictions of the T-matrix formalism is a nice illustration of the formalism's value and ability to provide intuitive physical insight at a moderate mathematical cost.

CHAPTER 4

Multiple scattering of incoherent light

We provide a fully analytical description of a two-level atom interacting with a broadband light field. The problem we present is a typical example of a physical situation which occurs very commonly in practice, but is not straightforwardly solvable. However, we show in this chapter that, remarkably, only a limited number of elementary calculations are required to treat the problem. The presented results are not only highly intuitive, but also allow us to study the nontrivial nonlinear response of a two-level atom to incident spontaneous emission. In addition, our results allow for a first-order estimation of the saturation of a passive two-level atom in the vicinity of an incoherently pumped atom, extending the formalism presented in chapter 3.

4.1 Introduction

The interaction of a two-level atom and a monochromatic field has always been a very popular topic in quantum physics. The attraction of this system is owe to the relatively modest mathematical tools needed to describe the problem, combined with a rich physical behavior, able to accurately predict many interesting phenomena such as superradiance [1, 5, 33, 35, 50, 98] or the Mollow triplet [85].

The effect of an incident field on an atom's dynamics is classically described by the optical Bloch equations [12, 107]. This set of equations allows one to obtain expressions for the average atomic level populations and coherences in the presence of an incident field. If the incident light is monochromatic, the optical Bloch equations are easily dealt with. For non-monochromatic (henceforth referred to as

broadband) incident light, however, solving the optical Bloch equations is in general a far from trivial but physically very relevant matter due to the common appearance of broadband fields in practical situations [2, 14, 26, 38, 41, 43, 61, 91, 131–133].

In this chapter, we show how to transparently describe the interaction of a two-level atom and a broadband incident wave. Our presentation is based on a multiple-scattering approach, in contrast to relevant work on, e.g., chaotic fields [134]. An everyday (and practically important) example of a broadband field is the field of spontaneous fluorescent photons emitted by an atom. The spectrum corresponding to fluorescence has a Lorentzian frequency distribution, and is therefore broadband. Obviously, we intuitively expect that if the spectrum of the incident field is far detuned from to the resonance frequency of the atom, or very broad compared to the atom's natural line width, no significant interaction will take place. Likewise, if the incident field has a very narrow frequency distribution, we expect that the interaction will resemble the one induced by a monochromatic incident wave. In this chapter, we show that only a few elementary calculations are required to quantify the interaction of such a broadband field and a two-level atom. We find that not just the incident spectrum itself, but in addition the overlap of the incident spectrum and the natural Lorentzian emission line of the atom itself determines the interaction strength.

In order to simplify the calculations, we will impose a very general restriction on the incident field. More precisely, we consider in this chapter the class of statistically stationary incident fields. The mathematical simplifications these fields allow for, and the fact that many fields encountered in practice are statistically stationary, is the reason why they are treated in so many textbooks on, e.g., quantum optics or magnetic resonance. An important property of statistically stationary fields is that two-time averages $\langle E(t)E(t')\rangle$ of the field $E(t)$ only depend on the time difference $t - t'$, which implies that field components at different frequencies are uncorrelated [65].

In addition, we will apply a standard approximation to the evolution of the atom itself: we will average out the contribution of rapidly oscillating non-resonant terms. For a monochromatic incident wave, for example, this approximation simply implies that all components oscillating at twice the incident wave frequency are neglected. For a monochromatic incident wave, this approximation is referred to in the literature as the Rotating Wave Approximation (RWA) and was applied as such in chapter 2. Since we deal in this chapter with fields which are in general broadband, we will extend the standard approximation found in textbooks, and refer to the extension as the Generalized Rotating Wave Approximation (GRWA).

In the following, we will start in section 4.2 by formulating the optical Bloch equations for a two-level atom interacting with a general broadband field. A Fourier transform will lead to a better understanding of the behavior of the system in frequency space. Application of the GRWA will return steady-state solutions for the optical Bloch equations. In section 4.3 we demonstrate that our results can be applied to describe spontaneous emission. Moreover, we show our general solution reduces to the well-known monochromatic limit found in literature if the spectral width of the broadband field decreases to zero. We then show in section 4.4 that

our results can be straightforwardly used to determine the T-matrix of an atom irradiated by a broadband field. As an important application of the above results, we present in section 4.5 a first-order estimation of the saturation of a passive two-level atom in the vicinity of an incoherently pumped atom, thereby extending the formalism presented in chapter 3.

4.2 The optical Bloch equations

We consider a two-level atom ac with lower level a and upper level c, separated by an energy difference $\hbar\omega_{ca}$; the corresponding atomic Hamiltonian is given by

$$\hat{H}_c \equiv \hbar\omega_{ca}\hat{S}^+_{ac}\hat{S}^-_{ac}, \tag{4.1}$$

where the operators $\hat{S}^+_{ac}$ and $\hat{S}^-_{ac}$ respectively raise and lower the atomic state. The atom in its excited state can decay radiatively to its lower level at a rate Γ_{ca}. In connection with the atomic systems used in previous chapters, we can regard the atom as the three-level atom abc introduced in section 2.2 in the absence of a pump: it is clear from Figure 2.1 and the Master equation (2.13) that the highest lying level b does not participate in the atomic dynamics if the pump intensity is zero, and the atom reduces to a two-level ac system. The atom interacts with an incident time-dependent real-valued field $\boldsymbol{E}_e(t)$ through the interaction Hamiltonian

$$\hat{\tilde{V}}_{AE}(t) \equiv \hbar\Omega_e(t)(\hat{S}^+_{ac} + \hat{S}^-_{ac}). \tag{4.2}$$

The Rabi frequency $\Omega_e(t) \equiv -\frac{1}{\hbar}\boldsymbol{d}_{ac}\cdot\boldsymbol{E}_e(t)$ quantifies the interaction strength between the atom and the incident field, with $\boldsymbol{d}_{ac}$ the ac transition dipole moment. Similar to the general description of chapter 2, the system dynamics can be described in terms of a density matrix $\hat{\sigma}(t)$ which evolves according to the Master equation

$$\begin{aligned}\frac{d}{dt}\hat{\sigma} &= \hat{\mathcal{L}}\hat{\sigma} \\ &\equiv \hat{\mathcal{L}}_{nd}\hat{\sigma} + \hat{\mathcal{L}}_d\hat{\sigma}.\end{aligned} \tag{4.3}$$

The non-dissipative part of the Lindblad operator can now be written as

$$\hat{\mathcal{L}}_{nd}\hat{\sigma} \equiv -\frac{i}{\hbar}[\hat{H}_c + \hat{\tilde{V}}_{AE}, \hat{\sigma}], \tag{4.4}$$

and the dissipative part as

$$\hat{\mathcal{L}}_d\hat{\sigma} \equiv -\frac{\Gamma_{ca}}{2}\left(\hat{S}^+_{ac}\hat{S}^-_{ac}\hat{\sigma} + \hat{\sigma}\hat{S}^+_{ac}\hat{S}^-_{ac}\right) + \Gamma_{ca}\hat{S}^-_{ac}\hat{\sigma}\hat{S}^+_{ac}. \tag{4.5}$$

Using (4.4) and (4.5), we can expand the Master equation (4.3) in terms of density matrix elements $\sigma_{ij} \equiv \langle i|\,\hat{\sigma}\,|j\rangle$ as

$$\dot{\sigma}_{cc} = +i\Omega_e(t)\left(\sigma_{ca} - \sigma_{ac}\right) - \Gamma_{ca}\sigma_{cc}, \tag{4.6a}$$
$$\dot{\sigma}_{aa} = -i\Omega_e(t)\left(\sigma_{ca} - \sigma_{ac}\right) + \Gamma_{ca}\sigma_{cc}, \tag{4.6b}$$
$$\dot{\sigma}_{ac} = -i\Omega_e(t)\left(\sigma_{cc} - \sigma_{aa}\right) + i\omega_{ca}\sigma_{ac} - \frac{\Gamma_{ca}}{2}\sigma_{ac}, \tag{4.6c}$$
$$\dot{\sigma}_{ca} = +i\Omega_e(t)\left(\sigma_{cc} - \sigma_{aa}\right) - i\omega_{ca}\sigma_{ca} - \frac{\Gamma_{ca}}{2}\sigma_{ca}. \tag{4.6d}$$

Equations (4.6) can be found in many elementary books on quantum optics [30], and are often referred to as the *optical Bloch equations*. The matrix elements $\sigma_{aa}(t)$ and $\sigma_{cc}(t)$ are the ensemble-averaged populations of the lower and upper atomic level, respectively. They are related by $\sigma_{aa}(t) + \sigma_{cc}(t) = 1$, expressing conservation of population. The off-diagonal elements are related to the dipole moment induced by the incident field; we will elaborate more on the atom's transition dipole moment in section 4.4. The Rabi frequency $\Omega_e(t)$ is real-valued and time dependent; in the conventional case of a monochromatic incident wave $\boldsymbol{E}_e(t) \equiv \boldsymbol{E}_0\cos\omega_0 t$ which is often found in the literature, the definition $\Omega_e \equiv -\frac{1}{\hbar}\boldsymbol{d}_{ac}\cdot\boldsymbol{E}_0$ is mostly used, explicitly removing the oscillatory time dependence of the field from the Rabi frequency (obviously, the optical Bloch equations then contain extra factors $e^{\pm i\omega_0 t}$ and the interaction Hamiltonian (4.2) reduces to (2.8)). However, we will see that for a more general time dependence, as the one we deal with here, it is beneficial to use our definition and consider an explicit time-dependent atom-field coupling (and continue henceforth to denote the coupling by the term Rabi frequency).

Our aim in this section is to derive steady-state solutions for equations (4.6). The statistical properties of the field are especially advantageous in the frequency domain, since if the two-time average $\langle\Omega_e(t)\Omega_e(t+\tau)\rangle$ of the real-valued field $\Omega_e(t)$ only depends on τ, one can deduce (see, e.g., [65, 79]) that in the frequency domain

$$\langle\Omega_e(\omega)\Omega_e(\omega')\rangle = J_e(\omega)\delta(\omega+\omega'), \tag{4.7}$$

where the Fourier transform of $\Omega_e(t)$ is defined as

$$\Omega_e(\omega) \equiv \frac{1}{2\pi}\int_{-\infty}^{+\infty}\Omega_e(t)e^{-i\omega t}dt, \tag{4.8a}$$
$$\Omega_e(t) = \int_{-\infty}^{+\infty}\Omega_e(\omega)e^{i\omega t}d\omega, \tag{4.8b}$$

and $J_e(\omega)$ is the spectral density function of the incident radiation. We will see that the appearance of a delta function in (4.7) will highly facilitate the calculations further on. In what follows, we will Fourier transform the optical Bloch equations. We therefore define the population difference $\Delta\pi(t)$ and its Fourier transform $\Delta\pi(\omega)$ as

$$\Delta\pi(t) \equiv \sigma_{cc}(t) - \sigma_{aa}(t) \equiv \int_{-\infty}^{+\infty} \Delta\pi(\omega) e^{-i\omega t} dt. \tag{4.9}$$

In the spirit of the Rotating Wave Approximation, the coherences

$$\sigma_{ac}(t) \equiv \int_{-\infty}^{+\infty} \sigma_{ac}(\omega) e^{i\omega t} d\omega, \tag{4.10a}$$

$$\sigma_{ca}(t) \equiv \int_{-\infty}^{+\infty} \sigma_{ca}(\omega) e^{i\omega t} d\omega, \tag{4.10b}$$

can be approximated by

$$\sigma_{ac}(t) \approx \int_{0}^{+\infty} \sigma_{ac}(\omega) e^{i\omega t} d\omega, \tag{4.11a}$$

$$\sigma_{ca}(t) \approx \int_{-\infty}^{0} \sigma_{ca}(\omega) e^{i\omega t} d\omega, \tag{4.11b}$$

where the contribution of the non-resonating part of the coherences has been omitted. The restriction of the integration interval in expressions (4.11) has the simple meaning that quickly oscillating terms are not taken into account, as mentioned in the introduction of this chapter. This approximation is a straightforward generalization of the Rotating Wave Approximation as applied in chapter 2 (in which case $\sigma_{ca}(t) = \sigma_{ac}^*(t) = \sigma_{ca}(0)e^{-i\omega_0 t}$ with ω_0 the frequency of the incident field). We refer to the extension (4.11) as the *Generalized Rotating Wave Approximation*. This approximation is justified if $J_e(\omega)$ is only appreciably different from zero near the atomic resonance.

If we now split the Fourier transform $\Omega_e(\omega)$ of the Rabi frequency $\Omega_e(t)$ into a positive- and a negative-frequency part

$$\begin{aligned} \Omega_e(t) &= \int_{0}^{+\infty} \Omega_e(\omega) e^{i\omega t} d\omega + \int_{-\infty}^{0} \Omega_e(\omega) e^{i\omega t} d\omega \\ &\equiv \Omega_e^+(t) + \Omega_e^-(t), \end{aligned} \tag{4.12}$$

we see that neglecting all highly non-resonant terms in (4.6) results in slightly

altered optical Bloch equations:

$$\dot{\sigma}_{cc} = +i\Omega_e^+(t)\sigma_{ca} - i\Omega_e^-(t)\sigma_{ac} - \Gamma_{ca}\sigma_{cc}, \tag{4.13a}$$
$$\dot{\sigma}_{aa} = -i\Omega_e^+(t)\sigma_{ca} + i\Omega_e^-(t)\sigma_{ac} + \Gamma_{ca}\sigma_{cc}, \tag{4.13b}$$
$$\dot{\sigma}_{ac} = -i\Omega_e^+(t)\left(\sigma_{cc} - \sigma_{aa}\right) + i\omega_{ca}\sigma_{ac} - \frac{\Gamma_{ca}}{2}\sigma_{ac}, \tag{4.13c}$$
$$\dot{\sigma}_{ca} = +i\Omega_e^-(t)\left(\sigma_{cc} - \sigma_{aa}\right) - i\omega_{ca}\sigma_{ca} - \frac{\Gamma_{ca}}{2}\sigma_{ca}. \tag{4.13d}$$

The proper combination of rotating and counter-rotating terms ensure that equations (4.13) are far simpler to deal with than the original Bloch equations (4.6), as we will show now. Fourier transforming equation (4.13a) and (4.13b) gives

$$\begin{aligned}(\Gamma_{ca} + i\omega)\Delta\pi(\omega) = &+2i\int_0^{+\infty}\Omega_e(\omega')\sigma_{ca}(\omega-\omega')d\omega' \\ &- 2i\int_{-\infty}^{0}\Omega_e(\omega')\sigma_{ac}(\omega-\omega')d\omega' - \Gamma_{ca}\delta(\omega).\end{aligned} \tag{4.14}$$

Fourier transforming (4.13c) and (4.13d), on the other hand, gives

$$(i\omega - i\omega_{ca} + \frac{\Gamma_{ca}}{2})\sigma_{ac}(\omega) = -i\int_0^{+\infty}\Omega_e(\omega'')\Delta\pi(\omega-\omega'')d\omega'', \tag{4.15a}$$
$$(i\omega + i\omega_{ca} + \frac{\Gamma_{ca}}{2})\sigma_{ca}(\omega) = +i\int_{-\infty}^{0}\Omega_e(\omega'')\Delta\pi(\omega-\omega'')d\omega''. \tag{4.15b}$$

If we now substitute the previous expressions in (4.14), we find

$$\begin{aligned}&(\Gamma_{ca} + i\omega)\Delta\pi(\omega) + \Gamma_{ca}\delta(\omega) = \\ &= -2\int_0^{+\infty}d\omega'\int_{-\infty}^{0}d\omega''\Omega_e(\omega')\Omega_e(\omega'')\Delta\pi(\omega-\omega'-\omega'')\times \\ &\left(\frac{1}{i\omega - i\omega' + i\omega_{ca} + \frac{\Gamma_{ca}}{2}} + \frac{1}{i\omega - i\omega'' - i\omega_{ca} + \frac{\Gamma_{ca}}{2}}\right),\end{aligned} \tag{4.16}$$

which is a self-consistent equation in the population difference. In steady-state, we can write

$$\Delta\pi(\omega) = \Delta\pi(\omega=0)\delta(\omega), \tag{4.17}$$

which is appropriate since we are interested in the regime for which the populations are time-independent. Substitution of (4.17) in (4.16) and phase-averaging yields

$$\Gamma_{ca}\Delta\pi(\omega=0)+\Gamma_{ca}=-2\Delta\pi(\omega=0)\int_0^{+\infty}d\omega' J_e(\omega')\frac{\Gamma_{ca}}{(\omega'-\omega_{ca})^2+(\frac{\Gamma_{ca}}{2})^2}, \quad (4.18)$$

and therefore

$$\Delta\pi(\omega)=-\frac{1}{1+2\int_0^{+\infty}d\omega' J_e(\omega')\frac{1}{(\omega'-\omega_{ca})^2+(\frac{\Gamma_{ca}}{2})^2}}\delta(\omega). \quad (4.19)$$

We can conclude that in steady-state, we find the desired solution

$$\sigma_{cc}^{st}\equiv 1-\sigma_{aa}^{st}=\frac{1}{2}\frac{S}{S+1}, \quad (4.20a)$$

$$\sigma_{ca}^{st}\equiv(\sigma_{ac}^{st})^*=\frac{1}{S+1}\int_{-\infty}^{0}\frac{i\Omega_e(\omega)}{-i\omega_{ca}-i\omega-\frac{\Gamma_{ca}}{2}}e^{i\omega t}d\omega, \quad (4.20b)$$

with

$$S\equiv 2\int_0^{+\infty}d\omega J_e(\omega)\frac{1}{(\omega_{ca}-\omega)^2+(\frac{\Gamma_{ca}}{2})^2}. \quad (4.21)$$

Expressions (4.20) are the key result of this section. The influence of the spectral properties of the incident field enters the dynamics of the density matrix through a single interaction parameter S. The expression (4.21) for S is surprisingly simple and appealing: it is the overlap integral of the spectral density of the incident field, and the natural Lorentzian emission line of the two-level system itself. The structure of the interaction parameter confirms what we intuitively expect: resonant fields with a narrow distribution interact strongly with the atom, while the interaction with broad, far off-resonance fields is far less pronounced [134]. As examples, we will in the next section focus on two specific and interesting values for the saturation.

4.3 Examples

4.3.1 The coherent limit

As a first demonstration of equations (4.20), we will verify that the well-known expressions for an incident *monochromatic* field can be retrieved from our results. We consider a real-valued monochromatic incident field $\boldsymbol{E}_e(t)\equiv\boldsymbol{E}_0\cos(\omega_0 t)$ with

$\omega_0 > 0$. The corresponding Rabi frequency is

$$\Omega_e(\omega) \equiv \frac{\Omega_0}{2}\left(\delta(\omega-\omega_0)+\delta(\omega+\omega_0)\right), \tag{4.22}$$

therefore

$$\begin{aligned}&\Omega_e(\omega)\Omega_e(-\omega') = \\ &\frac{\Omega_0^2}{4}\Big(\delta(\omega-\omega')\delta(\omega-\omega_0)+\delta(\omega-\omega')\delta(\omega+\omega_0) \\ &\quad+\delta(\omega+\omega')\delta(\omega-\omega_0)+\delta(\omega+\omega')\delta(\omega+\omega_0)\Big).\end{aligned} \tag{4.23}$$

Of the 4 terms appearing in (4.23), only the first remains in the (G)RWA, yielding

$$J_e(\omega) = \frac{\Omega_0^2}{4}\delta(\omega-\omega_0), \tag{4.24}$$

which transforms expressions (4.20) into

$$\sigma_{cc}^{st} = (\frac{\Omega_0}{2})^2 \frac{1}{(\omega_0-\omega_{ca})^2+(\frac{\Gamma_{ca}}{2})^2+\frac{\Omega_0^2}{2}}, \tag{4.25a}$$

$$\sigma_{ca}^{st} = \frac{\Omega_0}{2}e^{-i\omega_0 t}\frac{1}{(\omega_0-\omega_{ca})+i\frac{\Gamma_{ca}}{2}+\frac{1}{2}\frac{\Omega_0^2}{(\omega_0-\omega_{ca})-i\frac{\Gamma_{ca}}{2}}}, \tag{4.25b}$$

which corresponds exactly to the solutions for incident monochromatic fields found in the literature [30], justifying our method. In connection with previous chapters, we note that equations (4.25) can also be readily deduced from the set of differential equations (2.17), (2.18) and the expressions presented in Appendix A in the absence of a pumping field.

4.3.2 Spontaneous emission

As a second demonstration of equations (4.20), we consider the nontrivial case of an atom interacting with incident fluorescence emission centered around $\omega_0 \gg \Gamma_{ca}$. The incident field then has a Lorentzian spectrum with a width $\Gamma_{ca}(1+\kappa)$:

$$J_e(\omega) \equiv \frac{J_{tot}}{\pi}\frac{\frac{\Gamma_{ca}}{2}(1+\kappa)}{(\omega-\omega_0)^2+(\frac{\Gamma_{ca}}{2}(1+\kappa))^2}, \tag{4.26}$$

where the factor

$$J_{tot} \equiv \int_{-\infty}^{\infty} J_e(\omega) d\omega = \left\langle \Omega_e(t)^2 \right\rangle \tag{4.27}$$

is proportional to the total incident field energy. We find as an explicit solution for (4.21):

$$\begin{aligned} S &= 2 \int_0^{+\infty} d\omega J_e(\omega) \frac{1}{(\omega - \omega_{ca})^2 + (\frac{\Gamma_{ca}}{2})^2} \\ &\approx 2 \int_{-\infty}^{+\infty} d\omega \frac{1}{(\omega - \omega_0)^2 + (\frac{\Gamma_{ca}}{2}(1+\kappa))^2} \frac{1}{(\omega - \omega_{ca})^2 + (\frac{\Gamma_{ca}}{2})^2} \times \\ &\quad \frac{J_{tot}}{\pi} \frac{\Gamma_{ca}}{2} (1+\kappa) \\ &= 2 J_{tot} \frac{(2+\kappa)}{(\omega_0 - \omega_{ca})^2 + (\frac{\Gamma_{ca}}{2})^2 (2+\kappa)^2}, \end{aligned} \tag{4.28}$$

where the extension of the integral in (4.28) from 0 to $-\infty$ is justified by $\omega_0 \gg \Gamma_{ca}$. Equation (4.28) clearly shows that the atom-field interaction is weak for spectrally broad or far-detuned fields, as mentioned earlier. As a practical application of the above results, we will in the next section use the result (4.20) with (4.25) and (4.28) obtained here to determine the nonlinear response of an atom to incident broadband light.

4.4 Derivation of T-matrix of a dipole irradiated by broadband light

As was extensively elaborated on in chapters 2 and 3, the key property which quantifies the interaction strength between an atom and an incident light field is the atom's T-matrix, or equivalently, its dynamic polarizability. In the limit of low-intensity incident fields, the atomic response is linear and the induced polarization is proportional to the incident field. However, at higher incident intensities, the response is no longer linear since the atom will exhibit saturation effects, as illustrated by the nonlinear polarizability (2.25). By applying the general procedure presented in section 2.3, we now show how the general results presented above can be straightforwardly used to determine the T-matrix of an atom irradiated by broadband incident light.

We take the general case of an incident field $\boldsymbol{E}_e(t)$ consisting of a monochromatic cosine component with amplitude $\boldsymbol{E}_0$ and frequency ω_0, and a non-monochromatic component $\boldsymbol{E}_L(t)$, with a Lorentzian frequency distribution. The fields $\boldsymbol{E}_e(t)$ thus

obtained define a very general class, containing the special cases of incident monochromatic light, as well as pure incident spontaneous emission. The Lorentzian component of the incident field has a line width $\Gamma_{ca}(1+\kappa)$, $\kappa \geq -1$, centered around $\omega_0 \gg \Gamma_{ca}$:

$$\boldsymbol{E}_e(\omega) = \boldsymbol{E}_0 \frac{1}{2}\left(\delta(\omega+\omega_0) + \delta(\omega-\omega_0)\right) + \boldsymbol{E}_L(\omega). \tag{4.29}$$

The corresponding Rabi frequencies are

$$-\hbar\Omega_0 = \boldsymbol{d}_{ac} \cdot \boldsymbol{E}_0, \tag{4.30a}$$
$$-\hbar\Omega_L(\omega) = \boldsymbol{d}_{ac} \cdot \boldsymbol{E}_L(\omega), \tag{4.30b}$$

obeying

$$\langle \Omega_L(\omega)\Omega_L(\omega')\rangle = J_L(\omega)\delta(\omega+\omega'), \tag{4.31}$$

with $J_L(\omega)$ the spectral density of the incident Lorentzian field (4.26) with $J_{tot} \equiv \left\langle \Omega_L^2(t)\right\rangle$. Equations (4.29)-(4.31) fully describe the incident field. We now focus on the response of the atom to this incident field. Since the dynamic polarizability and the density matrix both describe the response of the atom to incident light, both quantities are related [75]:

$$\varepsilon_0 \overleftrightarrow{\alpha}(\omega) \cdot \boldsymbol{E}_e(\omega) \equiv \boldsymbol{d}_{ac}\sigma_{ca}(-\omega), \quad \omega > 0. \tag{4.32}$$

Relation (4.32) is a straightforward extension of expressions (2.23)-(2.25). The general result (4.20) allows for the dynamic polarizability to be written as

$$\overleftrightarrow{\alpha}(\omega) = -\overleftrightarrow{\alpha}_0 \frac{1}{2} \frac{\omega_{ca}}{\omega - \omega_{ca} + i\frac{\Gamma_{ca}}{2} + \frac{2\widetilde{S}(\omega)}{\omega-\omega_{ca}-i\frac{\Gamma_{ca}}{2}}}, \tag{4.33}$$

with the static polarizability $\overleftrightarrow{\alpha}_0$ defined in (2.27). The corresponding T-matrix of the atom is given by (2.28). The saturation appears in a surprisingly simple way as

$$\widetilde{S}(\omega) \equiv \frac{\Omega_0^2}{4} + \int_0^{+\infty} d\omega' J_L(\omega') \frac{(\omega-\omega_{ca})^2 + (\frac{\Gamma_{ca}}{2})^2}{(\omega'-\omega_{ca})^2 + (\frac{\Gamma_{ca}}{2})^2}. \tag{4.34}$$

Expressions (4.33) and (4.34) fully describe the response of a two-level atom to an

incident field of the general class (4.29). Two limits for the incident field are in particular interesting. First, for $J_L(\omega) \to 0$, the expression for the dynamic polarizability of a two-level atom irradiated by a monochromatic field is recovered, as given by expression (2.25) in the absence of a pump. Secondly, for $\Omega_0 \to 0$, we find the dynamic polarization of an atom irradiated by spontaneous emission only:

$$\overleftrightarrow{\alpha}(\omega) = -\overleftrightarrow{\alpha}_0 \frac{1}{2(S+1)} \frac{\omega_{ca}}{\omega - \omega_{ca} + i\frac{\Gamma_{ca}}{2}}, \tag{4.35}$$

with S given by

$$S = 2\frac{(2+\kappa)}{(\omega_0 - \omega_{ca})^2 + (\frac{\Gamma_{ca}}{2})^2(2+\kappa)^2} \int_{-\infty}^{\infty} d\omega J_L[\omega], \tag{4.36}$$

The saturation of an atom irradiated by spontaneous emission exhibits itself as a decrease of the amplitude of the atom's polarizability. Because of the induced saturation, the atom scatters incident probe light partially inelastically; the atom's albedo is defined as (2.34) and is given by

$$a = \frac{1}{1+S} \leq 1, \tag{4.37}$$

expressing the inelastic character of light scattering by the atom. In the next section, we focus on an important application of expression (4.35): we present a first-order estimation of the saturation of a two-level atom due to the fluorescence emission of a pumped atom in its vicinity.

4.5 Saturation of a passive atom in the vicinity of a pumped atom

In chapter 3, we described the interaction of N passive atoms interacting with a pumped atom in the framework of single-frequency multiple scattering of light. We elaborated on the broadband character of the light emitted by the pumped atom and the limitations of a single-frequency approach in the description of N-atom systems with gain. We now proceed to extend the formalism of chapter 3 and present a first-order estimation of the saturation of a passive atom induced by an incoherently pumped atom in its vicinity; more specifically, we determine how the T-matrix of the first is affected by the presence of the latter.

4.5.1 Estimation of the saturation induced by the pumped atom

In what follows, we focus on the simplest nontrivial case $N = 2$; the system under consideration then consists of two identical atoms in free space. As mentioned ear-

lier in this chapter, we focus on atoms of the *abc*-type, as graphically depicted in Figure 2.1. Following the notation introduced in chapters 2, the transition dipole moments associated with the atoms are denoted $\boldsymbol{d}_{ac}^{(j)} = d_{ac}\boldsymbol{\mu}_{ac}^{(j)}$ with $\boldsymbol{\mu}_{ac}^{(j)}$ the unit vector parallel to $\boldsymbol{d}_{ac}^{(j)}$. One of the atoms is incoherently pumped with associated pumping parameter W. The passive atom is positioned at $\boldsymbol{r}_2$, while the position of the pumped atom defines the origin $\boldsymbol{r}_1 = \boldsymbol{0}$ of the system's coordinate space.

Our aim is to derive an expression for the T-matrix of the passive atom, taking into account the saturation induced by the pumped atom. As we discussed in chapter 2, the light emitted by the pumped atom has a Lorentzian spectral distribution with spectral width $\Gamma_{ca}(1+W)$, W being the pump parameter defined as (2.20). The T-matrix of the passive atom can, according to (4.35) and (2.28), be written as

$$\overleftrightarrow{\hat{T}}(\omega) = t(\omega)\delta(\boldsymbol{r}-\boldsymbol{r}_2)\hat{\mathbb{1}} \otimes \left(\boldsymbol{\mu}_{ac}^{(2)} \otimes \boldsymbol{\mu}_{ac}^{(2)}\right), \tag{4.38}$$

with

$$t(\omega) = \frac{1}{(S+1)}\frac{3\pi}{\omega_{ca}/c}\frac{\Gamma_{ca}}{\left(\omega-\omega_{ca}+i\frac{\Gamma_{ca}}{2}\right)}, \tag{4.39}$$

where "$\otimes$" denotes the direct product of vectors, and where $\hat{\mathbb{1}}$ is a unit operator with matrix elements $\langle \boldsymbol{r}|\hat{\mathbb{1}}|\boldsymbol{r}'\rangle = \delta(\boldsymbol{r}-\boldsymbol{r}')$. The central emission frequency of the gain atom ω_0 is equal to its resonance frequency ω_{ca}. Hence, we can deduce from (4.28) that the saturation in (4.39) induced by the gain atom is quantified by

$$S = 2\left\langle \Omega_1(t)^2 \right\rangle \frac{1}{(2+W)}\frac{1}{(\Gamma_{ca}/2)^2}, \tag{4.40}$$

where the Rabi frequency $\Omega_1(t)$ is defined as

$$\left\langle \Omega_1(t)^2 \right\rangle = \frac{1}{\hbar^2}\left\langle \left| \boldsymbol{d}_{ac}^{(2)} \cdot \boldsymbol{E}_1(t,\boldsymbol{r}_2) \right|^2 \right\rangle, \tag{4.41}$$

with $\boldsymbol{E}_1(t,\boldsymbol{r})$ the field generated by the pumped atom. Expanding the field in its Fourier components yields

$$\left\langle \Omega_1(t)^2 \right\rangle = \frac{d_{ac}^2}{\hbar^2}\left\langle \left| \int_{-\infty}^{+\infty} \boldsymbol{\mu}_{ac}^{(2)} \cdot \boldsymbol{E}_1(\omega,\boldsymbol{r}_2) e^{i\omega t} d\omega \right|^2 \right\rangle. \tag{4.42}$$

We now make the following approximation: we assume that the light scattered by

the passive atom does not influence the photon emission rate of the pumped atom. In other words, we only take scattering events into account which correspond to scattering by the passive atom of a photon emitted by the pumped atom; no subsequent interaction of scattered photons with the gain atom is taken into account. Under the above approximation, the pumped atom acts as a source $\boldsymbol{S}_1(\omega) = S_1(\omega)\boldsymbol{\mu}_{ac}^{(1)}$ and the field it generates is given by

$$\boldsymbol{E}_1(\omega, \boldsymbol{r}) = \overleftrightarrow{G}_0(\omega, \boldsymbol{r}) \cdot \boldsymbol{S}_1(\omega), \tag{4.43}$$

where the Green function $\overleftrightarrow{G}_0(\omega, \boldsymbol{r})$ is introduced in the previous chapter and is defined as (3.45). The statistical character of the spontaneous emission of the pumped atom translates into

$$\langle S_1(\omega) S_1^*(\omega') \rangle \equiv \frac{\widetilde{J}_1}{\pi} \frac{\frac{\Gamma_{ca}}{2}(1+W)}{(\omega - \omega_{ca})^2 + \left(\frac{\Gamma_{ca}}{2}\right)^2 (1+W)^2} \delta(\omega - \omega'), \tag{4.44}$$

where the first factor stems from the Lorentzian distribution of the spectrum and the delta function originates from the extension of (4.7) to complex-valued fields. The previous relation allows us to rewrite (4.42) as

$$\left\langle \Omega_1(t)^2 \right\rangle = \frac{d_{ac}^2}{\hbar^2} \int_{-\infty}^{+\infty} d\omega \frac{\widetilde{J}_1}{\pi} \frac{\Gamma_{ca}}{2} (1+W) \frac{\left| \boldsymbol{\mu}_{ac}^{(1)} \cdot \overleftrightarrow{G}_0(\omega, \boldsymbol{r}_1 - \boldsymbol{r}_2) \cdot \boldsymbol{\mu}_{ac}^{(2)} \right|^2}{(\omega - \omega_{ca})^2 + \left(\frac{\Gamma_{ca}}{2}\right)^2 (1+W)^2}. \tag{4.45}$$

The norm $\widetilde{J}_1$ quantifies the intensity of the pumped atom's emitted radiation; once $\widetilde{J}_1$ is known and the above integral is evaluated, the T-matrix of the passive atom can be deduced from expressions (4.39), (4.40) and (4.45). We now proceed to determine $\widetilde{J}_1$ and evaluate (4.45).

The total time-averaged power emitted by the pumped atom is given by the angle-integrated radial energy flow

$$\langle p(t) \rangle \equiv \left\langle \int_{4\pi} \boldsymbol{P}(t, \boldsymbol{r}) \cdot \mathbf{1}_r r^2 d\Omega \right\rangle \tag{4.46}$$

where $\mathbf{1}_r \equiv \boldsymbol{r}/r$ is the unit vector in the radial direction. The time-averaged Poynting vector $\boldsymbol{P}(t, \boldsymbol{r})$ is defined in Appendix C as

$$\langle \boldsymbol{P}(t, \boldsymbol{r}) \rangle \equiv \frac{1}{2} \left\langle \mathrm{Re}\left[\boldsymbol{E}_1(t, \boldsymbol{r}) \times \boldsymbol{H}_1^*(t, \boldsymbol{r}) \right] \right\rangle, \tag{4.47}$$

with the magnetic field given by

$$\boldsymbol{H}_1(\omega, \boldsymbol{r}) = \frac{1}{i\omega\mu_0} \boldsymbol{\nabla} \times \boldsymbol{E}_1(\omega, \boldsymbol{r}). \tag{4.48}$$

The Poynting vector allows us to reformulate (4.46) as

$$\langle p(t) \rangle = \frac{1}{2} \mathrm{Re} \left[\left\langle \int_{4\pi} (\boldsymbol{E}_1(t, \boldsymbol{r}) \times \boldsymbol{H}_1^*(t, \boldsymbol{r})) \cdot \mathbf{1}_r r^2 d\Omega \right\rangle \right]. \tag{4.49}$$

Insertion of (4.48) in (4.49) and straightforward manipulation yields, using (4.43) and (4.44),

$$\langle p(t) \rangle = \frac{1}{3} \widetilde{J}_1 \frac{c\varepsilon_0}{4\pi}. \tag{4.50}$$

Since the system under consideration has no energy loss channels (except for the Stokes shift $\omega_{ba} - \omega_{ca}$ which we neglect for clarity), the total time-averaged photon absorption rate equals the system's time-averaged photon emission rate. In chapter 5, we will show that the absorbed power is equal to

$$\langle p(t) \rangle \equiv \hbar\omega_{ca} W \Gamma_{ca} \left(\frac{1}{1+W} \right), \tag{4.51}$$

which is intuitively obvious, since the number of absorbed pump photons is proportional to the applied pump power $W\Gamma_{ca}\hbar\omega_{ca}$ and the time-averaged population of the gain atom's lower level $1/(1+W)$, the latter expression being a direct consequence of expression (2.19).

Combining both expressions for the time-averaged emitted power (4.50) and (4.51) allows us to express the saturation term (4.45) as

$$\left\langle \Omega_1(t)^2 \right\rangle = \Gamma_{ca}^2 W \hbar\omega_{ca} \frac{d_{ac}^2}{\hbar^2} \frac{6}{c\varepsilon_0} \int_{-\infty}^{+\infty} d\omega \frac{\left| \boldsymbol{\mu}_{ac}^{(1)} \cdot \overleftrightarrow{G}_0(\omega, \boldsymbol{r}_1 - \boldsymbol{r}_2) \cdot \boldsymbol{\mu}_{ac}^{(2)} \right|^2}{(\omega - \omega_{ca})^2 + \left(\frac{\Gamma_{ca}}{2}\right)^2 (1+W)^2}. \tag{4.52}$$

The integral in (4.53) diverges for $\omega \to 0$ due to the implicitly assumed frequency-independence of the decay rate Γ_{ca}; in a more rigorous treatment, a frequency-dependent decay rate should be introduced (see, e.g., [79]). We can circumvent the above unphysical divergence by considering only the pole at $\omega = \omega_{ca} + i\frac{\Gamma_{ca}}{2}(1+W)$

and neglecting the artificial pole in $\omega = 0$, resulting in

$$\left\langle \Omega_1(t)^2 \right\rangle \approx 36\pi^2 \frac{W}{1+W} \frac{\Gamma_{ca}^2}{(\omega_{ca}/c)^2} \left| \boldsymbol{\mu}_{ac}^{(1)} \cdot \overleftrightarrow{G}_0(\omega_{ca}, \boldsymbol{r}_1 - \boldsymbol{r}_2) \cdot \boldsymbol{\mu}_{ac}^{(2)} \right|^2 . \tag{4.53}$$

In order to derive (4.53), we used the standard high-Q assumption $\omega_{ca} \gg \Gamma_{ca}$ and applied the well-known relation [30]

$$\Gamma_{ca} = \frac{1}{3\pi\varepsilon_0} \frac{\omega_{ca}^3}{\hbar c^3} d_{ac}^2 \tag{4.54}$$

between the dipole moment, the resonance frequency and the decay rate for frequencies near the resonance frequency. We can conclude from (4.40) and (4.53) that the T-matrix element (4.39) is characterized by a saturation

$$S = 2 \left(\frac{12\pi}{\omega_{ca}/c} \right)^2 \frac{W}{(1+W)(2+W)} \left| \boldsymbol{\mu}_{ac}^{(1)} \cdot \overleftrightarrow{G}_0(\omega_{ca}, \boldsymbol{r}_1 - \boldsymbol{r}_2) \cdot \boldsymbol{\mu}_{ac}^{(2)} \right|^2 . \tag{4.55}$$

Expression (4.39) with (4.55) is a first-order estimation of the saturation of a passive atom due to the spontaneous emission of a pumped atom in its vicinity. We now focus on the implications of this saturation on the threshold predictions of chapter 3.

4.5.2 Implications of the saturation induced by the pumped atom

In chapter 3, we showed that the presence of gain in an N-atom system allows for the presence of a threshold within the framework of single-frequency multiple scattering of light. We elaborated on the approximative nature of a single-frequency approach, and hinted at the importance of off-resonant interactions. The T-matrix element (4.39) shows that a first-order correction of the T-matrix of a passive atom in the vicinity of a pumped atom establishes itself as a decrease of the amplitude of the T-matrix by a factor $(S+1)^{-1}$. We now proceed to determine the effect of the above correction on the threshold predictions of chapter 3.

The condition which needs to be fulfilled in a two-atom system in order for the system to exhibit a threshold, is given by (3.44), including the extra saturation factor $(S+1)^{-1}$:

$$\frac{S/2}{(S+1)} \frac{(1-W)(2+W)}{16W} \frac{\Gamma_{ca}}{\left(\omega - \omega_{ca} + i\frac{\Gamma_{ca}}{2}\right)} \frac{\Gamma_{ca}}{\left(\omega - \omega_{ca} + i\frac{\Gamma_{ca}}{2}(1+W)\right)} = 1. \tag{4.56}$$

Importantly, equation (4.56) does *not* have any solutions for real W and ω. This observation stands in sharp contrast to the situation depicted in chapter 3, the latter

leading to a clear threshold as demonstrated by Figure 3.1. In other words, the saturation-induced first-order correction to the T-matrix of a passive atom derived above inhibits the manifestation of a threshold in a two-atom system with gain. This effect demonstrates the importance of the contribution of off-resonant light when describing N-atom systems with gain. The derivation presented above is approximative; we note that extending the above formalism beyond the presented first-order approximation is far from trivial within a T-matrix approach. Therefore, in the next chapter we will reconsider an N-atom system with gain and describe the system using the N-atom Master equation. We will show that, while being computationally much more involved, the Master equation incorporates off-resonant interactions to *all* scattering orders and, in that sense, provides a non-approximative description of an N-atom system with gain.

4.6 Summary

In this chapter, we have solved the optical Bloch equations for a two-level system interacting with a statistically stationary broadband field using the generalized rotating wave approximation. The resulting steady-state density matrix is similar to the situation one obtains with an incident monochromatic field; the difference between both results can be intuitively understood. We have applied the derived results to calculate the response of a two-level atom to a broadband field; the saturation of the response is characterized by the overlap integral of the spectral density of the incident field and the natural Lorentzian emission line of the atom itself. We then used the expression for the atomic T-matrix to determine the effect of off-resonant interactions in the description of few-atom systems with gain. We showed that the contribution of these interactions is significant in a first-order scattering approximation and leads to a vanishing of the threshold predicted in chapter 3. In the next chapter, we proceed beyond the above first-order approximation and present a quantum-mechanical study of N-atom systems with gain, including off-resonant interactions in all scattering orders.

CHAPTER 5

Few-atom systems with gain: a quantum optical approach

Using a density matrix approach, we study the simplest microscopic systems that exhibit both gain and feedback: clusters of 2 to 5 atoms, one of which is pumped. The other atoms supply feedback through multiple scattering of light. We show that, if the atoms are in each other's near-field, the system exhibits large gain narrowing and spectral mode redistribution. The observed phenomena are more pronounced if the feedback is enhanced. The presented few-atom system is the simplest exactly solvable microscopic system which shows the approach to laser oscillation.

5.1 Introduction

In chapter 3, we introduced a few-atom system with gain as the simplest microscopic system displaying both gain and optical feedback. Using the T-matrix of a pumped atom derived in chapter 2, we described clusters of N atoms with gain within the framework of single-frequency multiple scattering of light. We elaborated on the nontrivial implications of the introduction of gain in a multiple-scattering formalism, and showed in chapter 4 that saturation due to off-resonant light is of crucial importance.

In this chapter, we proceed beyond the limitations of the multiple-scattering formalism presented in the previous chapters, and present a study of N-atom systems with gain within a quantum mechanical framework. More precisely, we will derive the Master equation of N atoms in free space, one of which interacts with an external pump field. The advantages of a Master-equation approach are twofold. First,

by considering the system's full Master equation, we ensure that all off-resonant contributions to the saturation of the atoms are taken into account in all scattering orders. Secondly, the Master equation allows for a transparent description of the spectral and statistical properties of the light emitted by the system, in contrast to a multiple-scattering approach.

We start in section 5.2 by deriving the N-atom Master equation. The derivation will be presented in two phases. First, we consider the passive N-atom system and show how its evolution can be described in terms of a density matrix. In a second step, we include the interaction of one of the atoms with an external pump field; we demonstrate how the details of the atomic pumping scheme affect the resulting Master equation. In section 5.3, we elaborate on the procedure of solving the Master equation. We show that introducing the quantum regression theorem and expressing the Master equation in terms of atomic operators leads to a dramatic increase of computational efficiency. In section 5.4 we use the above solving procedure to discuss the properties of N atoms with gain. Remarkably, this few-atom system, though very simple, shows surprisingly strong spectral gain narrowing and mode redistribution, indicating an approach to laser oscillation. In addition, we demonstrate that the observed phenomena become more pronounced as the number of atoms increases, in correspondence with the intuitive $N \to \infty$ limit. In addition, we elaborate on the nontrivial character of the system's second-order photon correlations. Finally, in section 5.5, we connect the few-atom systems considered here to macroscopic laser systems. In particular, we relate standard laser concepts such as threshold behavior and mode redistribution to the characteristics of the presented N-atom systems.

5.2 The Master equation of N atoms with gain

5.2.1 The Master equation of N passive atoms

In the spirit of the presentation in [71], we start by considering a collection of N identical passive atoms coupled to a three-dimensional multimode electromagnetic field. Each of the atoms has two relevant energy levels a and c, separated by an energy difference $\hbar\omega_{ca}$. In relation to the previous chapters, we can regard the atoms to be of the three-level type abc introduced in section 2.2 in the absence of a pump. As we discussed in section 4.2, the upper level b does not participate in the atomic dynamics if no external pump field is present; the atoms can then be regarded as two-level ac systems. The total Hamiltonian of the atoms and the electromagnetic field can be written as

$$\hat{H}(t) = \sum_{j=1}^{N} \hat{H}_c^{(j)}(t) + \sum_{j=1}^{N} \hat{V}_{AR}^{(j)}(t) + \hat{H}_R(t). \tag{5.1}$$

The atomic Hamiltonian is given by

$$\sum_{j=1}^{N} \hat{H}_c^{(j)}(t) = \hbar\omega_{ca} \sum_{j=1}^{N} \hat{S}_{ac}^{(j)+}(t)\hat{S}_{ac}^{(j)-}(t), \tag{5.2}$$

where $\hat{S}_{ac}^{(j)+}(t)$ and $\hat{S}_{ac}^{(j)-}(t)$ respectively raise and lower the state of atom j at time t. The atoms are coupled to the field through the interaction Hamiltonian

$$\sum_{j=1}^{N} \hat{V}_{AR}^{(j)}(t) = -\sum_{j=1}^{N} \hat{\boldsymbol{d}}^{(j)}(t) \cdot \hat{\boldsymbol{E}}(t, \boldsymbol{r}_j), \tag{5.3}$$

where $\boldsymbol{r}_j$ is the position vector of atom j,

$$\hat{\boldsymbol{d}}^{(j)}(t) \equiv \boldsymbol{d}_{ac}^{(j)} \left(\hat{S}_{ac}^{(j)+}(t) + \hat{S}_{ac}^{(j)-}(t) \right) \tag{5.4}$$

is the dipole operator of atom j with $\boldsymbol{d}_{ac}^{(j)}$ the atom's transition dipole moment, and

$$\hat{\boldsymbol{E}}(t, \boldsymbol{r}) \equiv \sum_{\boldsymbol{k}\lambda} \boldsymbol{\epsilon}_{\boldsymbol{k}\lambda} \left(\frac{\hbar\omega_{\boldsymbol{k}\lambda}}{2\varepsilon_0 V} \right)^{1/2} \left(\hat{a}_{\boldsymbol{k}\lambda}(t) e^{i\boldsymbol{k}\cdot\boldsymbol{r}} + \hat{a}_{\boldsymbol{k}\lambda}^{\dagger}(t) e^{-i\boldsymbol{k}\cdot\boldsymbol{r}} \right) \tag{5.5}$$

is the electric-field operator, where V is the quantization volume. The operators $\hat{a}_{\boldsymbol{k}\lambda}(t)$ and $\hat{a}_{\boldsymbol{k}\lambda}^{\dagger}(t)$ respectively annihilate and create a photon with polarization $\boldsymbol{\epsilon}_{\boldsymbol{k}\lambda}$ and frequency $\omega_{\boldsymbol{k}\lambda}$ at time t; they obey the standard commutation relations

$$\left[\hat{a}_{\boldsymbol{k}\lambda}(t), \hat{a}_{\boldsymbol{k}'\lambda'}^{\dagger}(t) \right] = \delta_{\lambda\lambda'} \delta(\boldsymbol{k} - \boldsymbol{k}'). \tag{5.6}$$

Finally, the multimode electric field is described by the Hamiltonian

$$\hat{H}_R(t) \equiv \sum_{\boldsymbol{k}\lambda} \hbar\omega_{\boldsymbol{k}\lambda} \hat{a}_{\boldsymbol{k}\lambda}^{\dagger}(t) \hat{a}_{\boldsymbol{k}\lambda}(t). \tag{5.7}$$

The total Hamiltonian (5.1) fully describes the N-atom system under consideration and its coupling to the electromagnetic field. Our aim is to derive the N-atom Master equation, thereby describing the system in terms of atomic operators only.

If $\hat{Q}(t)$ is an arbitrary combination of atomic operators, then $\hat{Q}(t)$ evolves as

$$\frac{d}{dt}\hat{Q}(t) = \frac{i}{\hbar} \left[\hat{H}(t), \hat{Q}(t) \right], \tag{5.8}$$

which can be expanded, using (5.1), as

$$\begin{aligned}\frac{d}{dt}\hat{Q}(t) =& i\omega_{ca}\sum_{j=1}^{N}\left[\hat{S}_{ac}^{(j)+}(t)\hat{S}_{ac}^{(j)-}(t),\hat{Q}(t)\right]\\ &-\frac{i}{\hbar}\sum_{j=1}^{N}\sum_{\boldsymbol{k}\lambda}K_{\boldsymbol{k}\lambda}^{(j)}\left(e^{i\boldsymbol{k}\cdot\boldsymbol{r}_j}\left[\hat{S}_{ac}^{(j)+}(t)+\hat{S}_{ac}^{(j)-}(t),\hat{Q}(t)\right]\hat{a}_{\boldsymbol{k}\lambda}(t)\right)\\ &-\frac{i}{\hbar}\sum_{j=1}^{N}\sum_{\boldsymbol{k}\lambda}K_{\boldsymbol{k}\lambda}^{(j)}\left(e^{-i\boldsymbol{k}\cdot\boldsymbol{r}_j}\hat{a}_{\boldsymbol{k}\lambda}^{\dagger}(t)\left[\hat{S}_{ac}^{(j)+}(t)+\hat{S}_{ac}^{(j)-}(t),\hat{Q}(t)\right]\right), \qquad (5.9)\end{aligned}$$

were we used the shorthand notation

$$K_{\boldsymbol{k}\lambda}^{(j)} \equiv \left(\frac{\hbar\omega_{\boldsymbol{k}\lambda}}{2\varepsilon_0 V}\right)^{1/2}\boldsymbol{d}_{ac}^{(j)}\cdot\boldsymbol{\epsilon}_{\boldsymbol{k}\lambda}. \qquad (5.10)$$

We now proceed to eliminate the field operators from equation (5.9). The field operators $\hat{a}_{\boldsymbol{k}\lambda}(t)$ satisfy

$$\begin{aligned}\frac{d}{dt}\hat{a}_{\boldsymbol{k}\lambda}(t) =& \frac{i}{\hbar}\left[\hat{H}(t),\hat{a}_{\boldsymbol{k}\lambda}(t)\right]\\ =& -i\omega_{\boldsymbol{k}\lambda}\hat{a}_{\boldsymbol{k}\lambda}(t)+\frac{i}{\hbar}\sum_{j=1}^{N}K_{\boldsymbol{k}\lambda}^{(j)}\left(\hat{S}_{ac}^{(j)+}(t)+\hat{S}_{ac}^{(j)-}(t)\right)e^{-i\boldsymbol{k}\cdot\boldsymbol{r}_j}, \qquad (5.11)\end{aligned}$$

from which we can deduce that

$$\begin{aligned}\hat{a}_{\boldsymbol{k}\lambda}(t) =& \hat{a}_{\boldsymbol{k}\lambda}(0)e^{-i\omega_{\boldsymbol{k}\lambda}t}\\ &+\frac{i}{\hbar}\sum_{j=1}^{N}K_{\boldsymbol{k}\lambda}^{(j)}\int_0^t dt'\left(\hat{S}_{ac}^{(j)+}(t')+\hat{S}_{ac}^{(j)-}(t')\right)e^{-i\boldsymbol{k}\cdot\boldsymbol{r}_j+i\omega_{\boldsymbol{k}\lambda}(t'-t)}. \qquad (5.12)\end{aligned}$$

Using the explicit time-dependent field operators (5.12), we can simplify the evolution (5.9) of the atomic operator $\hat{Q}(t)$. The second term of (5.9) can be rewritten as

$$\begin{aligned}&-\frac{i}{\hbar}\sum_{j=1}^{N}\hat{\boldsymbol{E}}_0^{+}(t,\boldsymbol{r}_j)\cdot\boldsymbol{d}_{ac}^{(j)}\left[\hat{S}_{ac}^{(j)+}(t)+\hat{S}_{ac}^{(j)-}(t),\hat{Q}(t)\right]+\sum_{j,j'=1}^{N}\sum_{\boldsymbol{k}\lambda}K_{\boldsymbol{k}\lambda}^{(j)}K_{\boldsymbol{k}\lambda}^{(j')}e^{-i\boldsymbol{k}\cdot\boldsymbol{r}_{jj'}}\times\\ &\frac{1}{\hbar^2}\int_0^t dt' e^{i\omega_{\boldsymbol{k}\lambda}(t'-t)}\left[\hat{S}_{ac}^{(j)+}(t)+\hat{S}_{ac}^{(j)-}(t),\hat{Q}(t)\right]\left(\hat{S}_{ac}^{(j')+}(t')+\hat{S}_{ac}^{(j')-}(t')\right), \qquad (5.13)\end{aligned}$$

with

$$\hat{\boldsymbol{E}}_0^+(t,\boldsymbol{r}) \equiv \sum_{\boldsymbol{k}\lambda} \Big(\frac{\hbar\omega_{\boldsymbol{k}\lambda}}{2\varepsilon_0 V}\Big)^{1/2} \boldsymbol{\epsilon}_{\boldsymbol{k}\lambda} e^{i\boldsymbol{k}\cdot\boldsymbol{r}-i\omega_{\boldsymbol{k}\lambda}t} \hat{a}_{\boldsymbol{k}\lambda}(0) \tag{5.14}$$

the positive-frequency part of the quantum vacuum field operator. Following the convention of the previous chapters, the vector $\boldsymbol{r}_{jj'}$ is defined as $\boldsymbol{r}_{jj'} \equiv \boldsymbol{r}_j - \boldsymbol{r}_{j'}$. Expression (5.9) with (5.13) and the complex conjugate of the latter is an integro-differential equation for $\hat{Q}(t)$ in which the only field operators are free-field operators; the electromagnetic field has therefore effectively been eliminated.

We now proceed to further simplify the evolution equation for $\hat{Q}(t)$. The sum over the electromagnetic field modes in (5.13) can be replaced in the continuum limit by

$$\sum_{\boldsymbol{k}\lambda} \to \frac{V}{(2\pi)^3}\int \boldsymbol{d}k \sum_{\epsilon\perp\boldsymbol{k}} = \frac{V}{(2\pi)^3}\int_0^{+\infty} k^2 dk \int_{4\pi} d\Omega_k \sum_{\epsilon\perp\boldsymbol{k}}, \tag{5.15}$$

where the sum is over the two states of polarization orthogonal to $\boldsymbol{k}$. The atomic operators, which oscillate close to the atomic frequency ω_{ca}, can be rewritten in terms of more slowly varying dynamical variables

$$\hat{S}_{ac}^{(j)+}(t) = e^{+i\omega_{ca}t}\hat{\tilde{S}}_{ac}^{(j)+}(t), \tag{5.16a}$$

$$\hat{S}_{ac}^{(j)-}(t) = e^{-i\omega_{ca}t}\hat{\tilde{S}}_{ac}^{(j)-}(t), \tag{5.16b}$$

similar to the substitutions introduced in the Rotating Wave Approximation [30] discussed in chapter 2 and 4. We stress, however, that the presented derivation of the N-atom Master equation is at this stage not approximative but still exact. Using expressions (5.15) and (5.16), we can rewrite (5.13) as

$$\begin{aligned}
&-\frac{i}{\hbar}\sum_{j=1}^{N} \hat{\boldsymbol{E}}_0^+(t,\boldsymbol{r}_j)\cdot\boldsymbol{d}_{ac}^{(j)}\left[\hat{S}_{ac}^{(j)+}(t)+\hat{S}_{ac}^{(j)-}(t),\hat{Q}(t)\right] \\
&+\frac{1}{2\varepsilon_0\hbar}\sum_{j,j'=1}^{N}\int \boldsymbol{d}k\frac{\omega}{8\pi^3}e^{-i\boldsymbol{k}\cdot\boldsymbol{r}_{jj'}}\boldsymbol{d}_{ac}^{(j')}\cdot\left(1-\frac{1}{k^2}\boldsymbol{k}\otimes\boldsymbol{k}\right)\cdot\boldsymbol{d}_{ac}^{(j)}\int_0^t dt' e^{i\omega(t'-t)}\times \\
&\quad\left[\hat{S}_{ac}^{(j)+}(t)+\hat{S}_{ac}^{(j)-}(t),\hat{Q}(t)\right]\left(e^{+i\omega_{ca}t'}\hat{\tilde{S}}_{ac}^{(j')+}(t')+e^{-i\omega_{ca}t'}\hat{\tilde{S}}_{ac}^{(j')-}(t')\right),
\end{aligned} \tag{5.17}$$

where we let $\omega_{\boldsymbol{k}\lambda} \to \omega$ and used the notation $k \equiv |\boldsymbol{k}| = \omega/c$. In the derivation of

(5.17), the sum over polarizations is simplified as

$$\sum_{\boldsymbol{\epsilon}\perp\boldsymbol{k}} \boldsymbol{\epsilon}_{\boldsymbol{k}\lambda} \otimes \boldsymbol{\epsilon}_{\boldsymbol{k}\lambda} = 1 - \frac{1}{k^2}\boldsymbol{k}\otimes\boldsymbol{k}. \tag{5.18}$$

We now proceed by introducing an approximation in order to simplify the calculations. We replace the slowly varying operators (5.16) at time t' by their most recent values, thereby reducing the integro-differential equation for $\hat{Q}(t)$ to an ordinary differential equation. This approximation is often referred to as the short memory or *Markov* approximation [20, 79]. In the Markov approximation, we can simplify expression (5.17) as

$$\begin{aligned} -\frac{i}{\hbar}\sum_{j=1}^{N} \hat{\boldsymbol{E}}_0^+(t,\boldsymbol{r}_j)\cdot\boldsymbol{d}_{ac}^{(j)}\left[\hat{S}_{ac}^{(j)+}(t)+\hat{S}_{ac}^{(j)-}(t),\hat{Q}(t)\right] + \frac{1}{2\varepsilon_0\hbar}\sum_{j,j'=1}^{N}\int \boldsymbol{d}k\frac{\omega}{8\pi^3}\times \\ e^{-i\boldsymbol{k}\cdot\boldsymbol{r}_{jj'}}\boldsymbol{d}_{ac}^{(j')}\cdot\left(1-\frac{1}{k^2}\boldsymbol{k}\otimes\boldsymbol{k}\right)\cdot\boldsymbol{d}_{ac}^{(j)}\left[\hat{S}_{ac}^{(j)+}(t)+\hat{S}_{ac}^{(j)-}(t),\hat{Q}(t)\right]\times \\ \left(\hat{S}_{ac}^{(j')+}(t)\int_0^t dt' e^{i(\omega_{ca}+\omega)(t'-t)} + \hat{S}_{ac}^{(j')-}(t)\int_0^t dt' e^{+i(\omega-\omega_{ca})(t'-t)}\right). \end{aligned} \tag{5.19}$$

The physical motivation of the Markov approximation can be explained in terms of the different time scales involved in the system's evolution. The most important values for t' in the evolution of the slowly varying atomic operators (5.16) are of the order $t-|\boldsymbol{r}_{jj'}/c|$; in addition, we assume that the time required for a light signal to travel from one atom to another (which is of the order $|\boldsymbol{r}_{jj'}|/c$) is small compared to the time required for secular changes in the atomic levels (which is of the order $1/\Gamma_{ca}$). Under the above conditions, the slowly varying atomic operators at t' can be replaced by their value at time t. (As a side remark, we note that the Markov approximation is well-known and implicitly assumed in many quantum optical descriptions, where it leads to, e.g., the single-exponential decay of a single isolated two-level atom in free space.)

We now continue to further simplify expression (5.19). The typical times we consider are large compared to a single optical cycle ($t \gg 1/\omega_{ca}$); the integration interval in the time integration of (5.19) can therefore in good approximation be extended to $[0,+\infty[$. We can then use

$$\begin{aligned} \lim_{t\to\infty}\int_0^t dt' e^{i(\omega\pm\omega_{ca})(t'-t)} &= \lim_{t\to\infty}\int_0^t d\tau e^{-i(\omega\pm\omega_{ca})\tau} \\ &= -i\mathcal{P}\frac{1}{\omega\pm\omega_{ca}} + \pi\delta(\omega\pm\omega_{ca}), \end{aligned} \tag{5.20}$$

where $\mathcal{P}$ denotes the (Cauchy) Principal Value; discarding terms which oscillate at

high frequencies such as $\hat{S}_{ac}^{(j)+}(t)\hat{S}_{ac}^{(j')+}(t)$ then transforms (5.19) into

$$-\frac{i}{\hbar}\sum_{j=1}^{N}\hat{\boldsymbol{E}}_0^+(t,\boldsymbol{r}_j)\cdot\boldsymbol{d}_{ac}^{(j)}\left[\hat{S}_{ac}^{(j)+}(t),\hat{Q}(t)\right]+i\sum_{j,j'=1}^{N}\delta^{(jj')+}\left[\hat{S}_{ac}^{(j)-}(t),\hat{Q}(t)\right]\hat{S}_{ac}^{(j')+}(t)$$
$$+\sum_{j,j'=1}^{N}(i\delta^{(jj')-}+\frac{1}{2}\Gamma^{(jj')})\left[\hat{S}_{ac}^{(j)+}(t),\hat{Q}(t)\right]\hat{S}_{ac}^{(j')-}(t). \tag{5.21}$$

The coupling constants $\delta^{(jj')\pm}$ and $\Gamma^{(jj')}$ are defined as

$$\delta^{(jj')\pm}\equiv-\frac{1}{2\pi}\mathcal{P}\int_0^{+\infty}\frac{\omega^3}{\omega_{ca}^3}d\omega\frac{1}{\omega\pm\omega_{ca}}F^{(jj')}(\omega), \tag{5.22a}$$
$$\Gamma^{(jj')}\equiv F^{(jj')}(\omega_{ca}), \tag{5.22b}$$

with

$$F^{(jj')}(\omega)\equiv\frac{3}{2}\Gamma_{ca}\Big([\boldsymbol{\mu}_{ac}^{(j)}\cdot\boldsymbol{\mu}_{ac}^{(j')}-(\boldsymbol{\mu}_{ac}^{(j)}\cdot\boldsymbol{r}_{jj'})(\boldsymbol{\mu}_{ac}^{(j')}\cdot\boldsymbol{r}_{jj'})]\frac{\sin(\omega|\boldsymbol{r}_{jj'}|/c)}{\omega|\boldsymbol{r}_{jj'}|/c}$$
$$+[\boldsymbol{\mu}_{ac}^{(j)}\cdot\boldsymbol{\mu}_{ac}^{(j')}-3(\boldsymbol{\mu}_{ac}^{(j)}\cdot\boldsymbol{r}_{jj'})(\boldsymbol{\mu}_{ac}^{(j')}\cdot\boldsymbol{r}_{jj'})][\frac{\cos(\omega|\boldsymbol{r}_{jj'}|/c)}{(\omega|\boldsymbol{r}_{jj'}|/c)^2}-\frac{\sin(\omega|\boldsymbol{r}_{jj'}|/c)}{(\omega|\boldsymbol{r}_{jj'}|/c)^3}]\Big), \tag{5.23}$$

where we used relation (4.54) which relates Γ_{ca} to $\boldsymbol{d}_{ca}$, and defined $\boldsymbol{\mu}_{ac}^{(j)}\equiv\boldsymbol{d}_{ac}^{(j)}/|\boldsymbol{d}_{ac}^{(j)}|$, in accordance with the notation introduced in previous chapters. Combining expression (5.9) with (5.21) and its complex conjugate finally yields the passive N-atom Master equation

$$\frac{d}{dt}\left\langle\hat{Q}\right\rangle_0=i\omega_{ca}\sum_{j=1}^{N}\left\langle\left[\hat{S}_{ac}^{(j)+}\hat{S}_{ac}^{(j)-},\hat{Q}\right]\right\rangle_0+\sum_{\substack{j,j'=1\\j\neq j'}}^{N}i\delta^{(jj')}\left\langle\left[\hat{S}_{ac}^{(j)+}\hat{S}_{ac}^{(j')-},\hat{Q}\right]\right\rangle_0$$
$$-\frac{1}{2}\sum_{j,j'=1}^{N}\Gamma^{(jj')}\left\langle\hat{S}_{ac}^{(j)+}\hat{S}_{ac}^{(j')-}\hat{Q}+\hat{Q}\hat{S}_{ac}^{(j)+}\hat{S}_{ac}^{(j')-}-2\hat{S}_{ac}^{(j)+}\hat{Q}\hat{S}_{ac}^{(j')-}\right\rangle_0 \tag{5.24}$$

where we defined $\delta^{(jj')}$ as $\delta^{(jj')}\equiv\delta^{(jj')+}+\delta^{(jj')-}$. In the transition from expression (5.21) to the Master equation (5.24), we absorbed all frequency shifts into the atomic frequency ω_{ca} since these shifts are identical for all atoms and do not contribute to the phenomena of interest here. In addition, we considered the radiation field to be initially in vacuum as denoted by the brackets $\langle.\rangle_0$, thereby removing

the quantum vacuum field operators. The Master equation (5.24) is the key result of this derivation; it describes the time evolution of any atomic operator $\hat{Q}(t)$ in terms of atomic operators and atomic properties only. The atoms interact through the field with one another; due to the above elimination of the field, the atom-atom interaction is expressed in terms of an effective atom-atom coupling (5.22).

In relation to the scattering formalism of chapter 3, the coupling term (5.22a) can be simplified by standard contour integration as

$$\begin{aligned}\delta^{(jj')} =& \frac{3}{4}\Gamma_{ca}\Big(-[\boldsymbol{\mu}_{ac}^{(j)}\cdot\boldsymbol{\mu}_{ac}^{(j')} - (\boldsymbol{\mu}_{ac}^{(j)}\cdot\boldsymbol{r}_{jj'})(\boldsymbol{\mu}_{ac}^{(j')}\cdot\boldsymbol{r}_{jj'})](\frac{\cos(\omega_{ca}|\boldsymbol{r}_{jj'}|)}{\omega_{ca}|\boldsymbol{r}_{jj'}|}) \\ &+ [\boldsymbol{\mu}_{ac}^{(j)}\cdot\boldsymbol{\mu}_{ac}^{(j')} - 3(\boldsymbol{\mu}_{ac}^{(j)}\cdot\boldsymbol{r}_{jj'})(\boldsymbol{\mu}_{ac}^{(j')}\cdot\boldsymbol{r}_{jj'})][\frac{\sin(\omega_{ca}|\boldsymbol{r}_{jj'}|)}{(\omega_{ca}|\boldsymbol{r}_{jj'}|)^2} + \frac{\cos(\omega_{ca}|\boldsymbol{r}_{jj'}|)}{(\omega_{ca}|\boldsymbol{r}_{jj'}|)^3}]\Big).\end{aligned} \tag{5.25}$$

Comparing the coupling terms (5.22b) and (5.25) to the classical free-space Green function (3.46) shows that

$$2\delta^{(jj')} - i\Gamma^{(jj')} = 6\pi\frac{\Gamma_{ca}c}{\omega_{ca}}\boldsymbol{\mu}_{ac}^{(j)}\cdot\overleftrightarrow{G}_0(\omega_{ca},\boldsymbol{r}_{jj'})\cdot\boldsymbol{\mu}_{ac}^{(j')}. \tag{5.26}$$

Relation (5.26) illustrates the intimate connection between the above Master equation and the scattering formalism of chapter 3: integrating the atom-atom coupling over the *quantum* vacuum results in the *classical* retarded free-space Green function.

The coupling constants (5.22b) and (5.25) are expressed in terms of the natural decay rate Γ_{ca} of one atom, the orientation of the atomic transition dipole moments and the separation $x_{jj'} \equiv \omega_{ca}|\boldsymbol{r}_{jj'}|/c$ between different atoms. To illustrate the dependence of the atom-atom coupling on the atomic separation, Figure 5.1 shows both couplings for the case of parallel dipole moments and $\boldsymbol{r}_{jj'} \perp \boldsymbol{\mu}_{ac}^{(j)}, \boldsymbol{\mu}_{ac}^{(j')}$. For large separations ($x_{jj'} \gg 1$), both couplings $\delta^{(jj')}$ and $\Gamma^{(jj')}$ vanish. For atomic separations much smaller than the optical wavelength $\Gamma^{(jj')}$ and $\delta^{(jj')}$ exhibit a different behavior: while $\delta^{(jj')}$ diverges for small separations, $\Gamma^{(jj')}$ reduces to the single-atom decay rate Γ_{ca}. Because the coupling $\delta^{(jj')}$ appears as a frequency shift and the coupling $\Gamma^{(jj')}$ as a damping term, $\delta^{(jj')}$ is often referred to as the *coherent* atom-atom coupling while $\Gamma^{(jj')}$ is referred to as the *incoherent* atom-atom coupling [3].

We conclude the above derivation of the passive N-atom Master equation by connecting equation (5.24) to the density-matrix formalism introduced in chapter 2. The system of N atoms and the radiation field can be characterized by a total density matrix $\hat{\rho}(t)$, which evolves as

$$\frac{d}{dt}\hat{\rho}(t) = -\frac{i}{\hbar}\left[\hat{H}(t),\hat{\rho}(t)\right]. \tag{5.27}$$

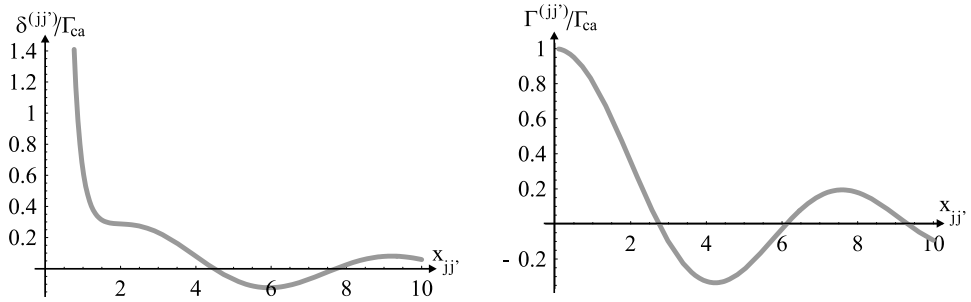

(a) The coherent coupling $\delta^{(jj')}$.

(b) The incoherent coupling $\Gamma^{(jj')}$.

Figure 5.1: The (a) coherent atom-atom coupling $\delta^{(jj')}$ and the (b) incoherent atom-atom coupling $\Gamma^{(jj')}$. Both couplings vary with the atomic separation $x_{jj'} \equiv \omega_{ca}|\boldsymbol{r}_{jj'}|/c$, and are shown for the case of parallel dipole moments $\boldsymbol{\mu}_{ac}^{(j)} \parallel \boldsymbol{\mu}_{ac}^{(j')}$ and $\boldsymbol{r}_{jj'} \perp \boldsymbol{\mu}_{ac}^{(j)}, \boldsymbol{\mu}_{ac}^{(j')}$.

The time average of an arbitrary operator $\hat{\tilde{Q}}(t)$ is related to the density matrix $\hat{\rho}(t)$ by

$$\left\langle \hat{\tilde{Q}}(t) \right\rangle \equiv \mathrm{Tr}_{\{A\},R}\left[\hat{\rho}(t)\hat{\tilde{Q}}(0)\right] = \mathrm{Tr}_{\{A\},R}\left[\hat{\rho}(0)\hat{\tilde{Q}}(t)\right], \tag{5.28}$$

where the trace stands for an integration over the atoms $\{A\} = A_1, \ldots, A_N$ and the electromagnetic field R. If the operator $\hat{\tilde{Q}}(t)$ is an arbitrary combination of atomic operators only, we replace the general operator $\hat{\tilde{Q}}(t)$ by the atomic operator $\hat{Q}(t)$ and simplify (5.28) as

$$\begin{aligned} \left\langle \hat{Q}(t) \right\rangle &= \mathrm{Tr}_{\{A\},R}\left[\hat{\rho}(t)\hat{Q}(0)\right] \\ &= \mathrm{Tr}_{\{A\}}\left[\mathrm{Tr}_R\left[\hat{\rho}(t)\right]\hat{Q}(0)\right] \\ &= \mathrm{Tr}_{\{A\}}\left[\hat{\sigma}(t)\hat{Q}(0)\right]. \end{aligned} \tag{5.29}$$

in terms of the atomic density matrix $\hat{\sigma}(t)$. Note that in order to write (5.29), we assumed that the total density matrix $\hat{\rho}(t)$ of the atoms and the field can be factorized into an atomic density matrix $\hat{\sigma}(t)$ and a field contribution $\hat{\rho}_R$

$$\hat{\rho}(t) \equiv \hat{\sigma}(t) \otimes \hat{\rho}_R, \tag{5.30}$$

thereby implying that correlations between the atoms and the field decay quickly enough in order not to affect the secular evolution of the atoms [24, 30]. The factorization (5.30) is often referred to as the *Born approximation*. In the Born approximation, atom-field interactions of second order in the atom-field coupling $\hat{V}_{AR}^{(j)}$ are neglected. (As a side remark, we note that the above Born approximation is fully consistent with the Master equation (5.24), though this may not seem apparent at first sight. We can demonstrate their compatibility by a Taylor expansion of the slowly varying atomic operators

$$\hat{\tilde{S}}_{ac}^{(j)\pm}(t') = \hat{\tilde{S}}_{ac}^{(j)\pm}(t) + (t'-t)\frac{d}{dt}\hat{\tilde{S}}_{ac}^{(j)\pm}(t) + \dots . \tag{5.31}$$

Since equation (5.9) reveals that the second term of (5.31) is of order $\boldsymbol{d}_{ac}^{(j)}$ or higher, retaining only the first term of (5.31) corresponds to approximating (5.17) up to second order in the atom-field interaction, in agreement with the Born approximation.)

If we combine both expressions (5.24) and (5.29) for the time average of $\hat{Q}(t)$ above, and consider the radiation field to be in a vacuum state ($\hat{\rho}_R \equiv |0\rangle\langle 0|$), we find the Master equation for the atomic density matrix in the *Born-Markov approximation*

$$\begin{aligned}\frac{d}{dt}\hat{\sigma} = &-i\omega_{ca}\sum_{j=1}^{N}\left[\hat{S}_{ac}^{(j)+}\hat{S}_{ac}^{(j)-},\hat{\sigma}\right] - \sum_{\substack{j,j'=1\\ j\neq j'}}^{N} i\delta^{(jj')}\left[\hat{S}_{ac}^{(j)+}\hat{S}_{ac}^{(j')-},\hat{\sigma}\right] \\ &- \frac{1}{2}\sum_{j,j'=1}^{N}\Gamma^{(jj')}\left(\hat{S}_{ac}^{(j)+}\hat{S}_{ac}^{(j')-}\hat{\sigma} + \hat{\sigma}\hat{S}_{ac}^{(j)+}\hat{S}_{ac}^{(j')-} - 2\hat{S}_{ac}^{(j)-}\hat{\sigma}\hat{S}_{ac}^{(j')+}\right),\end{aligned} \tag{5.32}$$

where we dropped the subscript denoting the vacuum state of the field for notational simplicity. Comparing (5.24) and (5.32) reveals a strong resemblance between both equations; however, we note that both evolution equations differ in a subtle way through the different ordering of the atomic raising and lowering operators and the sign of the commutator terms.

5.2.2 Gain and the N-atom Master equation

The Master equation (5.32), or equivalently, equation (5.24), fully describes the dynamics of a passive N-atom system in terms of atomic operators and properties only. We now proceed to incorporate gain in the system by including the interaction of one of the atoms with an external pump field.

In chapter 2 we discussed two different schemes allowing for the implementation of gain in an atomic system. The three-level scheme *abc* depicted in Figure 2.1 is

the simplest level scheme in terms of the number of levels required for its description, but the scheme's gain is inherently nonlinear due to the power broadening discussed in section 2.4. On the other hand, the four-level system *abcd* depicted in Figure 2.7 does not exhibit similar broadening, but has several major drawbacks in the light of our current interests. First, the four-level scheme *abcd* does not scatter light in the absence of an external pump. Since we are describing a system of N identical atoms and we obviously do not desire the passive atoms to be transparent, we must necessarily pump all N atoms. Secondly, the presence of gain provided by the scheme *abcd* is independent of the applied pump intensity as discussed in section 2.5.3; modeling N identical atoms as four-level systems *abcd* and exciting all of them with an external pump field therefore implies all the atoms to be in gain (or conversely, none of them). Thirdly, and perhaps practically most importantly, a four-level system *abcd* cannot be reduced to an effective two-level system, in contrast to a three-level system *abc*. The reduction of a multilevel system to an effective two-level system is of practical importance because of the resulting computational benefit, as we will illustrate further on. The difference between the four-level scheme *abcd* and the three-level scheme *abc* in terms of their ability to be reduced to an effective two-level system can be understood in terms of the feedback loop in both schemes in the presence of an incident probe. If the levels b and d involved in the pump transition are eliminated from the four-level scheme, the remaining levels a and c do not interact directly with the pump field. Consequently, the finite rate at which the pump provides feedback is removed; in other words, in the presence of an incident probe the equilibrium between the finite pump rate and the stimulated (and spontaneous) emission rate is distorted when eliminating levels b and d. A similar argument does not hold for the three-level scheme, because in the *abc* scheme the lower level a is shared between the $a \rightarrow c$ scattering transition of interest and the $a \rightarrow b$ pump transition. Considering the above arguments, we restrict ourselves henceforth to implementations of gain through schemes of the *abc* type.

The Master equation of one atom of the type *abc*, interacting with an external pump field at the $a \rightarrow b$ transition is given by

$$\begin{aligned}\frac{d}{dt}\hat{\sigma} \equiv & -i[\frac{1}{\hbar}\hat{V}_{AE} + \omega_{ca}\hat{S}^{+}_{ac}\hat{S}^{-}_{ac}, \hat{\sigma}] - \frac{\Gamma_{ca}}{2}\left(\hat{S}^{+}_{ac}\hat{S}^{-}_{ac}\hat{\sigma} + \hat{\sigma}\hat{S}^{+}_{ac}\hat{S}^{-}_{ac}\right) \\ & + \Gamma_{ca}\hat{S}^{-}_{ac}\hat{\sigma}\hat{S}^{+}_{ac} - W\frac{\Gamma_{ca}}{2}\left(\hat{S}^{-}_{ac}\hat{S}^{+}_{ac}\hat{\sigma} + \hat{\sigma}\hat{S}^{-}_{ac}\hat{S}^{+}_{ac}\right) + W\Gamma_{ca}\hat{S}^{+}_{ac}\hat{\sigma}\hat{S}^{-}_{ac}, \qquad (5.33)\end{aligned}$$

in terms of the atom's density matrix $\hat{\sigma}$. The parameter W is defined as (2.20) and quantifies the pump intensity. The Hamiltonian $\hat{V}_{AE}$ is defined as (2.8) and expresses the interaction of the atom with an incident probe field. The above Master equation is equivalent to the Master equation (2.13) presented in chapter 2 in the limit of $\Gamma_{bc} \rightarrow \infty$ and finite W, as can be straightforwardly checked. The interaction of the pump and the atom appears in (5.33) as a damping term; one can intuitively explain the physical processes involved in the pump process by explicitly calculating the evolution of the density matrix elements $\sigma_{ij} \equiv \langle i|\hat{\sigma}|j\rangle$ in the absence of a probe

field

$$\frac{d}{dt}\sigma_{cc} = -\Gamma_{ca}\sigma_{cc} + W\Gamma_{ca}\sigma_{aa}, \tag{5.34a}$$

$$\frac{d}{dt}\sigma_{aa} = +\Gamma_{ca}\sigma_{cc} - W\Gamma_{ca}\sigma_{aa}, \tag{5.34b}$$

$$\frac{d}{dt}\sigma_{ca} = \frac{d}{dt}\sigma_{ac}^{*} = -(1+W)\frac{\Gamma_{ca}}{2}\sigma_{ca}, \tag{5.34c}$$

revealing that the rate at which population is transferred from the lower level a to the excited level c is given by $W\Gamma_{ca}\sigma_{aa}$, as we expect. In addition, the steady-state population distribution corresponding to equations (5.34) is given by

$$\sigma_{cc}^{st} = \frac{W}{1+W} = 1 - \sigma_{aa}^{st}, \tag{5.35}$$

in accordance with expression (2.19).

The Master equation (5.33) reveals how gain can be implemented in the above Master equation formalism using a description in terms of effective two-level systems only. Combining expression (5.33) with the passive N-atom Master equation (5.32) yields the N-atom Master equation of N atoms with a single atom in gain [100, 114]

$$\begin{aligned}\frac{d}{dt}\hat{\sigma} =& -i\omega_{ca}\sum_{j=1}^{N}\left[\hat{S}_{ac}^{(j)+}\hat{S}_{ac}^{(j)-},\hat{\sigma}\right] - \sum_{\substack{j,j'=1\\ j\neq j'}}^{N} i\delta^{(jj')}\left[\hat{S}_{ac}^{(j)+}\hat{S}_{ac}^{(j')-},\hat{\sigma}\right]\\ &- \frac{1}{2}\sum_{j,j'=1}^{N}\Gamma^{(jj')}\left(\hat{S}_{ac}^{(j)+}\hat{S}_{ac}^{(j')-}\hat{\sigma} + \hat{\sigma}\hat{S}_{ac}^{(j)+}\hat{S}_{ac}^{(j')-} - 2\hat{S}_{ac}^{(j)-}\hat{\sigma}\hat{S}_{ac}^{(j')+}\right)\\ &- W\frac{\Gamma_{ca}}{2}\left(\hat{S}_{ac}^{(1)-}\hat{S}_{ac}^{(1)+}\hat{\sigma} + \hat{\sigma}\hat{S}_{ac}^{(1)-}\hat{S}_{ac}^{(1)+}\right) + W\Gamma_{ca}\hat{S}_{ac}^{(1)+}\hat{\sigma}\hat{S}_{ac}^{(1)-},\end{aligned} \tag{5.36}$$

in terms of the atomic density matrix, or equivalently,

$$\begin{aligned}\frac{d}{dt}\left\langle\hat{Q}\right\rangle_0 =& i\omega_{ca}\sum_{j=1}^{N}\left\langle\left[\hat{S}_{ac}^{(j)+}\hat{S}_{ac}^{(j)-},\hat{Q}\right]\right\rangle_0 + \sum_{\substack{j,j'=1\\ j\neq j'}}^{N} i\delta^{(jj')}\left\langle\left[\hat{S}_{ac}^{(j)+}\hat{S}_{ac}^{(j')-},\hat{Q}\right]\right\rangle_0\\ &- \frac{1}{2}\sum_{j,j'=1}^{N}\Gamma^{(jj')}\left\langle\left(\hat{S}_{ac}^{(j)+}\hat{S}_{ac}^{(j')-}\hat{Q} + \hat{Q}\hat{S}_{ac}^{(j)+}\hat{S}_{ac}^{(j')-} - 2\hat{S}_{ac}^{(j)+}\hat{Q}\hat{S}_{ac}^{(j')-}\right)\right\rangle_0\\ &- W\frac{\Gamma_{ca}}{2}\left\langle\hat{S}_{ac}^{(1)-}\hat{S}_{ac}^{(1)+}\hat{Q} + \hat{Q}\hat{S}_{ac}^{(1)-}\hat{S}_{ac}^{(1)+}\right\rangle_0 + W\Gamma_{ca}\left\langle\hat{S}_{ac}^{(1)-}\hat{Q}\hat{S}_{ac}^{(1)+}\right\rangle_0,\end{aligned} \tag{5.37}$$

in terms of an arbitrary atomic operator $\hat{Q}(t)$. The atom which interacts with the external pump field is labeled "1". Expressions (5.36) and (5.37) are the key result of this section: they describe the interaction of N (effective) two-level atoms, one of which interacts with an external pump field, taking into account atom-atom interactions through off-resonant light in all scattering orders. The Master equations (5.36) and (5.37) are written in a compact form and are as such not straightforwardly numerically solvable; in the next section, we focus on a practical approach to the solution of the above equations.

5.3 Solving the N-atom Master equation with gain

5.3.1 Physical quantities of interest

The Master equation (5.37) fully describes a system of N atoms with one atom in gain within the Born-Markov approximation. Our current aim is to provide a general description of N-atom systems in terms of (ideally) experimentally observable quantities. In what follows, we present an overview of the characteristics of an atomic system using the correlation functions of the emitted light.

The first type of correlation function we will focus on is the time-averaged field-field correlation or *spectrum*, defined in the statistically stationary regime as

$$\langle \mathcal{I}(\omega, \boldsymbol{r}) \rangle \equiv \lim_{t\to\infty} \varepsilon_0 \frac{1}{2\pi} \int_{-\infty}^{\infty} d\tau e^{-i\omega\tau} \left\langle \hat{\boldsymbol{E}}^-(t+\tau, \boldsymbol{r}) \cdot \hat{\boldsymbol{E}}^+(t, \boldsymbol{r}) \right\rangle, \tag{5.38}$$

with $\hat{\boldsymbol{E}}^+(t, \boldsymbol{r})$ and $\hat{\boldsymbol{E}}^-(t, \boldsymbol{r})$ respectively the positive- and negative-frequency part of the electric-field operator (5.5), given by

$$\hat{\boldsymbol{E}}^-(t, \boldsymbol{r}) = \left(\hat{\boldsymbol{E}}^+(t, \boldsymbol{r})\right)^\dagger = \sum_{\boldsymbol{k}\lambda} \boldsymbol{\epsilon}_{\boldsymbol{k}\lambda} \left(\frac{\hbar\omega_{\boldsymbol{k}\lambda}}{2\varepsilon_0 V}\right)^{1/2} \hat{a}^\dagger_{\boldsymbol{k}\lambda}(t) e^{-i\boldsymbol{k}\cdot\boldsymbol{r}}. \tag{5.39}$$

The spectrum (5.38) is expressed in units of Js/m^3. The integration over all frequencies of the spectrum and application of the delta-function representation

$$\delta(t) \equiv \frac{1}{2\pi} \int_{-\infty}^{+\infty} d\omega e^{-i\omega t}, \tag{5.40}$$

yields the steady-state intensity

$$\begin{aligned} \langle \mathcal{I}(\boldsymbol{r}) \rangle &\equiv \lim_{t\to\infty} \langle \mathcal{I}(t, \boldsymbol{r}) \rangle \\ &\equiv \lim_{t\to\infty} \int_{-\infty}^{\infty} d\omega e^{i\omega t} \langle \mathcal{I}(\omega, \boldsymbol{r}) \rangle = \lim_{t\to\infty} \varepsilon_0 \left\langle \hat{\boldsymbol{E}}^-(t, \boldsymbol{r}) \cdot \hat{\boldsymbol{E}}^+(t, \boldsymbol{r}) \right\rangle, \end{aligned} \tag{5.41}$$

emitted by the system.

The second type of correlation function of interest is the time-averaged intensity-intensity correlation, defined in the statistically stationary regime as

$$\left\langle \mathcal{G}^{(2)}(\boldsymbol{r},\boldsymbol{r}')\right\rangle \equiv \lim_{t\to\infty}\varepsilon_0^2\left\langle :\hat{I}(t,\boldsymbol{r})\hat{I}(t,\boldsymbol{r}'):\right\rangle, \tag{5.42}$$

where the colons denote normal ordering for the operators, and where the intensity operator is defined as

$$\hat{I}(t,\boldsymbol{r}) \equiv \hat{\boldsymbol{E}}^{-}(t,\boldsymbol{r})\cdot\hat{\boldsymbol{E}}^{+}(t,\boldsymbol{r}). \tag{5.43}$$

Expressions (5.38) and (5.42) are expressed in terms of electric-field operators; since we aim at a description using the Master equation (5.37), we need to express both correlation functions in terms of atomic operators only. Combining (5.5), (5.12), (5.15) and (5.18) shows that the positive-frequency part of $\hat{\boldsymbol{E}}(t,\boldsymbol{r})$ can be written as

$$\begin{aligned}\hat{\boldsymbol{E}}^{+}(t,\boldsymbol{r}) =&\hat{\boldsymbol{E}}_0^{+}(t,\boldsymbol{r}) + i\frac{1}{16\varepsilon_0\pi^3}\int \omega\boldsymbol{d}k(1-\frac{1}{k^2}\boldsymbol{k}\otimes\boldsymbol{k})\cdot\boldsymbol{d}_{ac}^{(j)}\times\\ &\sum_{j=1}^{N} e^{i\boldsymbol{k}\cdot\boldsymbol{R}_j}\int_0^t dt'\left(\hat{S}_{ac}^{(j)+}(t')+\hat{S}_{ac}^{(j)-}(t')\right)e^{i\omega(t'-t)},\end{aligned} \tag{5.44}$$

where we defined $\boldsymbol{R}_j \equiv \boldsymbol{r}-\boldsymbol{r}_j$. Using similar arguments as the ones used in the derivation of the Master equation, we can deduce that [108]

$$\begin{aligned}\hat{\boldsymbol{E}}^{+}(t,\boldsymbol{r}) =&\hat{\boldsymbol{E}}_0^{+}(t,\boldsymbol{r})\\ &+\frac{1}{4\pi\varepsilon_0}\frac{\omega_{ca}^2}{c^2}\sum_{j=1}^{N}\frac{1}{|\boldsymbol{R}_j|}\left(\boldsymbol{d}_{ac}^{(j)}-\frac{1}{|\boldsymbol{R}_j|^2}\boldsymbol{R}_j(\boldsymbol{R}_j\cdot\boldsymbol{d}_{ac}^{(j)})\right)\hat{S}_{ac}^{(j)-}(t-|\boldsymbol{R}_j|/c),\end{aligned} \tag{5.45}$$

in the far-field ($|\boldsymbol{R}_j|\omega_{ca}/c \gg 1, \forall j$). Expression (5.45) denotes that the positive-frequency part of the electric field is proportional to the sum of atomic lowering operators at a retarded time. In other words, the detection of a photon in the far-field at time t requires the decay of (or photon scattering off) an atom j at an earlier time $t-|\boldsymbol{R}_j|\omega_{ca}/c$.

Combining expression (5.45) with expressions (5.38), (5.41) and (5.42) reveals that we need to calculate two different types of atomic-operator combinations in order to evaluate the above correlation functions of interest. On one hand, expanding

the intensity-intensity correlation (5.38) or the intensity (5.41) in terms of atomic operators requires the steady-state value of atomic operators of the type

$$\left\langle \hat{S}_{ac}^{(j)+}(t)\hat{S}_{ac}^{(i)-}(t)\right\rangle . \tag{5.46}$$

On the other hand, the spectrum (5.38) can be written in terms of operator combinations of the type

$$\left\langle \hat{S}_{ac}^{(j)+}(t)\hat{S}_{ac}^{(i)-}(0)\right\rangle . \tag{5.47}$$

We now proceed to show how both types of operator combinations (5.46) and (5.47) can be evaluated using the Master equation (5.37).

5.3.2 Categorization of operator expectation values

The Master equation (5.37) expresses the evolution in time of an arbitrary atomic operator $\hat{Q}(t)$. A close observation of equation (5.37) reveals that each of its terms adds zero net excitation to the system. In other words, the Master equation consists only of contributions for which every atomic raising operator is compensated for by a lowering operator (and vice versa). A direct consequence of this particular property is that the evolution equations of the atomic operators with a given net excitation form a closed set [114]. For example, for the case $N = 2$, the evolution equations of the operators

$$\begin{aligned} &\hat{S}_{ac}^{(1)+}\hat{S}_{ac}^{(1)-}, \quad \hat{S}_{ac}^{(2)+}\hat{S}_{ac}^{(2)-}, \quad \hat{S}_{ac}^{(1)+}\hat{S}_{ac}^{(2)-}, \\ &\hat{S}_{ac}^{(2)+}\hat{S}_{ac}^{(1)-}, \quad \hat{S}_{ac}^{(1)+}\hat{S}_{ac}^{(1)-}\hat{S}_{ac}^{(2)+}\hat{S}_{ac}^{(2)-}, \end{aligned} \tag{5.48}$$

form a closed set, thereby coupling operators with zero net excitation only to other operator combinations with zero net excitation. The set (5.48) is a nontrivial irreducible set of operator combinations; other zero-excitation operators are related to operators (5.48) through completeness relations

$$\hat{S}_{ac}^{(j)+}\hat{S}_{ac}^{(j)-} + \hat{S}_{ac}^{(j)-}\hat{S}_{ac}^{(j)+} \equiv \hat{1}, \qquad \forall j, \tag{5.49}$$

with $\hat{1}$ the unity operator. The above procedure shows that in a two-atom system, the evolution of all zero-excitation operators is governed by a 5×5 matrix. Compared to the dimensions of the evolution matrix corresponding to the Master equation in terms of the density matrix (5.36), the dimensionality involved in determining the steady-state value of operators (5.46) is much smaller. Hence, in

N	# equations using (5.36)	# equations using (5.37)
2	16	5
3	64	19
4	256	56
5	1024	251
...	...	...
n	2^{2n}	$\frac{2n!}{(n!)^2} - 1$

Table 5.1: The total number of differential equations required in a density matrix description versus the number of equations required to evaluate the intensity and intensity-intensity correlations in an N-atom system.

the evaluation of the intensity-intensity correlation function (5.42) or the intensity (5.41), proper use of the Master equation (5.37) versus (5.36) reduces the dimensionality of the problem and the associated computational effort. To illustrate the computational benefit of the above reduction procedure, Table 5.1 compares the number of equations required in a description in terms of the system's density matrix to the number of equations required to evaluate zero-excitation operators (5.46). We observe that computational benefit associated with the above reduction is considerable and increases as the number of atoms N increases.

Using the above procedure, correlation functions of the type (5.46) can be straightforwardly efficiently evaluated. We now focus on the evolution of two-time operators of the type (5.47). The quantum regression theorem [22] states that if a set of operators

$$\hat{\boldsymbol{Q}}(t) \equiv \left(\hat{Q}_1, \hat{Q}_2, \ldots, \hat{Q}_n\right)(t) \tag{5.50}$$

evolves as

$$\frac{d}{dt}\left\langle \hat{\boldsymbol{Q}}(t)\right\rangle = \mathcal{M}\left\langle \hat{\boldsymbol{Q}}(t)\right\rangle, \tag{5.51}$$

with $\mathcal{M}$ the matrix describing the evolution, then two-time operator expectation values obey

$$\frac{d}{dt}\left\langle \hat{\boldsymbol{Q}}(t)\hat{Q}_i(0)\right\rangle = \mathcal{M}\left\langle \hat{\boldsymbol{Q}}(t)\hat{Q}_i(0)\right\rangle, \qquad 1 \leq i \leq n. \tag{5.52}$$

Application of the quantum regression theorem to the operators of the type (5.47) shows that their evolution can be derived from the evolution of single-time operators such as $\hat{S}_{ac}^{(j)+}(t)$. For the case $N = 2$, for example, evaluation of two-time averages

N	# equations using (5.36)	# equations using (5.37)
2	16	4
3	64	15
4	256	56
5	1024	210
...	...	...
n	2^{2n}	$\frac{(2n)!}{(n+1)!(n-1)!}$

Table 5.2: The total number of differential equations required in a density matrix description versus the number of equations required to evaluate the spectrum in an N-atom system.

(5.47) requires the evolution matrix of the closed set of evolution equations of the single-excitation operators

$$\hat{S}_{ac}^{(1)+}, \quad \hat{S}_{ac}^{(2)+}, \quad \hat{S}_{ac}^{(1)+}\hat{S}_{ac}^{(1)-}\hat{S}_{ac}^{(2)+}, \quad \hat{S}_{ac}^{(1)+}\hat{S}_{ac}^{(2)+}\hat{S}_{ac}^{(2)-}. \tag{5.53}$$

The dimensionality of the above list implies that the evolution of all two-time averages of the type (5.47) is, for $N = 2$, governed by a 4×4 matrix. Table 5.2 compares the dimensions of the evolution matrix using the quantum regression theorem to the dimensionality involved using the full Master equation (5.36). Similarly to the evaluation of expectation values (5.46), we observe that using the Master equation (5.37) versus (5.36) results in a considerable reduction of the computational effort.

We conclude this discussion by summarizing that a proper categorization of the atomic operators based on their net excitation, combined with the quantum regression theorem, allows for a straightforward determination of expectation values of the type (5.46) and (5.47). (As a side remark, we note that this categorization is only possible in the absence of an external probe field, since the Hamiltonian (2.8) corresponding to the interaction of an atom and an external probe field does not preserve the number of excitations.) Using the above reduction tools, we now proceed to simplify the expressions for the spectrum (5.38), the intensity (5.41) and the intensity-intensity correlation function (5.42) in terms of atomic operators; such simplification will allow us to characterize the system in terms of experimentally observable quantities.

5.3.3 Evaluation of correlation functions

The far-field spectrum (5.38) can be expressed in terms of atomic operators by means of substitutions (5.16) and (5.45) as

$$\langle \mathcal{I}(\omega, \boldsymbol{r}) \rangle = \varepsilon_0 \frac{d_{ac}^2}{(4\pi\varepsilon_0)^2} \frac{1}{2\pi r^2} \Big(\frac{\omega_{ca}}{c} \Big)^4 \sum_{i,j=1}^{N} e^{i\omega_{ca}\tau_{ij}} \boldsymbol{u}_i(\boldsymbol{r}) \cdot \boldsymbol{u}_j(\boldsymbol{r}) \times \lim_{t\to\infty} \int_{-\infty}^{+\infty} d\tau e^{-i(\omega-\omega_{ca})\tau} \left\langle \hat{\tilde{S}}_{ac}^{(i)+}(t+\tau) \hat{\tilde{S}}_{ac}^{(j)-}(t) \right\rangle, \tag{5.54}$$

with $r \equiv \boldsymbol{r}/|\boldsymbol{r}|$ and where τ_{ij} defined as $\tau_{ij} \equiv |\boldsymbol{R}_j|/c - |\boldsymbol{R}_i|/c$. The vector

$$\boldsymbol{u}_i(\boldsymbol{r}) \equiv \boldsymbol{\mu}_{ac}^{(i)} - (\boldsymbol{r} - \boldsymbol{r}_i) \frac{(\boldsymbol{r} - \boldsymbol{r}_i) \cdot \boldsymbol{\mu}_{ac}^{(i)}}{|(\boldsymbol{r} - \boldsymbol{r}_i)|^2} \tag{5.55}$$

is characteristic for the single-atom dipole radiation. According to the quantum regression theorem, we can write the two-time correlation functions in (5.54) as a sum of exponential functions, each with a weight $\beta_m^{(ij)}$ to be determined from (5.52):

$$\left\langle \hat{\tilde{S}}_{ac}^{(i)+}(\tau) \hat{\tilde{S}}_{ac}^{(j)-}(0) \right\rangle = \sum_{m=1}^{\kappa(N)} \beta_m^{(ij)} e^{(i\omega_m - \gamma_m)\tau}, \tag{5.56}$$

with

$$\kappa(N) \equiv \frac{(2N)!}{(N-1)!(N+1)!} \tag{5.57}$$

the number of eigenvalues of the evolution matrix of the atomic operators with one net excitation, as shown in Table 5.2. Expression (5.56) allows us to write the spectrum as

$$\langle \mathcal{I}(\omega, \boldsymbol{r}) \rangle = \varepsilon_0 \frac{d_{ac}^2}{(4\pi\varepsilon_0)^2} \frac{1}{\pi r^2} \Big(\frac{\omega_{ca}}{c} \Big)^4 \times \sum_{i,j=1}^{N} \sum_{m=1}^{\kappa(N)} \mathrm{Re} \left[\frac{\beta_m^{(ij)} e^{i\omega_{ca}\tau_{ij}}}{i(\omega - \omega_{ca} - \omega_m) + \gamma_m} \right] \boldsymbol{u}_i(\boldsymbol{r}) \cdot \boldsymbol{u}_j(\boldsymbol{r}), \tag{5.58}$$

denoting that the spectrum of the light emitted by N atoms is a superposition of $\kappa(N)$ Lorentzian contributions, each of which is characterized by a central frequency $\omega_{ca} + \omega_m$ and spectral width γ_m. Integrating the spectrum over all frequencies yields the intensity

$$\langle \mathcal{I}(\boldsymbol{r}) \rangle = \lim_{t\to\infty} \varepsilon_0 \frac{d_{ac}^2}{(4\pi\varepsilon_0)^2} \frac{1}{r^2} \Big(\frac{\omega_{ca}}{c} \Big)^4 \sum_{i,j=1}^{N} e^{i\omega_{ca}\tau_{ij}} \boldsymbol{u}_i(\boldsymbol{r}) \cdot \boldsymbol{u}_j(\boldsymbol{r}) \left\langle \hat{\tilde{S}}_{ac}^{(i)+}(t) \hat{\tilde{S}}_{ac}^{(j)-}(t) \right\rangle. \tag{5.59}$$

Finally, in a similar way as the spectrum and the intensity, the far-field intensity-intensity correlation function (5.42) can be rewritten in terms of atomic operators as

$$\left\langle \mathcal{G}^{(2)}(\boldsymbol{r},\boldsymbol{r}')\right\rangle = \varepsilon_0^2 \frac{d_{ac}^4}{(4\pi\varepsilon_0)^4}\left(\frac{\omega_{ca}}{c}\right)^8 \frac{1}{r^4} \sum_{i,j,n,m=1}^{N} e^{i\omega_{ca}\tau_{im}} e^{i\omega_{ca}\tau'_{jn}} \times (\boldsymbol{u}_i(\boldsymbol{r})\cdot\boldsymbol{u}_m(\boldsymbol{r}))\,(\boldsymbol{u}_j(\boldsymbol{r}')\cdot\boldsymbol{u}_n(\boldsymbol{r}')) \times \lim_{t\to\infty}\left\langle \hat{\tilde{S}}_{ac}^{(i)+}(t)\hat{\tilde{S}}_{ac}^{(j)+}(t)\hat{\tilde{S}}_{ac}^{(n)-}(t)\hat{\tilde{S}}_{ac}^{(m)-}(t)\right\rangle. \tag{5.60}$$

with $\tau'_{jn} \equiv |\boldsymbol{r}'-\boldsymbol{r}_n|/c - |\boldsymbol{r}'-\boldsymbol{r}_j|/c$. Expressions (5.58), (5.59) and (5.60) are the key results of this section: they express experimentally observable physical quantities in terms of expectation values of atomic operators only. Using the above mathematical framework, we now focus on the physical properties of the system under consideration and proceed in the next section to present an overview of the characteristics of an N-atom system with gain.

5.4 Characteristics of an N-atom system with gain

The correlation functions derived above allow us to characterize systems of N atoms with gain in terms of the properties of the emitted light. Besides depending on the atomic properties, the system characteristics vary with the atoms' spatial configuration and the orientation of the transition dipole moments. We focus henceforth on configurations of atoms with interatomic distances of the order c/ω_{ca} and smaller, since for much larger distances the feedback provided by the passive atoms is limited and only a very small fraction of the photons emitted by the pumped atom will be scattered.

We now proceed to focus on the spectrum and intensity of the emitted light and second-order photon correlations.

5.4.1 The spectrum

The flux $\langle\Phi(\omega,\boldsymbol{r})\rangle\, d\omega$ of photons detected in the frequency range $[\omega,\omega+d\omega]$ per unit area at a position $\boldsymbol{r}$ in the far-field is given by

$$\langle\Phi(\omega,\boldsymbol{r})\rangle\, d\omega = 2\frac{c}{\hbar\omega_{ca}}\langle\mathcal{I}(\omega,\boldsymbol{r})\rangle\, d\omega. \tag{5.61}$$

The flux is expressed in units $s^{-1}m^{-2}$. Expression (5.61) shows that, in general, the spectral information of the detected photons varies with the position $\boldsymbol{r}$ of the detector. To illustrate this dependence, Figure 5.2 depicts the far-field flux (5.61) emitted by a two-atom system with one of the atoms pumped. The flux is shown

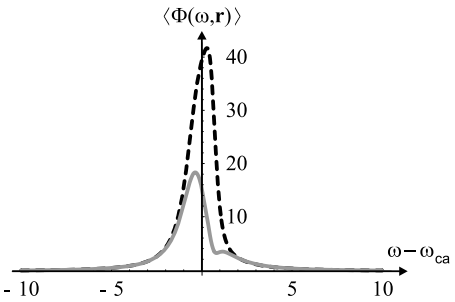

Figure 5.2: The angular flux function $\langle \Phi(\omega, \boldsymbol{r}) \rangle$ (in units of $|\boldsymbol{r}|^{-2}$) versus frequency (in units of Γ_{ca}). The system under consideration consists of two atoms, one of which is pumped. The atomic transition dipole moments are chosen parallel to each other ($\boldsymbol{\mu}_{ac}^{(1)} \parallel \boldsymbol{\mu}_{ac}^{(2)}$) and orthogonal to the axis connecting both atoms ($\boldsymbol{r}_{12} \perp \boldsymbol{\mu}_{ac}^{(1)}, \boldsymbol{\mu}_{ac}^{(2)}$). The position of the detector is taken in the far-field along the $\boldsymbol{r}_{12}$ axis (dashed line) and along the $\boldsymbol{\mu}_{ac}^{(1)} \times \boldsymbol{r}_{12}$ axis (solid line). The pump parameter is $W = 0.5$. The interatomic separation is $|\boldsymbol{r}_{12}| = c/\omega_{ca}$.

for two different positions of the detector. We observe that both the overall shape and the height of the flux depend on the detector's position. In addition, Figure 5.2 demonstrates that the spectrum is in general asymmetric in correspondence with the general structure of expression (5.58).

In what follows, we wish to disregard the role of the detector by considering the far-field angle-integrated flux

$$\begin{aligned}\langle \phi(\omega) \rangle \, d\omega &\equiv \int_{4\pi} r^2 d\Omega \, \langle \Phi(\omega, \boldsymbol{r}) \rangle \, d\omega \\ &= \frac{3\Gamma_{ca}}{(4\pi)^2} d\omega \sum_{i,j=1}^{N} \int_{4\pi} d\Omega e^{i\omega_{ca}\tau_{ij}} \boldsymbol{u}_i(\boldsymbol{r}) \cdot \boldsymbol{u}_j(\boldsymbol{r}) \times \\ &\quad \lim_{t\to\infty} \int_{-\infty}^{+\infty} d\tau e^{-i(\omega-\omega_{ca})\tau} \left\langle \hat{\tilde{S}}_{ac}^{(i)+}(t+\tau) \hat{\tilde{S}}_{ac}^{(j)-}(t) \right\rangle . \end{aligned} \tag{5.62}$$

The angle-integrated flux is expressed in units s^{-1}. The integration over a 4π solid angle in (5.62) can in the far-field be straightforwardly evaluated and yields

$$\int_{4\pi} d\Omega e^{i\omega_{ca}\tau_{ij}} \boldsymbol{u}_i(\boldsymbol{r}) \cdot \boldsymbol{u}_j(\boldsymbol{r}) = \frac{8\pi}{3\Gamma_{ca}} \left(\delta_{ij}\Gamma_{ca} + (1-\delta_{ij})\Gamma^{(ij)} \right), \tag{5.63}$$

with δ_{ij} the Kronecker delta and $\Gamma^{(ij)}$ given by (5.22b). Using (5.63), we can simplify expression (5.62) as

$$\langle\phi(\omega)\rangle\, d\omega = \frac{1}{2\pi} d\omega \sum_{i,j=1}^{N} \lim_{t\to\infty} \int_{-\infty}^{+\infty} d\tau e^{-i(\omega-\omega_{ca})\tau} \left\langle \hat{\tilde{S}}_{ac}^{(i)+}(t+\tau)\hat{\tilde{S}}_{ac}^{(j)-}(t)\right\rangle \times \left(\delta_{ij}\Gamma_{ca} + (1-\delta_{ij})\Gamma^{(ij)}\right). \tag{5.64}$$

For each atomic geometric configuration, the (angle-averaged) spectral properties of the emitted light vary with the applied pump intensity. If we increase the pump intensity, different modes in the system will be subject to different gain and, consequently, modes will compete for the available population inversion in the system. To indicate the effect of the pump intensity on the spectrum of the emitted light, Figure 5.3 shows the far-field angle-integrated flux for a four-atom configuration. The flux is shown for a typical low ($W = 1.77$) and a high ($W = 10.10$) pump intensity. At low pump intensity, the emission spectrum is broad, while at higher pump intensities we observe a significant spectral narrowing. Figure 5.3 further illustrates that the asymmetry of the spectrum typically reduces as the pump intensity increases, indicating the dominance of a single mode at high values of W.

The remarkable observed spectral narrowing is related to the collective behavior of the passive atoms acting as a cavity and the pumped atom providing gain. However, the cooperativity presented here is drastically different from the type of collective behavior found in superradiance [1, 5, 33, 35, 50, 98] or superfluorescence [16, 32, 51, 52, 115]: while we describe a stationary effect, superradiance and superfluorescence effects are essentially transient. Furthermore, the spectral width of a superradiant pulse broadens with the number of atoms, in sharp contrast to the spectral narrowing presented here. As a side remark, we note that atomic systems which do exhibit a narrowing in literature are either atomic ensembles in the very large atom-number limit [34] or atomic systems in a (macroscopic) cavity [53]; in relation to the latter type of work, Figure 5.3 clearly shows that, remarkably, gain narrowing is possible in the few-atom case even in the absence of a cavity.

The degree of gain narrowing which an atomic system exhibits depends to a large extent on the atomic configuration. If we wish to compare different configurations of atoms, we need to visualize the degree of observed gain narrowing. We proceed along the path originally considered by Shawlow and Townes [105] and compare the line width of the emitted light to the photon emission rate. Therefore, we determine the full width at half maximum $\Delta\omega$ of the far-field angle-integrated flux (5.64) and evaluate the spectral weight

$$\mathcal{J}(\Delta\omega) \equiv \int_{\Delta\omega} d\omega\, \langle\phi(\omega)\rangle\,, \tag{5.65}$$

within the range $\Delta\omega$. The spectral weight (5.65) corresponds to the total photon emission rate $n\Gamma_{ca}$ emitted by the N-atom system in the range $\Delta\omega$. Intuitively, the number n can be interpreted as the number of excitations in a cavity with decay

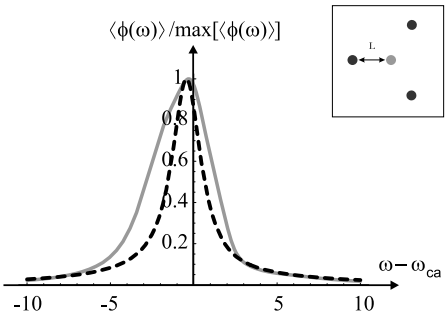

Figure 5.3: The normalized angle-integrated flux in the far-field versus frequency (in units of Γ_{ca}). The inset shows the configuration for which the spectrum is evaluated. The passive atoms (black) are positioned in an equilateral triangle, with the pumped atom (grey) in the center. All transition dipole moments are perpendicular to the plane of the atoms. The distance L in the inset is $0.7c/\omega_{ca}$. The spectrum is shown for a low pump intensity $W = 1.77$ (solid line) and a high pump intensity $W = 10.10$ (dashed line). The flux is normalized to its maximum to emphasize the spectral narrowing.

rate Γ_{ca}, as illustrated by Figure 5.4. If we take the limit $\Delta\omega \to +\infty$, we find

$$\begin{aligned}\lim_{\Delta\omega\to+\infty} \mathcal{J}(\Delta\omega) &= \int_{-\infty}^{+\infty} d\omega \, \langle\phi(\omega)\rangle \\ &= \sum_{i,j=1}^{N} \lim_{t\to\infty} \left\langle \hat{\tilde{S}}_{ac}^{(i)+}(t) \hat{\tilde{S}}_{ac}^{(j)-}(t) \right\rangle \left(\delta_{ij}\Gamma_{ca} + (1-\delta_{ij})\Gamma^{(ij)} \right). \quad (5.66)\end{aligned}$$

Insertion of expression (5.66) in the Master equation (5.37) shows that expression (5.66) can be further simplified as

$$\lim_{\Delta\omega\to+\infty} \mathcal{J}(\Delta\omega) = W\Gamma_{ca} \lim_{t\to\infty} \left\langle \hat{\tilde{S}}_{ac}^{(1)-}(t) \hat{\tilde{S}}_{ac}^{(1)+}(t) \right\rangle, \quad (5.67)$$

confirming that the total energy that flows into the system is entirely reradiated out of the system.

The photon number n is a measure for the power emitted by the N-atom system in the spectral range $\Delta\omega$. Since each of the passive atoms can on average store one excitation, the average photon emission rate $n\Gamma_{ca}$ cannot exceed $N\Gamma_{ca}$. In addition, the system's photon emission rate is limited by the rate (5.67) at which photons are absorbed by the system. The variation of $1/n$ with $\Delta\omega$ is represented in Figure 5.5. The photon emission rate and spectral width are shown for the same parameters as in Figure 5.3 for increasing pump intensity. We observe a large decrease of $\Delta\omega$, accompanied by an increase in the emission rate. The above restrictions on n imply that n cannot increase indefinitely; hence, there is a critical pump intensity

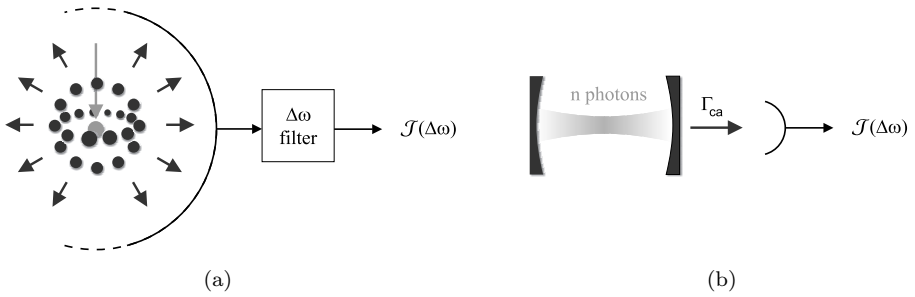

Figure 5.4: The photon emission rate $\mathcal{J}(\Delta\omega)$ of a pumped N-atom system (the pumped atom is grey, the passive atoms black) (a) in the spectral range $\Delta\omega$ equals the emission rate of a cavity (b) with decay rate Γ_{ca} and n steady-state intracavity photons.

at which saturation of the passive atoms sets in, as shown in the inset of Figure 5.5. The maximum value of n is relatively low compared to N due to the weak coupling between the atoms. Around the saturation point, the spectrum broadens while n remains locally constant. If the pump intensity increases beyond the saturation point of the passive atoms, the emission rate decreases. This effect can be attributed to power broadening of the three-level pumping scheme, as discussed in sections 2.4 and 5.2.2.

The observed relation between $1/n$ and $\Delta\omega$ below saturation is similar to the behavior found in many macroscopic lasers. As was shown by Shawlow and Townes and generalized by many others [63, 129], the quantum-limited laser line width $\Delta\omega_L$ due to diffusion is inversely proportional to the number n_L of photons in the laser mode:

$$\Delta\omega_L = \frac{1}{n_L}\frac{\Gamma_{ca}\gamma_c}{\Gamma_{ca}+\gamma_c}, \tag{5.68}$$

with γ_c the decay rate of the intracavity laser intensity. The Schawlow-Townes relation (5.68) is valid far below the laser threshold (far above the threshold, (5.68) still holds if multiplied with a factor 0.5 at the right-hand side); in the bad-cavity limit ($\gamma_c \gg \Gamma_{ca}$), the above relation reduces to

$$\Delta\omega_L = \frac{1}{n_L}\Gamma_{ca}, \tag{5.69}$$

which depends on the atomic decay rate only. Although the N-atom systems under consideration do not strictly obey condition (5.69), it is striking that our simple microscopic system exhibits a similar behavior considering the small number of atoms involved.

If the number of atoms increases, the system's storage capacity grows. Hence,

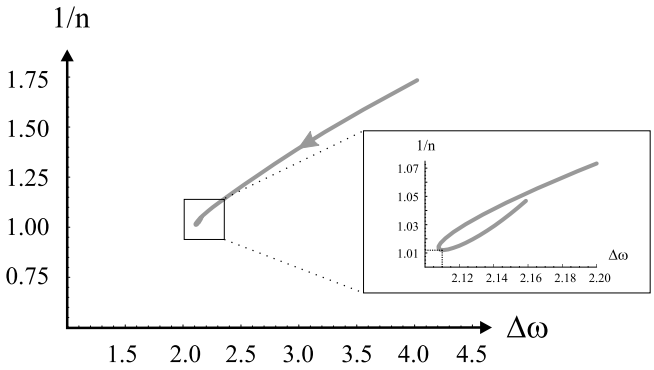

Figure 5.5: The photon emission rate (relative to Γ_{ca}) in the range $\Delta\omega$ versus $\Delta\omega$ (in units of Γ_{ca}). The pump intensity W ranges from 1.76 to 13.43, while the inset focusses on the behavior around the saturation point. The arrow denotes an increase of the pump. The same configuration as in Figure 5.3 is used, with $L = 0.7c/\omega_{ca}$. The dashed lines in the inset denote the position of $\Delta\omega_{min}$ and n_{max}^{-1}.

the maximum value n_{max} which n can attain increases with N. For each given number of atoms, there is an infinite number of possible configurations in which the atoms can be positioned. Since the dipole-dipole coupling depends on the configuration, both n_{max} and the corresponding width $\Delta\omega_{min}$ will, for a given N, vary with the geometry.

In order to compare different configurations of atoms, we determine how many excitations can be stored with a given coherence time $\Delta\omega_{min}^{-1}$. For each number of atoms N, we consider those configurations which attain their saturation point at a given value of $\Delta\omega_{min}$. We then determine the corresponding number of excitations n_{max}. Figure 5.6 shows the calculated n_{max} for three different values of the coherence time. For every number of atoms, different configurations exist which yield the same saturation value $\Delta\omega_{min}$. In general, such configurations each have a different n_{max} associated with them, as represented by the identically colored symbols. We see that the effect of an increase in N is twofold. First, we observe that, for a fixed coherence time, the maximum number of excitations increases with N. This trend indicates that, as the storage capacity of the system grows, more photons with a given coherence time $\Delta\omega_{min}^{-1}$ can be emitted by the system. Secondly, when comparing different values of $\Delta\omega_{min}$ in Figure 5.6, we see that, if the required coherence time increases, a larger capacity is needed to attain a given number of excitations n_{max}. This relation between the number of excitations and the storage capacity is in accordance with the intuitive limiting case $N \to \infty$, $1/n_{max} \to 0$ and $\Delta\omega_{min} \to 0$.

We conclude the discussion on the spectral properties of the emitted light by considering the efficiency η with which incident pump photons are converted into

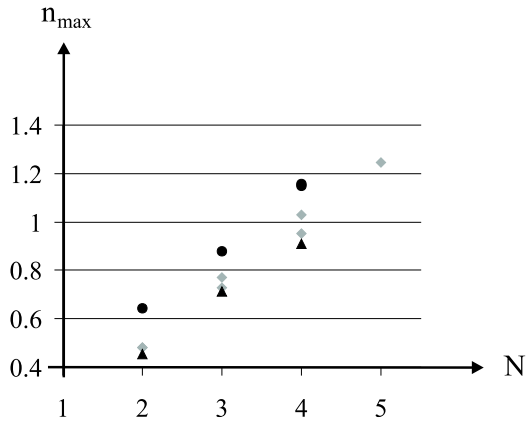

Figure 5.6: The relation between the maximum excitations number n_{max} and N. Multiple symbols for a fixed N represent different configurations. Fixed symbol shapes represent fixed coherence times. The triangles are for a coherence time $0.47\Gamma_{ca}^{-1}$. The diamonds are for a coherence time $0.43\Gamma_{ca}^{-1}$. The circles are for a coherence time $0.29\Gamma_{ca}^{-1}$.

photons in the range $\Delta\omega_{min}$. The efficiency η is defined as the ratio of the output rate and the input rate

$$\eta \equiv \frac{n_{max}}{W\left\langle \hat{S}_{ac}^{(1)-}\hat{S}_{ac}^{(1)+}\right\rangle}. \tag{5.70}$$

The numerical value of the efficiency depends on the number of atoms and the configuration, but we find as a general trend that the efficiency increases with N. For $\Delta\omega_{min}^{-1} = 0.43\Gamma_{ca}^{-1}$ considered in Figure 5.6, for example, the efficiency increases from $\eta = 20\%$ for $N = 2$ to $\eta = 24\%$ for $N = 5$. This increase indicates that adding more atoms leads to a better photon confinement, as we expect.

5.4.2 Second-order photon correlations

We now proceed to discuss angular correlations between simultaneously emitted photons. The intensity-intensity correlation function (5.60) can be normalized as

$$g^{(2)}(\boldsymbol{r},\boldsymbol{r}') \equiv \frac{\left\langle \mathcal{G}^{(2)}(\boldsymbol{r},\boldsymbol{r}')\right\rangle}{\left\langle \mathcal{I}(\boldsymbol{r})\right\rangle\left\langle \mathcal{I}(\boldsymbol{r}')\right\rangle}. \tag{5.71}$$

If the angular distribution of the emitted light is purely random, the normalized second-order correlation function (5.71) is equal to 1. A value of $g^{(2)}(\boldsymbol{r},\boldsymbol{r}') > 1$

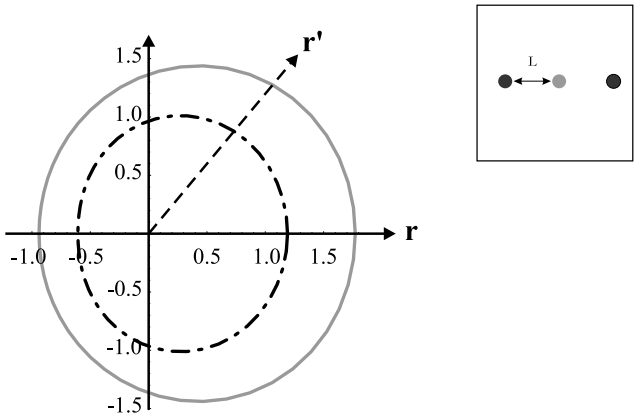

Figure 5.7: A polar plot of the normalized steady-state second-order correlation function $g^{(2)}(\boldsymbol{r}, \boldsymbol{r}')$ for a three-atom system. The inset shows the atomic configuration considered. The atoms are positioned in an axial configuration, with the pumped atom (grey) in the middle of the passive atoms (black). The distance L is $0.7c/\omega_{ca}$. All transition dipole moments are perpendicular to the atomic axis and to the plane of the polar plot. The position $\boldsymbol{r}$ is taken along the atomic axis in the far-field. The pump parameter is taken $W = 1.5$ (solid line) and $W = 10$ (dash-dotted lined).

indicates a larger correlation between a photon emitted in the $\boldsymbol{r}$ direction and a photon simultaneously emitted in the direction of $\boldsymbol{r}'$ as compared to the random case. Conversely, a $g^{(2)}(\boldsymbol{r}, \boldsymbol{r}') < 1$ indicates a reduced angular correlation with respect to the random situation. Figure 5.7 shows the normalized second-order correlation function (5.71) for a three-atom system. The atoms are positioned in an axial configuration; the middle atom interacts with an external pumping field. One of the detection directions $\boldsymbol{r}$ is fixed along the atomic axis while the other detection direction $\boldsymbol{r}'$ is varied. We observe that the angular correlation between two simultaneously emitted photons is highest for photons emitted in the same direction ($\boldsymbol{r} = \boldsymbol{r}'$), while the correlation is lowest for emission in opposite directions ($\boldsymbol{r} = -\boldsymbol{r}'$).

Similar to the spectral properties described above, the second-order correlation depends on the atomic configuration considered. To illustrate this geometric effect, Figure 5.8 shows the second-order correlation function (5.71) for the four-atom system of Figure 5.3; this configuration has a threefold rotational symmetry. Comparing Figure 5.8 to 5.7 shows that the photons' angular correlations tend to exhibit a high symmetry if the underlying rotational symmetry of the atomic geometry is high.

We conclude this discussion on second-order photon correlations by considering the correlation function (5.71) for photons emitted simultaneously in the same direction. A $g^{(2)}(\boldsymbol{r}, \boldsymbol{r})$ value of 1 denotes that the photons are emitted at random and the corresponding emission statistics is described by a Poissonian distribution.

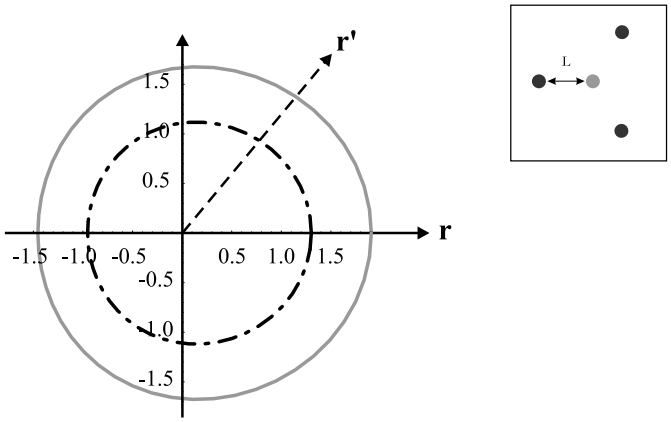

Figure 5.8: A polar plot of the normalized steady-state second-order correlation function $g^{(2)}(\boldsymbol{r}, \boldsymbol{r}')$ for a four-atom system. The inset shows the atomic configuration considered. The passive atoms (black) are positioned in an equilateral triangle with the pumped atom (grey) in the middle. All transition dipole moments are perpendicular to the atomic plane and to the plane of the polar plot. The position $\boldsymbol{r}$ is taken in the far-field along the axis connecting the pumped atom with one of the passive ones. The pump parameter is taken $W = 1.5$ (solid line) and $W = 10$ (dash-dotted line).

If $g^{(2)}(\boldsymbol{r}, \boldsymbol{r}) < 1$ the emitted photons are antibunched and the distribution is sub-Poissonian. For a single pumped atom, for example, the second-order correlation function reduces to zero, since a single atom cannot emit two photons at the same time. Values of $g^{(2)}(\boldsymbol{r}, \boldsymbol{r}) > 1$ denote a bunching of the emitted photons; the associated statistics are then super-Poissonian. For single-mode chaotic light, for example, the correlation function $g^{(2)}(\boldsymbol{r}, \boldsymbol{r})$ attains the value 2. To illustrate the effect of the pump on the normalized second-order correlation function, Figure 5.9 shows $g^{(2)}(\boldsymbol{r}, \boldsymbol{r})$ for the detection direction and atomic configurations considered in Figures 5.7 and 5.8. We observe that at low pump intensities the emitted photons are strongly bunched while the bunching is less pronounced at high pump intensities. In addition, while the quantitative behavior of the second-order correlation for $N = 3$ differs from $N = 4$, both cases exhibit the same qualitative trend, i.e., the correlation decreases with the absorbed power. The graphs in Figure 5.9 are shown up to the saturation point; at higher pump intensities (not shown in the graphs) the photon absorption rate decreases and the correlation drops and attains its limiting value $g^{(2)}(\boldsymbol{r}, \boldsymbol{r}) = 0$ in the limit $W \to \infty$, indicating a decoupling of the pumped atom and the passive atoms in correspondence with the power broadening mechanism mentioned above.

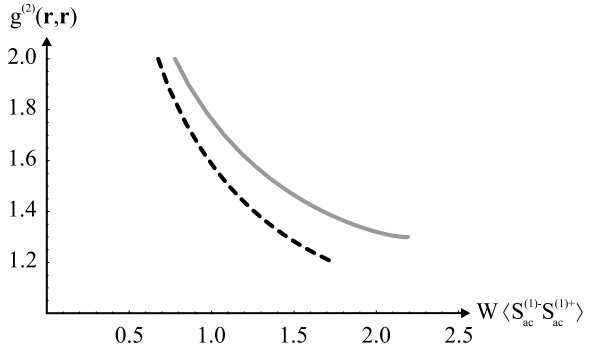

Figure 5.9: The normalized steady-state second-order correlation function $g^{(2)}(\boldsymbol{r},\boldsymbol{r})$ for an N-atom system versus the rate at which the system absorbs pump photons. The correlation function is shown for the three-atom configuration of Figure 5.7 (dashed line) and the four-atom configuration of Figure 5.8 (solid line). The direction of $\boldsymbol{r}$ is identical to the direction of $\boldsymbol{r}$ in Figures 5.7 and 5.8: along the atomic axis for the three-atom system and along a mid-perpendicular of the equilateral triangle for the four-atom system. The correlation functions are shown up to the point at which saturation sets in.

5.5 Comparison to macroscopic lasers

The physical properties of the N-atom systems under consideration result from the interplay between two key processes: the optical gain provided by the pumped atom, and the optical feedback provided by the passive atoms. Since the combination of gain and feedback is the core concept governing many laser-related phenomena, it is interesting to briefly elaborate on the above physical properties in terms of their counterparts in standard laser systems.

5.5.1 Mode competition

In section 5.4.1 we showed that the light emitted by an N-atom system can exhibit pronounced spectral narrowing as the applied pump intensity increases. In addition, we observed that the spectrum tends to symmetrize at high pump intensities, denoting the dominance of a single Lorentzian contribution to the spectrum. The spectral symmetrization can be interpreted in terms of *mode competition*, a well-known laser dynamic behavior [112]. As the far-field spectrum symmetrizes, the weights of the modes in which the N-atom system emits light are redistributed. To illustrate this mode redistribution, the far-field angle-integrated flux (5.64) can be written, using (5.56), as

$$\langle \phi(\omega) \rangle \, d\omega = \sum_{m=1}^{\kappa(N)} \mathrm{Re}\left[\frac{1/\pi}{i(\omega - \omega_{ca} - \omega_m) + \gamma_m} \tilde{\beta}_m \right] d\omega, \tag{5.72}$$

with as weight coefficients

$$\tilde{\beta}_m \equiv \sum_{i,j=1}^{N} \beta_m^{(ij)} \left(\delta_{ij}\Gamma_{ca} + (1-\delta_{ij}\Gamma^{(ij)}) \right). \tag{5.73}$$

We note that one must exert caution in the interpretation of the above mode weight coefficients. First, the contributions to the spectrum are not to be considered as modes in the strict sense due to the irreversible decay rate γ_m associated with each term; we will henceforth refer to the contributions to the spectrum as *pseudo modes*. Secondly, the weight coefficients (5.73) do not add up to 1 but obey, according to (5.66) and (5.67)

$$\sum_{m=1}^{\kappa(N)} \mathrm{Re}\left[\tilde{\beta}_m\right] = \int_{-\infty}^{\infty} \langle \phi(\omega) \rangle \, d\omega = W\Gamma_{ca} \lim_{t\to\infty} \left\langle \hat{\tilde{S}}_{ac}^{(1)-}(t) \hat{\tilde{S}}_{ac}^{(1)+}(t) \right\rangle, \tag{5.74}$$

expressing energy conservation. Finally, the weight coefficients (5.73) are in general complex-valued and their real part is not strictly positive. Taking into account the above considerations, we can consider the weight coefficients $\tilde{\beta}_m$ to denote to what extent each pseudo mode dominates the spectrum. To illustrate the system's mode redistribution as the pump intensity varies, Figure 5.10 shows the distribution of weight coefficients corresponding to the spectra of Figure 5.3. Since four atoms are involved, the number of pseudo modes is $\kappa(4) = 56$ according to Table 5.2. We observe that at low pump intensity the spectrum consists of two Lorentzian contributions while at high pump intensity a single pseudo mode dominates the spectrum. In addition, Figure 5.10 shows that the real part of the weight coefficients is larger at higher pump intensities; this enlargement indicates that the redistribution of weights occurs not only relative to the weights of other pseudo modes, but in absolute terms as well. In other words, one pseudo mode carries away most of the available gain in the system, analogous to the mode competition process in standard lasers.

5.5.2 Threshold behavior

One of the hallmarks of many laser systems is the manifestation of a threshold in the emitted power with varying pump intensity. As is elaborated on in [130], the details of the laser threshold depend strongly on the specific characteristics of the system. In addition, the concept of a laser threshold is, strictly speaking, well-defined only in the thermodynamic limit [99]. However, for reasons of comparison, we can consider the dependence of the emitted power in an N-atom system on the applied pump intensity. Figure 5.10(a) shows the dependence of the photon emission rate $\mathcal{J}(\Delta\widetilde{\omega})$

$$\mathcal{J}(\Delta\widetilde{\omega}) \equiv \int_{\omega_{ca}-\Gamma_{ca}/4}^{\omega_{ca}-\Gamma_{ca}/4} d\omega \, \langle \phi(\omega) \rangle \,, \tag{5.75}$$

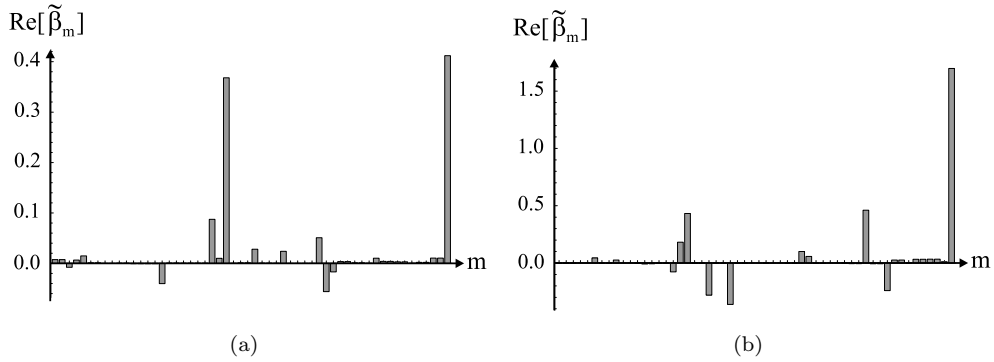

Figure 5.10: The real part of the spectral weights $\tilde{\beta}_m$ (in units of Γ_{ca}) which make up the far-field angle-integrated flux for the two cases considered in Figure 5.3. The index m is the mode number of each of the Lorentzian contributions to the flux. The total number of modes is 56. The weights are shown (a) for low pump ($W = 1.77$) intensity and (b) for high pump intensity ($W = 10.10$).

on the photon absorption rate. The atomic system under consideration is the axial three-atom system of Figure 5.7. The photon emission rate is shown for the range of pump intensities below the power broadening regime. The emission rate (5.75) is the rate at which photons are detected by a narrow band detector spectrally centered around the resonance frequency of a single atom. Figure 5.10(a) shows that the emitted power increases almost linearly with applied pump intensity; no features suggestive of a threshold are apparent. However, the spectrum of the emitted light is a superposition of $\kappa(N)$ Lorentzian contributions, each representing a different pseudo mode. Figure 5.10(b) focusses on the weight of the dominant pseudo mode which makes up the spectrum of Figure 5.10(a). Remarkably, the weight coefficient of the dominant pseudo mode does rise nonlinearly with increasing pump intensity; the weights of the other pseudo modes (not shown in the graph) are much smaller and do not exhibit similar behavior. The threshold-like increase of the weight coefficient of the dominant pseudo mode is, though reminiscent of the threshold prediction of chapter 3, not apparent in the full spectrum because of the large spectral overlap between different modes. The characteristics of a single mode will affect the full spectrum only if the system's gain narrowing is sufficiently pronounced (and the bandwidth of the detector sufficiently narrow). As we discussed in 5.4.1, a high degree of spectral narrowing in an N-atom system requires a high number of atoms. Therefore, the N-atom systems considered can exhibit threshold behavior in the emitted power only for high atom numbers.

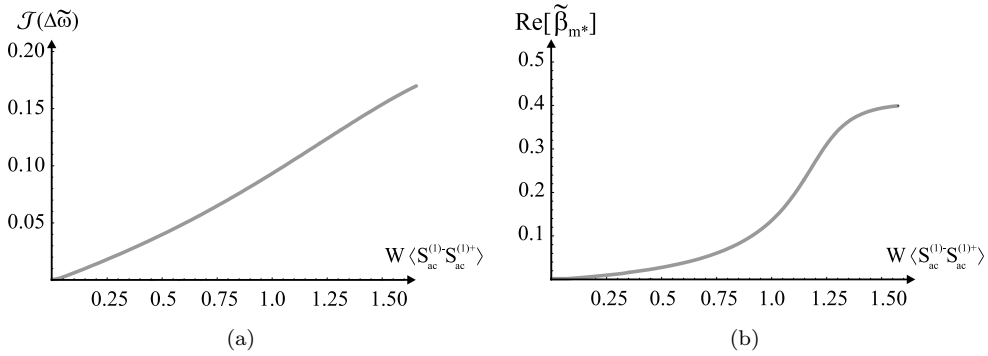

Figure 5.11: (a) The far-field angle-integrated photon emission rate $\mathcal{J}(\Delta\tilde{\omega})$ (in units of Γ_{ca}) in the range $\Delta\tilde{\omega} \equiv [\omega_{ca} - \Gamma_{ca}/4, \omega_{ca} + \Gamma_{ca}/4]$. The atomic system considered is the axial three-atom configuration of Figure 5.7. (b) The real part of the spectral weight $\tilde{\beta}_{m^*}$ (in units of Γ_{ca}) of the mode labeled m^* versus the absorbed power. The mode m^* of which the weight is shown is the mode that dominates the far-field angle-integrated flux at high pump values. The atomic system considered is the same as in (a).

5.5.3 Photon statistics

The interpretation of the second-order correlation in the N-atom systems under consideration is in general less intuitive than the interpretation of the corresponding first-order correlations. This observation is well-known in many types of lasers. Class-B lasers, for example, are characterized by a high cavity damping rate compared to the population inversion rate in the gain medium. The corresponding photon statistics of a class-B laser can remain thermal until far above threshold [130], in sharp contrast to common Poissonian behavior. Various other types of lasers, such as single-quantum dot microsphere lasers [13, 90, 92], exhibit similar behavior. On the other hand, single atoms in a cavity [17, 80, 86] exhibit pronounced photon antibunching with corresponding sub-Poissonian photon statistics. The above examples illustrate that the photon statistics of a laser depend strongly on the type of system under consideration; in addition, the intrinsic quantum nature of the presented analysis as opposed to classical laser theory further adds to the nontrivial character of the presented statistics.

5.6 Summary

In this chapter, we described the simplest microscopic systems which shows both gain and feedback. More precisely, we presented systems of only a few atoms in each other's near-field using an N-atom Master equation. We demonstrated that systems of N atoms with gain may show large gain narrowing and mode redistribution. Surprisingly, the presented systems exhibit behavior qualitatively similar to many macroscopic lasers. Adding more atoms to an N-atom system enhances the

observed spectral phenomena and allows more photons to propagate with a given coherence time. In addition, we discussed the nontrivial character of the statistics of the emitted photons. Finally, we elaborated on the connection between the physical properties of the presented N-atom systems and their counterparts in standard laser systems.

As mentioned above, the physical properties of an N-atom system in the presence of gain are determined by the system's photon storage capacity. Since the storage capacity in an N-atom system is limited by the number of atoms, we are computationally limited to systems which can store only a few photons. In the next chapter, we circumvent this computational restriction by altering the saturation of the passive atoms; this procedure will allow us to describe systems with storage capacities which are an order of magnitude larger than the ones presented sofar, leading to much more pronounced feedback-induced effects.

CHAPTER 6

One-atom laser oscillation with a single optical scatterer

We present an extension of the system presented in chapter 5 and consider a single atom interacting with one insaturable optical scattering object. The atom is pumped, providing gain to the system. The scatterer provides optical feedback through multiple scattering of light. We determine the dynamics of the atom-scatterer system by calculating the system's Master equation. We show that, if the atom and scatterer are in each other's near-field, the system exhibits large gain narrowing and threshold behavior in the emitted photon flux. To place the presented system in a broader perspective, we compare our results with a standard Jaynes-Cummings model and point out interesting deviations between both approaches. Finally, we relate the description of the atom and scatterer to the T-matrix formalism introduced in chapter 3.

6.1 Introduction

Microresonators have been a subject of considerable theoretical and experimental study over the last several years [120]. They show large potential in applications such as biological and chemical sensors [126], novel laser sources and dynamic filters in telecommunication [81, 103]. Additionally, microresonators are regarded as promising building blocks in the emerging field of quantum technology.

Systems in which microresonators are coupled to single atoms allow for a high control of light-matter interaction [40, 62, 101], which has led to significant progress in cavity QED and the ongoing drive towards quantum computing [11, 57, 95, 125]. In the interaction of a microresonator with a single atom, the introduction of gain

through optical pumping of the atom may lead to the realization of ultra small lasers such as single-quantum dot microsphere lasers [13, 90, 92]. Such systems are indicative of the current drive towards smaller laser systems, fueled by the desire for fast, low-power optical devices in highly integrated structures.

From a fundamental point of view, the drive towards miniaturization is continuously allowing for a better understanding of the microscopic processes governing laser oscillation: as laser systems are made smaller, a purely macroscopic description becomes inadequate and microscopic considerations should be taken into account, providing access to a wealth of interesting physical phenomena. In this chapter, we continue along this miniaturization trend and demonstrate its ultimate limit: the simplest microscopic system which shows pronounced many-photon laser behavior consists of a single two-level atom interacting with one insaturable optical scattering object. The atom is optically pumped, providing gain to the system. The scatterer supplies optical feedback through multiple scattering of light. The scatterer is characterized only by its polarizability, ensuring the validity of our model for a broad range of scatterers, such as plasmon resonances in a gold particle. We show that, depending on the applied pump intensity and the atom-scatterer coupling, the light emitted by the system can be highly coherent.

We start in section 6.2 by deriving the Master equation of an atom interacting with an insaturable scatterer. The presented derivation closely resembles the derivation of the N-atom Master equation as described in chapter 5 (we stress, though, that prior knowledge of chapter 5 is not required to appreciate the results presented in this chapter). The resulting atom-scatterer Master equation reveals the similarities between the description of an atom interacting with an optical scatterer and standard atom-field interaction. Section 6.3 focusses on the method of solving the Master equation in practice. In particular, we show to what extent this practical procedure deviates from solving the standard atom-field Master equation. Section 6.4 elaborates on the steady-state properties of the emitted light. We show that the system exhibits large gain narrowing and threshold behavior for increasing pump intensity. In addition, we determine the statistics of the emitted photons and show the nontrivial dependence of the second-order coherence of the emitted light on the optical feedback. Finally, in section 6.5 we elaborate in more detail on a few interesting features and consequences of the presented results. First, we compare our results with those obtained from a Jaynes-Cummings model and point out interesting deviations between both approaches. Secondly, we connect the presented results to the T-matrix formalism introduced in chapter 3.

6.2 The Master equation of an atom and an insaturable scatterer

We start by considering the system shown in Figure 6.1. An atom A interacts with an optical scatter S. The atom has two relevant energy levels a and c, separated by a frequency difference $\omega_{ca} \equiv \omega_c - \omega_a$. In relation to the previous chapters, we can regard the atom to be of the three-level type *abc* introduced in section 2.2. The

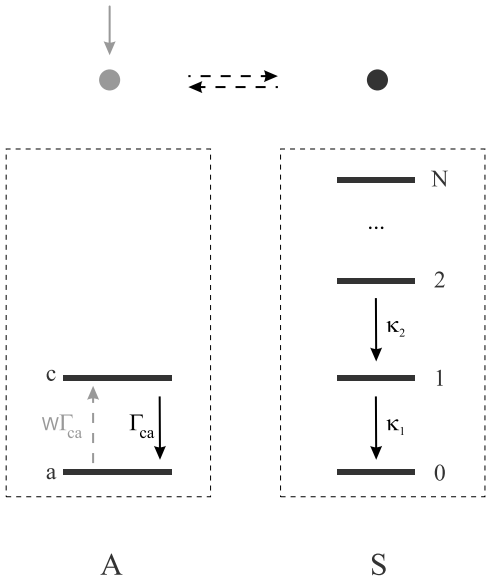

Figure 6.1: An atom A interacts with an optical scatterer S. The atom is incoherently pumped at a rate $W\Gamma_{ca}$. The scatterer has $N+1$ relevant excitations levels, each of which decays spontaneously to the adjacent lower-lying level.

atom is incoherently pumped with an external optical pump field; the corresponding pump rate is given by $W\Gamma_{ca}$ with W defined in (2.20). The scatterer S is fully characterized by the resonance behavior of its polarizability. We focus on frequencies near a resonance of S; the scatterer's energy diagram then corresponds to a damped harmonic oscillator with resonance frequency and decay rate determined by the resonance considered. Figure 6.1 shows the scatterer's $N+1$ lowest excitation levels with energy $\hbar\omega_j$. We consider scatterer resonances near the atomic transition frequency ω_{ca} and take $\omega_j \equiv j\omega_{ca}$. Each of the scatterer's energy levels decays at a rate $\kappa_j \equiv j\kappa$ to the adjacent lower-lying energy level. The transitions from level j to levels $j \pm 1$ are dipole-allowed, while all other transitions are considered forbidden. Extensions to multipole transitions are straightforward but lie outside the scope of this chapter [42].

We proceed with a general description of the atom-scatterer interaction. The total Hamiltonian $\hat{H}(t)$ describing the energies of the atom and scatterer, the electromagnetic field, and interactions is, in the standard electric dipole approximation, given by

$$\hat{H}(t) \equiv \hat{H}_c(t) + \hat{H}_S(t) + \hat{H}_R(t) + \hat{H}_{AR}(t) + \hat{H}_{SR}(t), \tag{6.1}$$

in the absence of a pump field (for didactic reasons, the pump will be included at a later stage of this presentation). The atomic Hamiltonian is given by

$$\hat{H}_c(t) \equiv \hbar\omega_{ca}\hat{S}^+_{ac}(t)\hat{S}^-_{ac}(t), \tag{6.2}$$

where $\hat{S}^+_{ac}(t)$ and $\hat{S}^-_{ac}(t)$ respectively create and annihilate an atomic excitation. The scatterer's Hamiltonian is given by

$$\hat{H}_S(t) \equiv \sum_{j=1}^{N} \hbar\omega_j \hat{S}^+_j(t)\hat{S}^-_j(t), \tag{6.3}$$

where $\hat{S}^+_j(t) = \left(\hat{S}^-_j(t)\right)^\dagger$ raises the scatterer's state from level $j-1$ to level j. The atom and scatterer are coupled to the three-dimensional multimode electromagnetic field (5.7) with Hamiltonian

$$\hat{H}_R(t) \equiv \sum_{\boldsymbol{k}\lambda} \hbar\omega_{\boldsymbol{k}\lambda}\hat{a}^\dagger_{\boldsymbol{k}\lambda}(t)\hat{a}_{\boldsymbol{k}\lambda}(t), \tag{6.4}$$

where the operators $\hat{a}^\dagger_{\boldsymbol{k}\lambda}(t)$ and $\hat{a}_{\boldsymbol{k}\lambda}(t)$ respectively create and annihilate a photon in the field mode $(\boldsymbol{k}, \lambda)$ at time t. The atom couples to the electromagnetic field through the Hamiltonian

$$\hat{V}_{AR}(t) = -\hat{\boldsymbol{d}}^{(A)}(t) \cdot \hat{\boldsymbol{E}}(t, \boldsymbol{r}_A), \tag{6.5}$$

where $\boldsymbol{r}_A$ is the atom's position vector, the electric-field operator $\hat{\boldsymbol{E}}(t, \boldsymbol{r})$ is given by (5.5) and the atomic dipole operator is defined as

$$\hat{\boldsymbol{d}}^{(A)}(t) \equiv \boldsymbol{d}^{(A)}_{ac}\left(\hat{S}^+_{ac}(t) + \hat{S}^-_{ac}(t)\right), \tag{6.6}$$

with $\boldsymbol{d}^{(A)}_{ac}$ the atom's transition dipole moment. The coupling of the scatterer to the electromagnetic field is expressed by the Hamiltonian

$$\hat{V}_{SR}(t) = -\hat{\boldsymbol{d}}^{(S)}(t) \cdot \hat{\boldsymbol{E}}(t, \boldsymbol{r}_S), \tag{6.7}$$

where $\boldsymbol{r}_S$ is the scatterer's position vector and where the dipole operator of the scatterer is defined as

$$\hat{\boldsymbol{d}}^{(S)}(t) \equiv \sum_{j=1}^{N} \boldsymbol{d}^{(S)}_j \left(\hat{S}^+_j(t) + \hat{S}^-_j(t)\right), \tag{6.8}$$

with $\boldsymbol{d}_j^{(S)}$ the transition dipole moment of the $(j-1) \rightarrow j$ transition. The decay rate κ_j and the transition dipole moment $\boldsymbol{d}_j^{(S)}$ are related according to expression (4.54) by

$$\kappa_j = j\kappa = \frac{1}{3\pi\varepsilon_0}\frac{\omega_{ca}^3}{\hbar c^3}\left(d_j^{(S)}\right)^2. \tag{6.9}$$

The above relation reveals that $d_j^{(S)} = \sqrt{j}d_{ac}^{(A)}$, which suggests the introduction of the operators [19]

$$\hat{b}_N^\dagger(t) \equiv \left(\hat{b}_N(t)\right)^\dagger \equiv \sum_{j=1}^{N} \sqrt{j}\hat{S}_j^+(t). \tag{6.10}$$

The operators $\hat{b}_N^\dagger(t)$ and $\hat{b}_N(t)$ respectively create and annihilate a scatterer excitation; the average number of excitations in the scatterer is given by

$$\left\langle \sum_{j=1}^{N} j\hat{S}_j^+(t)\hat{S}_j^-(t) \right\rangle = \left\langle \hat{b}_N^\dagger(t)\hat{b}_N(t) \right\rangle, \tag{6.11}$$

where the averaging is to be interpreted in a statistical sense, similar to chapter 5. In addition, the operators (6.10) obey the commutation relation

$$\left[\hat{b}_N(t), \hat{b}_N^\dagger(t)\right] = \hat{1} - N\hat{S}_N^+(t)\hat{S}_N^-(t), \tag{6.12}$$

from which we deduce that $\hat{b}_N^\dagger(t)$ and $\hat{b}_N(t)$ behave as standard boson creation and annihilation operations in the limit $N \rightarrow \infty$.

The dynamics of the atom-scatterer system can be expressed in terms of a Master equation [23, 30, 71, 107]. The Master equation describes the behavior of the density matrix of the atom-scatterer system. Alternatively, the Master equation allows us to determine the temporal evolution of the expectation value of any operator $\hat{Q}(t)$ acting on the atom and scatterer. The derivation of the atom-scatterer Master equation closely follows the derivation presented chapter 5; the resulting evolution of $\hat{Q}(t)$ is, in the Born-Markov approximation, given by

$$\frac{d}{dt}\left\langle \hat{Q} \right\rangle_0 = \left\langle \hat{\mathcal{L}}_{nd}\hat{Q} \right\rangle_0 + \left\langle \hat{\mathcal{L}}_d\hat{Q} \right\rangle_0. \tag{6.13}$$

We consider the radiation field to be in vacuum, as denoted by the subscript $\langle . \rangle_0$.

The non-dissipative part of the Master equation can be written as

$$\left\langle \hat{\mathcal{L}}_{nd}\hat{Q}\right\rangle_0 \equiv \frac{i}{\hbar}\left\langle [\hat{H}_c+\hat{H}_S+\hat{H}_{AS},\hat{Q}]\right\rangle_0, \tag{6.14}$$

with coupling Hamiltonian

$$\hat{H}_{AS} \equiv \hbar\delta^{(AS)}\hat{S}^+_{ac}\hat{b}_N + \text{H.c.}, \tag{6.15}$$

while the dissipative part of the Master equation is given by

$$\begin{aligned}\left\langle \hat{\mathcal{L}}_d\hat{Q}\right\rangle_0 \equiv &-\frac{\Gamma_{ca}}{2}\left\langle \hat{S}^+_{ac}\hat{S}^-_{ac}\hat{Q}-\hat{S}^+_{ac}\hat{Q}\hat{S}^-_{ac}\right\rangle_0 - \frac{\kappa}{2}\left\langle \hat{b}^\dagger_N\hat{b}_N\hat{Q}-\hat{b}^\dagger_N\hat{Q}\hat{b}_N\right\rangle_0\\ &-\frac{\Gamma^{(AS)}}{2}\left\langle \hat{S}^+_{ac}\hat{b}_N\hat{Q}+\hat{Q}\hat{S}^+_{ac}\hat{b}_N-2\hat{b}^\dagger_N\hat{Q}\hat{S}^-_{ac}\right\rangle_0\\ &-W\frac{\Gamma_{ca}}{2}\left\langle \hat{S}^-_{ac}\hat{S}^+_{ac}\hat{Q}-\hat{S}^-_{ac}\hat{Q}\hat{S}^+_{ac}\right\rangle_0 + \text{H.c.}.\end{aligned} \tag{6.16}$$

The coupling between the atom and the scatterer is quantified by the parameter

$$2\delta^{(AS)}-i\Gamma^{(AS)} = \frac{6\pi}{\omega_{ca}/c}\left(\Gamma_{ca}\kappa\right)^{1/2}\boldsymbol{\mu}^{(A)}_{ac}\cdot\overleftrightarrow{G}_0(\omega_{ca},\boldsymbol{r}_A-\boldsymbol{r}_S)\cdot\boldsymbol{\mu}^{(S)}, \tag{6.17}$$

with $\overleftrightarrow{G}_0$ the classical free-space Green function (3.46) and $\boldsymbol{\mu}^{(A)}_{ac}$ and $\boldsymbol{\mu}^{(S)}$ the normalized transition dipole moments of the atom and scatterer respectively. Similar to the derivation presented in chapter 5, the Master equation (6.13) is derived by integrating over the multimode electromagnetic field to which the atom and scatterer couple; this integration results in the appearance of the Green function (6.17) as an effective coupling term.

The resemblance of the atom-scatterer Master equation (6.13) and the N-atom Master equation (5.37) hints at the similar character of both systems: the vacuum-induced atom-scatterer coupling is identical to the coupling between two atoms (and hence, the coupling between two scatterers of the type currently considered). In other words, microscopic atomic and scatterer building blocks differ in a Master equation description only through their saturation character. The degree of saturation can be straightforwardly tweaked by replacing atomic raising and lowering operators by the corresponding scatterer operators (6.10); the number of levels taken into account then determines the resulting saturation character of the microscopic building blocks.

6.3 Solving the atom-scatterer Master equation

6.3.1 Physical quantities of interest

The Master equation (6.13) describes the interactions in an atom-scatterer system with gain within the Born-Markov approximation. Following the same presentation as in chapter 5, we aim at a description of the atom-scatterer system in terms of correlation functions of the emitted light. In what follows, we focus on the spectrum (5.38)

$$\langle \mathcal{I}(\omega, \boldsymbol{r}) \rangle \equiv \varepsilon_0 \frac{1}{2\pi} \int_{-\infty}^{\infty} d\tau e^{-i\omega\tau} \left\langle \hat{\boldsymbol{E}}^-(t+\tau, \boldsymbol{r}) \cdot \hat{\boldsymbol{E}}^+(t, \boldsymbol{r}) \right\rangle, \tag{6.18}$$

and the intensity-intensity correlation (5.42)

$$\left\langle \mathcal{G}^{(2)}(\boldsymbol{r}, \boldsymbol{r}') \right\rangle \equiv \lim_{t\to\infty} \varepsilon_0^2 \left\langle : \hat{I}(t, \boldsymbol{r}) \hat{I}(t, \boldsymbol{r}') : \right\rangle, \tag{6.19}$$

of the emitted light, where the colons denote normal ordering for the operators, and where the intensity operator is defined in (5.43) as

$$\hat{I}(t, \boldsymbol{r}) \equiv \hat{\boldsymbol{E}}^-(t, \boldsymbol{r}) \cdot \hat{\boldsymbol{E}}^+(t, \boldsymbol{r}). \tag{6.20}$$

In analogy with expression (5.45), the positive-frequency part of the electric-field operator is given in the far-field by

$$\begin{aligned} \hat{\boldsymbol{E}}^+(t, \boldsymbol{r}) = \hat{\boldsymbol{E}}_0^+(t, \boldsymbol{r}) + \frac{1}{4\pi\varepsilon_0 r} \frac{\omega_{ca}^2}{c^2} \Big(& |\boldsymbol{d}^{(A)}| \boldsymbol{u}_A(\boldsymbol{r}) \hat{S}_{ac}^-(t - |\boldsymbol{R}_A|/c) \\ & + |\boldsymbol{d}^{(S)}| \boldsymbol{u}_S(\boldsymbol{r}) \hat{b}_N(t - |\boldsymbol{R}_S|/c) \Big), \end{aligned} \tag{6.21}$$

with $\hat{\boldsymbol{E}}_0^+(t, \boldsymbol{r})$ the positive-frequency part of the quantum vacuum electric field operator (5.14) and where we defined $\boldsymbol{R}_i \equiv \boldsymbol{r} - \boldsymbol{r}_i$ with $i = A, S$ and used notation (5.55)

$$\boldsymbol{u}_i(\boldsymbol{r}) \equiv \boldsymbol{\mu}_{ac}^{(i)} - \boldsymbol{R}_i \frac{\boldsymbol{R}_i \cdot \boldsymbol{\mu}_{ac}^{(i)}}{|\boldsymbol{R}_i|^2}, \qquad i = A, S \tag{6.22}$$

characteristic for the dipole radiation of the atom and scatterer.

6.3.2 Categorization of operator expectation values

The correlation functions (6.18) and (6.19) are expressed through (6.21) in terms of operators acting on the atom and scatterer only. The absence of any field operators in both correlation functions ensures that both expressions can be expanded using the Master equation (6.13). In the limit $N \to \infty$, the operators $\hat{b}_N^\dagger$ and $\hat{b}_N$ obey the standard boson commutation relations, as mentioned above. The Master equation (6.13) in the limit $N \to \infty$ strongly resembles the Master equation governing the interaction of an atom and a single electromagnetic field mode; we will elaborate in more detail on this similarity further on. Based on the similarity between both aforementioned Master equations, one might at first attempt to solve both equations in a similar way. However, standard atom-field interaction theory relies on an adiabatic elimination of the system's coherences. Since such elimination is not justified in the present atom-scatterer system, we proceed along a different path, discussed in Appendix D: we consider only the $N+1$ lowest levels of the scatterer, with N depending on the system parameters (such as the atom-scatterer separation and the pump intensity). If the average number of scatterer excitations $\left\langle \hat{b}_N^\dagger \hat{b}_N \right\rangle$ is then much smaller than $N/2$, our predictions coincide with the $N \to \infty$ situation.

The description of the atom-scatterer system thus effectively reduces to a description of the interaction of a two-level and an $(N+1)$-level system. Similar to the procedure described in section 5.3.2, we can simplify the expansion of the correlation functions (6.18) and (6.19) by a proper categorization of the operators acting on the atom and scatterer. The state space of the atom-scatterer system has $2(N+1)$ dimensions; the corresponding operator space has $4(N+1)^2$ dimensions. The latter may be spanned by products of operators $\hat{S}_j^{\pm}$ acting on either the atom ($j = ac$) or the scatterer ($j \in \{1, ..., N\}$). These product operators form a basis; each of these basis operators changes the number of excitations in the system by an integer number Δm with $-(N+1) \leq \Delta m \leq N+1$. As discussed in chapter 5, the quantum regression theorem ensures that only basis operators with the same Δm are coupled through their evolution equation; if only a few Δm subspaces are of interest, the increase in computational efficiency due to this categorization is considerable. Since we aim at the determination of the field-field and intensity-intensity correlations of the emitted light, we only need to focus on the subspaces $\Delta m = 1$ and $\Delta m = 0$. The dimensionality $\nu(N, \Delta m)$ of these subspaces is

$$\nu(N, 1) = 4N, \qquad \nu(N, 0) = 4N + 1, \tag{6.23}$$

in sharp contrast to the $4(N+1)^2$ dimensionality of the entire atom-scatterer operator space. Expressions (6.23) show that the dimensions of the matrix which describes an atom-scatterer system increase linearly with the system's storage capacity N; this scaling behavior is much more favorable than the corresponding scaling of N-atom systems shown in Tables 5.1 and 5.2. This difference in computational effort implies that, in practice, the storage capacities we can deal with in atom-scatterer systems are easily an order of magnitude larger than the capacities

in few-atom systems .

The above categorization of basis operators allows for an efficient description of atom-scatterer systems. The symbolic evolution matrices associated with the $\Delta m = 0$ and $\Delta m = 1$ subspaces are computer-generated for each N. In the next sections, we use the numerical inversion and diagonalization of these matrices to study the field-field and intensity-intensity correlations of the light emitted by the atom-scatterer system.

6.4 Characteristics of the atom-scatterer system

The spectral distribution of the light emitted by the atom-scatterer system depends on the pump intensity and the atom-scatterer coupling. The latter is determined by the separation $|\boldsymbol{r}_A - \boldsymbol{r}_S|$ through expression (6.17). If the separation between the atom and the scatterer is much larger than the wavelength $2\pi c/\omega_{ca}$, the optical feedback in the system is insufficient for any observable feedback-related phenomena to occur. We therefore focus on atom-scatterer separations of the order of the wavelength and smaller.

6.4.1 The spectrum

We demonstrated in section 5.3.3 that, as a general result of the Master equation, the spectrum of the emitted light can be expressed as a sum of Lorentzian contributions. The total number of contributions is given by $\nu(N, 1)$; each of these Lorentzians is characterized by a central frequency, a spectral width and a spectral weight. Similar to the description of N-atom systems, the weight of each Lorentzian expresses to what extent each contribution dominates the total spectrum; varying the pump intensity induces mode competition in the system.

To study the effect of a varying pump intensity on the spectrum of the emitted light, we determine the angle-integrated far-field photon flux

$$\langle \phi(\omega) \rangle \, d\omega = \frac{c}{\hbar \omega_{ca}} \int_{4\pi} r^2 d\Omega \, \langle \mathcal{I}(\omega, \boldsymbol{r}) \rangle \, d\omega, \tag{6.24}$$

expressed in s^{-1}. The flux (6.24) measures the total number of photons detected in the far-field in the frequency range $[\omega, \omega + d\omega]$. Figure 6.2 visualizes the effect of the pump intensity on the photon flux. The flux is shown for a typical low ($W = 3$) and a high ($W = 30$) pump intensity. At low pump intensity, the emission spectrum is broad, while at higher pump intensities the spectrum is much narrower than the natural line width Γ_{ca}. In addition, we observe that an increase of the pump intensity reduces the asymmetry of the spectrum, which denotes that a single mode dominates the spectrum at high pump intensities. The symmetrization of the spectrum for increasing pump is similar to the corresponding behavior of an N-atom system discussed in chapter 5.

Comparing Figure 6.2 to the spectrum of a four-atom system shown in Figure

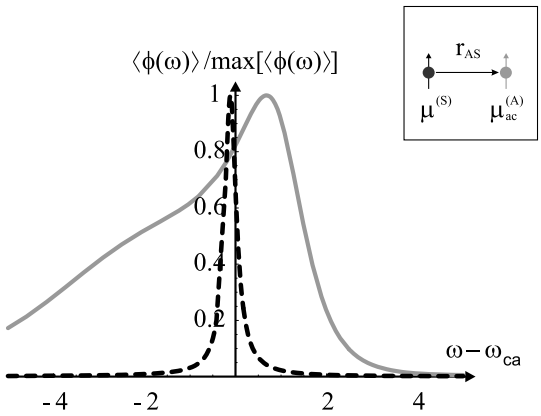

Figure 6.2: The normalized far-field angle-integrated photon flux versus frequency (in units of Γ_{ca}) of an atom-scatterer system. The decay rates of the atom and scatterer are chosen equal ($\Gamma = \kappa$). The atom-scatterer distance is $|\boldsymbol{r}_A - \boldsymbol{r}_S| = 0.52c/\omega_{ca}$. The inset shows the orientation of the transition dipole moments of the atom and scatterer. The spectrum is shown for a low pump intensity $W = 3$ (solid line) and a high pump intensity $W = 30$ (dashed line). At high pump intensity we observe pronounced gain narrowing.

5.3 reveals that the manifestation of gain narrowing in an atom-scatterer system is much more pronounced than the narrowing in a few-atom system; this observation is intimately related to the Schawlow-Townes effect described in section 5.4.1 and the large storage capacity of the scatterer compared to the capacity of a few-atom system.

To visualize the spectral properties of the emitted light for a broad range of pump intensities, we determine the spectral full width at half maximum $\Delta\omega$ and the maximum photon flux of the far-field angle-integrated flux for the same atom-scatterer configuration as in Figure 6.2. We vary the number of scatterer levels N until a further increase of N no longer affects the spectrum; the system dynamics then correspond to the $N \to \infty$ situation. Figure 6.3 show how $\Delta\omega$ and $\max[\langle\phi(\omega)\rangle]$ vary with the rate $W\Gamma_{ca}\left\langle \hat{S}_{ac}^{-}\hat{S}_{ac}^{+}\right\rangle$ at which pump photons are absorbed by the system. We observe that the spectral width $\Delta\omega$ decreases while the peak spectral photon flux increases with the pump photon absorption rate. Both $\Delta\omega$ and $\max[\langle\phi(\omega)\rangle]$ exhibit saturation behavior at high pump intensities and small N. We observe that at higher N, saturation sets in at higher pump photon absorption rates, indicating that the observed saturation is caused by the finiteness of N. Additionally, we observe that the pump photon absorption rate has a maximum in the limit $N \to \infty$. This limitation is a natural consequence of the power broadening inherent to the three-level pumping scheme, as discussed in section 2.4 and 5.2.2: the ground level of the gain atom broadens as the pump intensity increases, causing the atom and scatterer to effectively decouple at higher pump intensities, which imposes an intrinsic limit on the rate at which pump photons are absorbed. In relation to the threshold prediction of chapter 3, Figure 6.3 shows that the atom-

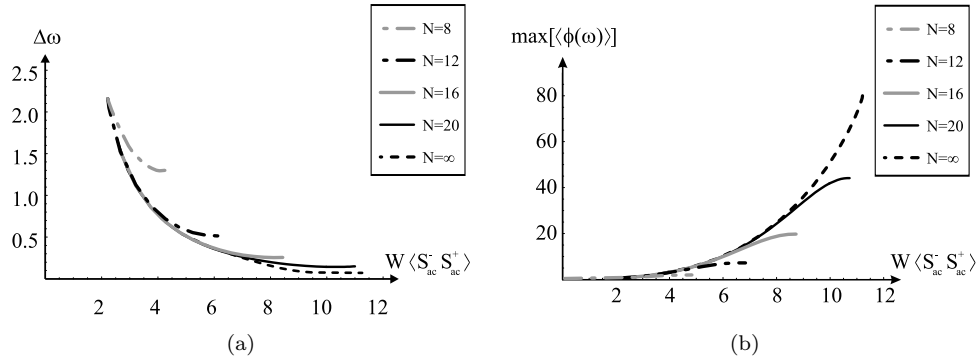

Figure 6.3: (a) The full width at half maximum $\Delta\omega$ (in units of Γ_{ca}) and (b) the maximum flux function $\max[\langle\phi(\omega)\rangle]$ of the angle-averaged far-field spectrum of an atom-scatterer system versus the pump photon absorption rate (in units of Γ_{ca}). The atom-scatterer configuration is the identical to the configuration of Figure 6.2. The number of resonator levels is $N = 8$ (grey dash-dotted line), $N = 12$ (black dash-dotted line), $N = 16$ (grey solid line), $N = 20$ (black solid line). These graphs are shown up to the regime at which saturation. The black dashed line represents $N = 32$, which practically coincides with the $N \to \infty$ limit.

scatterer system under consideration exhibits a smooth crossover from a spectrally broad regime dominated by spontaneous emission at low pump intensities ($W < 1$) to a regime with high spectral density at high pump intensities ($W \gg 1$), indicative of laser oscillation in the system.

The spectral properties not only vary with the applied pump intensity, but also with the optical feedback in the system. The system's feedback is determined by the atom-scatterer separation through the coupling (6.17). To illustrate the effect of a change in separation, Figure 6.4 shows the far-field angle-integrated spectrum for a fixed pump intensity $W = 40$ and different atom-scatterer separations. We observe a dramatic increase of the system's photon emission rate and degree of spectral narrowing as the atom-scatterer separation is reduced. This effect indicates that a larger feedback causes the pump photons to be more efficiently converted into photons with energy near $\hbar\omega_{ca}$, accompanied by an enhancement of their coherence time $\Delta\omega^{-1}$.

The spectral properties of the atom-scatterer system can be attributed to the interplay of the system's two key ingredients: optical gain and optical feedback. The atom-scatterer is a laser system in which the optical feedback is provided by multiple scattering of light and the optical gain is incorporated by a single pumped atom. The spectral narrowing and threshold behavior shown in Figure 6.3 are indicative of the laser behavior in the system.

The coherence properties of the atom-scatterer laser system described sofar are associated with correlation functions of the electric field. In the next section, we focus on correlations of the field intensity to describe the statistical properties of

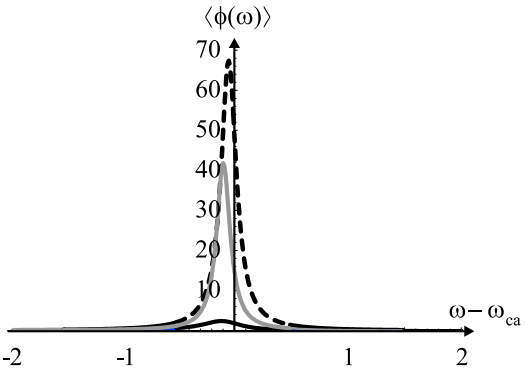

Figure 6.4: The flux function $\langle\phi(\omega)\rangle$ of an atom-scatterer system versus frequency (in units of Γ_{ca}). The decay rates of the atom and scatterer are chosen equal: $\Gamma = \kappa$. The spectrum is shown for $W = 40$. The atom-scatterer configuration is identical to the configuration of Figure 6.2 with $|\boldsymbol{r}_A - \boldsymbol{r}_S|$ equal to $0.62c/\omega_{ca}$ (black solid line), $0.52c/\omega_{ca}$ (grey solid line) and $0.42c/\omega_{ca}$ (black dashed line). The spectra shown illustrate that the spectral width strongly depends on the atom-scatterer separation.

the emitted photons.

6.4.2 Second-order photon correlations

We proceed by considering the normalized intensity-intensity correlation function (5.71)

$$g^{(2)}(\boldsymbol{r}, \boldsymbol{r}') \equiv \frac{\left\langle \mathcal{G}^{(2)}(\boldsymbol{r}, \boldsymbol{r}') \right\rangle}{\langle \mathcal{I}(\boldsymbol{r}) \rangle \langle \mathcal{I}(\boldsymbol{r}') \rangle}, \tag{6.25}$$

using definitions (6.19) and (5.41). As we discussed in chapter 5, a random angular distribution of the emitted photons corresponds to $g^{(2)}(\boldsymbol{r}, \boldsymbol{r}') = 1$; a normalized second-order correlation function larger than unity denotes an increased angular correlation with respect to the random one, while a value lower than unity reveals a reduced correlation.

In general, the second-order correlation function (6.25) depends on the pump intensity, the atom-scatterer coupling and the positions $\boldsymbol{r}$ and $\boldsymbol{r}'$ at which photons are detected. To illustrate the effect of an increased pump intensity on the second-order coherence, we determine $g^{(2)}(\boldsymbol{r}, \boldsymbol{r})$ for the same parameters as in Figure 6.3. In analogy with the calculation of the system's spectral properties, we increase N until the statistics no longer vary with N; the resulting correlation function then corresponds to the $N \to \infty$ limit. Figure 6.5 shows the resulting variation of $g^{(2)}(\boldsymbol{r}, \boldsymbol{r})$ with the rate at which pump photons are absorbed. We observe that $g^{(2)}(\boldsymbol{r}, \boldsymbol{r}) \gg 1$ at small pump rates; as the photon absorption rate increases, the

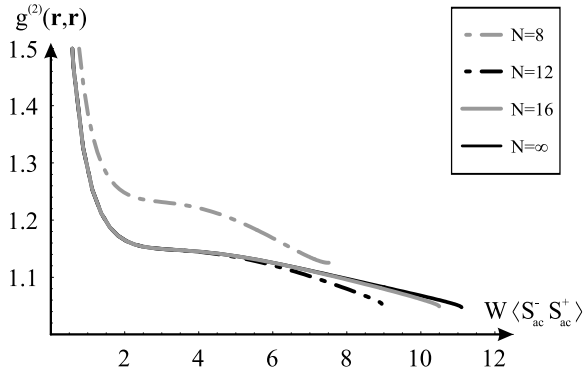

Figure 6.5: The normalized intensity-intensity correlation function $g^{(2)}(\boldsymbol{r},\boldsymbol{r})$ versus the rate at which the system absorbs pump photons (in units of Γ_{ca}). The detection position $\boldsymbol{r}$ is in the far-field, along the atom-scatterer axis ($\boldsymbol{r}/|\boldsymbol{r}| = (\boldsymbol{r}_S - \boldsymbol{r}_A)/|\boldsymbol{r}_S - \boldsymbol{r}_A|$). The atom-scatterer configuration is identical to the configuration of Figure 6.2. The number of resonator levels is $N = 8$ (grey dash-dotted line), $N = 12$ (black dash-dotted line), $N = 16$ (grey solid line). These graphs are shown up to the regime at which saturation of the scatterer or power broadening of the atom sets in. The black solid curve represents $N = 20$, which coincides with the $N \to \infty$ limit for the correlation function shown.

correlation decreases and approaches the coherent limit $g^{(2)}(\boldsymbol{r},\boldsymbol{r}) = 1$. Similarly to the spectral properties mentioned above, the second-order correlation exhibits saturation behavior at small N. It is interesting to note that $g^{(2)}(\boldsymbol{r},\boldsymbol{r})$ attains a limiting value at much lower values of N compared to the absorption rate. For the configuration shown in Figure 6.5, for example, the limiting value of $g^{(2)}(\boldsymbol{r},\boldsymbol{r})$ varies only marginally above $N = 12$, while the photon absorption rate saturates only around $N = 20$. This contrast indicates that, for N large enough, a further increase of N leads to a higher photon output rate without increasing the photons' second-order coherence.

Similar to the description of angular correlations in chapter 5, we can evaluate the normalized intensity-intensity correlation function (6.25) for simultaneously emitted photons detected at different positions $\boldsymbol{r}$ and $\boldsymbol{r}'$. Figure 6.6(a) shows the resulting correlation functions for two different pump intensities. In correspondence with Figure 6.5 we observe that the second-order correlations decrease as the pump increases. In addition, the geometrical symmetry of $g^{(2)}(\boldsymbol{r},\boldsymbol{r}')$ increases with increasing pump intensity. In other words, the atom-scatterer system tends to exhibit random angular correlations at high pump intensity, in contrast to, e.g., the three-atom system of Figure 5.7. The different symmetry of the angular correlations of the three-atom system and the atom-scatterer system are, besides being due to the obvious configurational difference, related to the different number of stored excitations in these systems. The number of photons which contribute to the correlation functions of interest is typically much higher in an atom-scatterer system than in a few-atom system due to the aforementioned difference in storage capacity. Since the statistics are derived from the emitted photons, the correlations in a few-atom

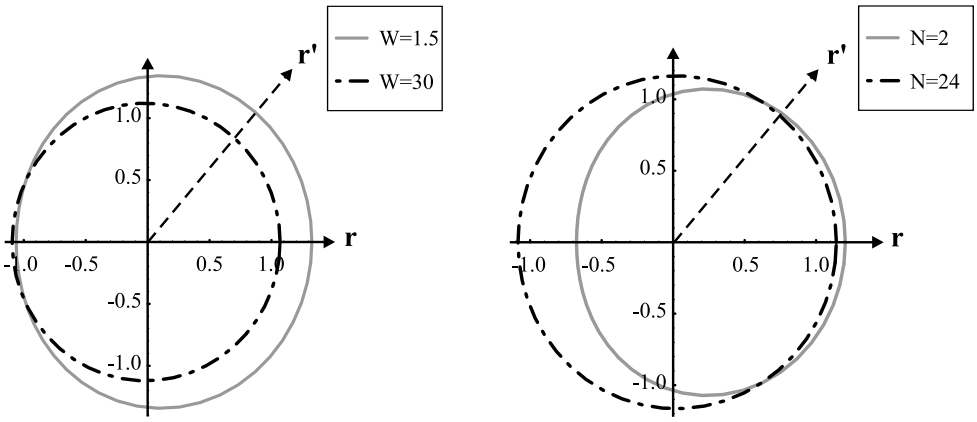

(a) (b)

Figure 6.6: A polar plot of the normalized second-order correlation function $g^{(2)}(\boldsymbol{r}, \boldsymbol{r}')$. One detection position $\boldsymbol{r}$ is in the far-field, along the atom-scatterer axis ($\boldsymbol{r}/|\boldsymbol{r}| = (\boldsymbol{r}_S - \boldsymbol{r}_A)/|\boldsymbol{r}_S - \boldsymbol{r}_A|$). The other detection point $\boldsymbol{r}'$ is varied in the plane perpendicular to the transition dipole moments of the atom and scatterer. The atom-scatterer configuration is identical to the configuration of Figure 6.2. Figure (a) shows $g^{(2)}(\boldsymbol{r}, \boldsymbol{r}')$ for $N = 24$ scatterer levels. The pump parameter is $W = 1.5$ (grey solid line) and $W = 30$ (black dash-dotted line). Figure (b) shows $g^{(2)}(\boldsymbol{r}, \boldsymbol{r}')$ for a pump parameter $W = 10$. The number of scatterer levels is $N = 2$ (grey solid line) and $N = 24$ (black dash-dotted line).

system typically differ from those in an atom-scatterer system. Figure 6.6(b) illustrates the influence of the system's storage capacity on the second-order correlation function for the same configuration as in Figure 6.6(a). The angular correlation is shown for $N = 24$ (which coincides with the $N \to \infty$ limit) and $N = 2$ (in which case the system reduces to a two-atom system). We observe that, as mentioned above, the different saturation character of the $N = 24$ case as compared to the $N = 2$ case clearly affects the resulting second-order correlations.

6.4.3 Comparison to few-atom systems

The above discussion on the photons' second-order correlations demonstrates the challenging nature of interpreting higher-order photon correlations in the systems with gain of interest, as we pointed out in chapter 5. Comparing Figures 6.3 and 6.6 illustrates the well-known fact that a drastic change in first-order correlations is not necessarily accompanied by a large change in second-order correlations. The non-trivial statistics discussed above denote that the atom-scatterer system presented here is a laser in the bad-cavity limit [29, 49, 130]. The mode redistribution associated with the laser character of the atom-scatterer system is illustrated in Figure 6.7. Following the discussion on mode competition of section 5.5.1, we plot the weight coefficients $\tilde{\beta}_m$ of each of the Lorentzian contributions that make up the

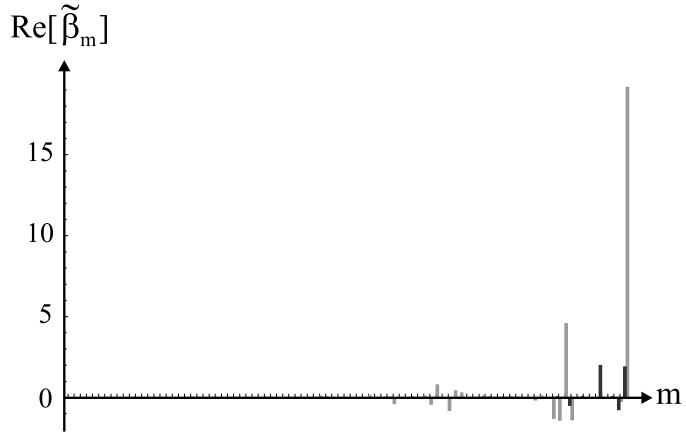

Figure 6.7: The real part of the spectral weights $\tilde{\beta}_m$ (in units of Γ_{ca}) which make up the far-field angle-integrated flux for the two cases considered in Figure 6.2. The index m is the mode number of each of the Lorentzian contributions to the flux. The total number of modes is $\nu(23,1) = 92$. The weights are shown at low pump intensity $W = 3$ (black) intensity and at high pump intensity $W = 30$ (grey).

spectrum

$$\langle \phi(\omega) \rangle \, d\omega = \sum_{m=1}^{\nu(N,1)} \mathrm{Re}\left[\frac{1/\pi}{i(\omega - \omega_{ca} - \omega_m) + \gamma_m} \tilde{\beta}_m \right] d\omega. \tag{6.26}$$

The expansion (6.26) is the atom-scatterer analogy of the N-atom expression (5.72). As an illustration, Figure 6.7 shows the weight distribution for the far-field angle-integrated spectra of Figure 6.2. We observe pronounced mode-competition effects with increasing pump intensity. In addition, comparing Figure 6.7 to the mode distribution as shown in Figure 5.10 for a four-atom system reveals that the large storage capacity of atom-scatterer systems ensures that gain-induced mode competition is much more pronounced in atom-scatterer systems compared to few-atom systems, as we expect.

6.5 The atom-scatterer system in a broader perspective

6.5.1 Comparison with a Jaynes-Cummings approach

The Master equation (6.13) describes the interaction of an atom and a harmonic scatterer in the Born-Markov approximation. Interestingly, the equation (6.13)

strongly resembles the Master equation describing the interaction of an atom with gain and a single field mode, given by

$$\begin{aligned}\frac{d}{dt}\left\langle \hat{Q}\right\rangle_0 =& \frac{i}{\hbar}\left\langle [\hat{H}_A+\hat{H}_S+\hat{\tilde{H}}_{AS},\hat{Q}]\right\rangle_0 - \frac{\Gamma_{ca}}{2}\left\langle \hat{S}^+_{ac}\hat{S}^-_{ac}\hat{Q}+\hat{Q}\hat{S}^+_{ac}\hat{S}^-_{ac}-2\hat{S}^+_{ac}\hat{Q}\hat{S}^-_{ac}\right\rangle_0 \\ &- \frac{\kappa}{2}\left\langle \hat{b}^\dagger_N\hat{b}_N\hat{Q}+\hat{Q}\hat{b}^\dagger_N\hat{b}_N-2\hat{b}^\dagger_N\hat{Q}\hat{b}_N\right\rangle_0 \\ &- W\frac{\Gamma_{ca}}{2}\left\langle \hat{S}^-_{ac}\hat{S}^+_{ac}\hat{Q}+\hat{Q}\hat{S}^-_{ac}\hat{S}^+_{ac}-2\hat{S}^-_{ac}\hat{Q}\hat{S}^+_{ac}\right\rangle_0, \end{aligned} \tag{6.27}$$

with as interaction Hamiltonian

$$\hat{\tilde{H}}_{AS} \equiv \hbar g\hat{S}^+_{ac}\hat{b}_N + \text{H.c.}, \tag{6.28}$$

in the limit $N \to \infty$. In the above equation, the operators $\hat{b}^\dagger_N$ and $\hat{b}_N$ are interpreted as operators which respectively create and annihilate a field excitation in the mode of interest. The coupling g in the atom-field Hamiltonian (6.28) is real-valued and quantifies the atom-field interaction strength; the interaction Hamiltonian (6.28) is often referred to as an interaction of the *Jaynes-Cummings* type [60, 110]. Comparing equations (6.13) and (6.27) reveals that the only mathematical difference between the atom-scatterer Master equation and the Master equation of an atom and a single field mode is the absence of an incoherent coupling term $\Gamma^{(AS)}$ in the latter. This mathematical distinction originates from a contrast in the underlying physical approach leading to the above descriptions: while the atom-field coupling (6.28) is established irrespective of the presence of a reservoir, the atom-scatterer coupling *results* from an integration over the reservoir. Figure 6.8 further illustrates this conceptual difference. In a Jaynes-Cummings description of atom-field interaction, the atom and field are modeled assuming both systems interact with separate (but identical) reservoirs. Integrating the system over both reservoirs results in spontaneous decay of the atom and field mode; the atom-field coupling is unaffected by this integration. Conversely, in an atom-scatterer system, the atom and scatterer interact with a single reservoir. Integrating the system over the reservoir results in spontaneous decay of the atom and field mode *and* the emergence of an effective coupling; this coupling is quantified by the free-space Green function (6.17).

We now focus on the condition under which an atom-scatterer system is well-described by a Jaynes-Cummings model. The coupling (6.17) induces two effects on the atom and scatterer, corresponding to the real and imaginary part of the Green function. First, the energy levels of the atom and scatterer are shifted; this shift is proportional to $\hbar\delta^{(AS)}$. Secondly, the atom-scatterer coupling changes the life times of the energy levels; the spontaneous decay rate of the coupled system therefore differs from the decay rates of the individual subsystems. This life-time effect can be attributed to the imaginary part $\Gamma^{(AS)}$ of the Green function (6.17). Consequently,

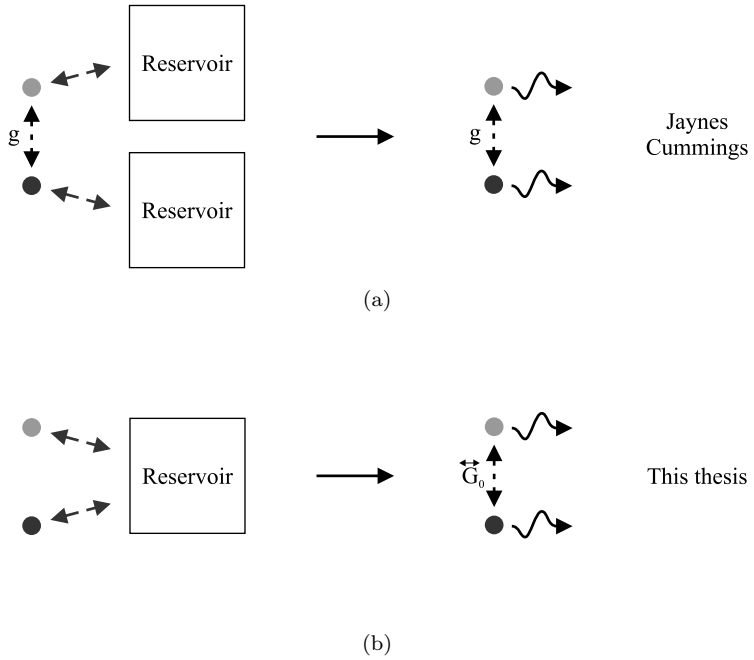

Figure 6.8: An illustration of the conceptual difference between atom-field coupling of the Jaynes-Cummings type and atom-scatterer coupling as described in this chapter. (a) An atom (grey dot) interacts with a single field mode (black dot). The atom and field interact with separate (but identical) reservoirs (dashed arrows). Integrating the system over both reservoirs (solid black arrow) results in spontaneous decay of the atom and field mode (curly arrows). The atom-field coupling g remains unaffected by the integration. (b) An atom (grey dot) interacts with a scatterer (black dot). The atom and scatterer interact with a single reservoir (dashed arrows). Integrating the system over the reservoir (solid black arrow) results in spontaneous decay of the atom and scatterer (curly arrows) and the emergence of an effective coupling.

a Jaynes-Cummings description can be in good approximation applied to describe an atom-scatterer system if the coupling induces only small changes in the decay rates of the atom and scatterer. Since the incoherent atom-scatterer coupling is proportional to $\sqrt{\Gamma_{ca}\kappa}$, we expect the induced change in decay rate to be negligible in the limiting cases $\Gamma_{ca} \gg \kappa$ and $\Gamma_{ca} \ll \kappa$. To illustrate the analogy between an atom-scatterer coupling and a coupling of the Jaynes-Cummings type, Figure 6.9 shows the far-field angle-integrated spectrum for different decay rates of the atom and scatterer. We compare the spectrum as obtained from the Master equation (6.13) with the spectrum obtained by taking $\Gamma^{(AS)} = 0$ while retaining $\delta^{(AS)}$. Figure 6.9(a) depicts the spectrum at low pump intensity ($W = 3$) for an atom and scatterer with equal decay rates $\Gamma_{ca} = \kappa$. A clear distinction between the $\Gamma^{(AS)} = 0$ and $\Gamma^{(AS)} \neq 0$ calculation is apparent which we expect given the equal decay rates of the atom and scatterer. Conversely, Figure 6.9(b) shows the spectrum obtained

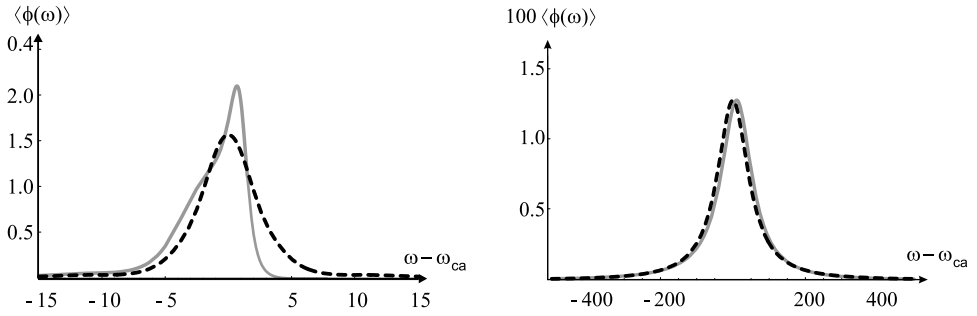

Figure 6.9: The far-field angle-integrated spectrum versus frequency (in units of Γ_{ca}). The atom-scatterer configuration is identical to the configuration of Figure 6.2. The spectrum is shown with (Jaynes-Cummings coupling, black dashed line) and without (coupling in this thesis, grey solid line) the $\Gamma^{(AS)} = 0$ approximation. The system parameters are (a) $W = 3$ and $\Gamma_{ca} = \kappa$ (b) $W = 3$ and $1000\Gamma_{ca} = \kappa$.

for an atom and scatterer with $1000\Gamma_{ca} = \kappa$; we observe that the large difference in decay rate of the atom and scatterer indeed leads to a better agreement between the above calculations.

6.5.2 Comparison with T-matrix formalism

We conclude this chapter by connecting the present atom-scatterer systems to the atomic systems and their description presented in chapters 2 to 5. In chapter 2, we demonstrated how the Master equation of a scattering systems allows for the determination of the system's T-matrix. Following a similar derivation, we can deduce that the T-matrix of the scatterer presented in Figure 6.1 is given by

$$\hat{\overleftrightarrow{T}}_S(\omega) = t_S(\omega)\delta(\boldsymbol{r} - \boldsymbol{r}_S)\hat{\mathbb{1}} \otimes \boldsymbol{\mu}^{(S)} \otimes \boldsymbol{\mu}^{(S)}, \tag{6.29}$$

with

$$t_s(\omega) \equiv \frac{3\pi}{\omega_{ca}/c} \frac{\kappa}{\left(\omega - \omega_{ca} + i\frac{\kappa}{2}\right)}, \tag{6.30}$$

where $\hat{\mathbb{1}}$ is a unit operator with matrix elements $\langle \boldsymbol{r}|\hat{\mathbb{1}}|\boldsymbol{r}'\rangle = \delta(\boldsymbol{r} - \boldsymbol{r}')$, introduced in chapter 2. Comparing (6.29) with the T-matrix of a two-level atom (2.28) confirms the intuitive notion that the T-matrix of a harmonic oscillator is identical to the T-matrix of a two-level atom, apart from the presence of a saturation term in the latter.

chapter	saturation of gain atom	saturation of passive scatterer(s)
3	none at threshold	none at threshold
4	-	broadband (first-order)
5	broadband	broadband
6	broadband	none

Table 6.1: A comparison of the saturation character of different scattering building blocks, depending on their description.

The T-matrix (6.29) allows us to compare the atom-scatterer systems presented here to the atomic systems of previous chapters. In the description of few-atom systems with gain in chapter 3, we limited ourselves to atomic saturation caused by an incident external probe field and neglected all off-resonant interactions. In section 3.4, we investigated the properties of a two-atom in the absence of an external probe. We defined a "threshold" characterizing the conditions under which a nonzero field can build up; at the threshold, the atoms are considered to be unsaturated. In chapter 4 we calculated a first-order estimation of the saturation of a passive atom due to incident broadband light. In chapter 5 we generalized this type of saturation and included atomic saturation due to off-resonant light in all scattering orders. The insaturable character of the scatterers presented above position the atom-scatterer systems between the insaturable atoms at threshold of chapter 3 and the saturable atoms of chapter 5. To illustrate this position of the atom-scatterer systems, Table 6.1 shows a comparison of the saturation character of the scattering building blocks presented in previous chapters.

6.6 Summary

The aim of this chapter was to present the simplest exactly solvable microscopic system which shows many-photon laser behavior. We have shown that a single pumped atom interacting with one optical scatterer exhibits pronounced gain narrowing and threshold behavior of the peak emission fluence. Both effects are more pronounced as the optical feedback increases. Conversely, the system's photon statistics exhibit nontrivial behavior; the system we presented is a laser in the bad-cavity limit. In order to position the atom-scatterer in a broader perspective, we compared our model to a standard Jaynes-Cummings model and elaborated on deviations between both approaches. Finally, we connected the atom-scatterer description to the atomic systems of the previous chapters. In relation to the threshold prediction presented in chapter 3, we showed that an increase of the applied pump intensity in atom-scatterer systems leads to a smooth crossover from a regime dominated by spontaneous emission to a regime where pronounced laser effects are apparent.

Afterword

In this thesis we have presented a study of the optical properties of few-atom systems with gain. The interest of these systems lies in their combination of both optical gain and optical feedback on a microscopic scale. When considering our results in the broad framework of current research on microscopic laser phenomena, we believe the conclusions of this thesis are relevant for a wide range of experimental realizations. As an outlook onto future related research, we now proceed to briefly discuss a few experimental considerations and implications of our work.

In chapter 2, we described the effect of gain on the optical properties of a single atom. We showed the atom's albedo depends strongly on the applied pumping intensity. This observation could lead to interesting experimental work on, e.g., coherent backscattering [64, 121], since the width of the coherent backscattering cone is closely related to the albedo of the scatterers in the multiple scattering medium considered. Similarly, coherent backscattering experiments are expected to reveal interesting atomic saturation effects as described in chapter 3 and 4 [109].

In chapter 5, we demonstrated that a system of only a few atoms positioned in each other's near-field shows large gain narrowing and mode redistribution. From an experimental point of view, we are convinced that our model applies to a broad spectrum of experiments, such as laser cooled ions [37, 39]. Selective excitation of the ions can be achieved by tuning the polarization of the pump field and the positioning of the ions. Another possible experimental path would be to implement the atoms as quantum dots [47] which form, if bound to DNA, bioconjugated superstructures [44, 69]. While the energy transfer in those structures is somewhat different from the one presented in this thesis, we anticipate gain narrowing to remain conceptually valid. As a third experimental realization, we expect our results to stimulate experimental work on cold atoms [113] interacting with pumping fields. Compared to our current system, the number of atoms in a cold-atom cloud is very high; we therefore trust the phenomena described above to be much more pronounced.

Finally, the atom-resonator system introduced in chapter 6 allows for an intuitive and simple description of the effect of saturation on the interaction of an atom and a harmonic oscillator. In this context, we believe our results are ideally suited to describe the interaction of a single emitter and a microcavity [62]. In such experiment, multipole interactions [42] will induce quantitative differences with respect to the results presented here, but qualitatively our predictions remain unaltered.

APPENDIX A

Expansion of the Master equation in the dressed-state basis

The aim of this Appendix is to show the expansion of the Master equation (2.13) in the basis $\{|1(N)\rangle, |2(N)\rangle, |c, N+1\rangle\}$ defined in 2.10. The reduced density matrix elements which are diagonal in the atomic states evolve as

$$\begin{aligned}\dot{\sigma}_{1,1}^{N,N} = &-i\frac{\Omega_e}{2}\sin(\theta)\left(\sigma_{c,1}^{N+1,N}e^{i\omega t} - \sigma_{1,c}^{N,N+1}e^{-i\omega t}\right) \\ &+ \Gamma_{ca}\sin^2(\theta)\sigma_{c,c}^{N+1,N+1} - \Gamma_{bc}\cos^2(\theta)\sigma_{1,1}^{N,N} \\ &+ \frac{\Gamma_{bc}}{2}\sin(\theta)\cos(\theta)\left(\sigma_{1,2}^{N,N} + \sigma_{1,2}^{N,N}\right),\end{aligned} \tag{A.1}$$

$$\begin{aligned}\dot{\sigma}_{2,2}^{N,N} = &-i\frac{\Omega_e}{2}\cos(\theta)\left(\sigma_{c,2}^{N+1,N}e^{i\omega t} - \sigma_{2,c}^{N,N+1}e^{-i\omega t}\right) \\ &+ \Gamma_{ca}\cos^2(\theta)\sigma_{c,c}^{N+1,N+1} - \Gamma_{bc}\sin^2(\theta)\sigma_{2,2}^{N,N} \\ &+ \frac{\Gamma_{bc}}{2}\sin(\theta)\cos(\theta)\left(\sigma_{1,2}^{N,N} + \sigma_{1,2}^{N,N}\right),\end{aligned} \tag{A.2}$$

$$\begin{aligned}\dot{\sigma}_{c,c}^{N+1,N+1} = &-i\frac{\Omega_e}{2}\sin(\theta)\left(\sigma_{1,c}^{N,N+1}e^{-i\omega t} - \sigma_{c,1}^{N+1,N}e^{i\omega t}\right)\\ &- i\frac{\Omega_e}{2}\cos(\theta)\left(\sigma_{2,c}^{N,N+1}e^{-i\omega t} - \sigma_{c,2}^{N+1,N}e^{i\omega t}\right)\\ &- \Gamma_{ca}\sigma_{c,c}^{N+1,N+1} + \Gamma_{bc}\cos^2(\theta)\sigma_{1,1}^{N+1,N+1}\\ &- \Gamma_{bc}\sin(\theta)\cos(\theta)(\sigma_{1,2}^{N+1,N+1} + \sigma_{2,1}^{N+1,N+1})\\ &+ \Gamma_{bc}\sin^2(\theta)\sigma_{2,2}^{N+1,N+1},\end{aligned} \tag{A.3}$$

while the elements which are off-diagonal in the atomic states evolve as

$$\begin{aligned}\dot{\sigma}_{1,2}^{N,N} = &-i\frac{\Omega_e}{2}\left(\sin(\theta)\sigma_{c,2}^{N+1,N}e^{i\omega t} - \cos(\theta)\sigma_{1,c}^{N,N+1}e^{-i\omega t}\right)\\ &- \frac{\Gamma_{bc}}{2}(\sigma_{1,2}^{N,N} - \sin(\theta)\cos(\theta)\sigma_{2,2}^{N,N} - \sin(\theta)\cos(\theta)\sigma_{1,1}^{N,N})\\ &+ \Gamma_{ca}\sin(\theta)\cos(\theta)\sigma_{c,c}^{N+1,N+1} - \frac{i}{\hbar}(E_1^N - E_2^N)\sigma_{1,2}^{N,N},\end{aligned} \tag{A.4}$$

$$\begin{aligned}\dot{\sigma}_{1,c}^{N,N+1}e^{-i\omega t} = &-i\frac{\Omega_e}{2}\left(\sin(\theta)\sigma_{c,c}^{N+1,N+1} - \sin(\theta)\sigma_{1,1}^{N,N} - \cos(\theta)\sigma_{1,2}^{N,N}\right)\\ &- \frac{\Gamma_{bc}}{2}\left(\cos^2(\theta)\sigma_{1,c}^{N,N+1}e^{-i\omega t} - \sin(\theta)\cos(\theta)\sigma_{2,c}^{N,N+1}e^{-i\omega t}\right)\\ &- \frac{\Gamma_{ca}}{2}\sigma_{1,c}^{N,N+1} + \frac{i}{\hbar}(E_c^{N+1} - E_1^N)\sigma_{1,c}^{N,N+1}e^{-i\omega t},\end{aligned} \tag{A.5}$$

$$\begin{aligned}\dot{\sigma}_{2,c}^{N,N+1}e^{-i\omega t} = &-i\frac{\Omega_e}{2}\left(\cos(\theta)\sigma_{c,c}^{N+1,N+1} - \cos(\theta)\sigma_{2,2}^{N,N} - \sin(\theta)\sigma_{1,2}^{N,N}\right)\\ &+ \frac{\Gamma_{bc}}{2}\left(\sin(\theta)\cos(\theta)\sigma_{1,c}^{N,N+1}e^{-i\omega t} - \sin^2(\theta)\sigma_{2,c}^{N,N+1}e^{-i\omega t}\right)\\ &- \frac{\Gamma_{ca}}{2}\sigma_{2,c}^{N,N+1} + \frac{i}{\hbar}(E_c^{N+1} - E_2^N)\sigma_{2,c}^{N,N+1}e^{-i\omega t},\end{aligned} \tag{A.6}$$

and

$$\dot{\sigma}_{2,1}^{N,N} = (\dot{\sigma}_{1,2}^{N,N})^*, \tag{A.7a}$$

$$\dot{\sigma}_{c,1}^{N+1,N} = (\dot{\sigma}_{1,c}^{N,N+1})^*, \tag{A.7b}$$

$$\dot{\sigma}_{c,2}^{N+1,N} = (\dot{\sigma}_{2,c}^{N,N+1})^*. \tag{A.7c}$$

APPENDIX B

The Kramers-Kronig relations for a point dipole with gain

The goal of this Appendix is generalize the Kramers-Kronig relations to the case of a point dipole with gain. The Kramers-Kronig relations relate the real and imaginary part of a response function α as [10]

$$\mathrm{Re}\left[\alpha(\omega)\right] = \frac{1}{\pi}\mathcal{P}\int_{-\infty}^{+\infty}\frac{\mathrm{Im}[\alpha](x)}{x-\omega}dx, \tag{B.1a}$$

$$\mathrm{Im}\left[\alpha(\omega)\right] = -\frac{1}{\pi}\mathcal{P}\int_{-\infty}^{+\infty}\frac{\mathrm{Re}[\alpha](x)}{x-\omega}dx, \tag{B.1b}$$

where ω denotes frequency, and $\mathcal{P}$ denotes the integral's (Cauchy) Principal Value. We will check relations (B.1) for the polarizability (2.26):

$$\overleftrightarrow{\alpha}(\omega) = -\overleftrightarrow{\alpha_0}\frac{1-W}{1+W}\frac{1}{2}\frac{\omega_0}{\omega-\omega_0+i\frac{\Gamma}{2}(1+W)}. \tag{B.2}$$

with W the pump parameter ($0 \leq W \leq +\infty$). For this particular polarizability, the right-hand side of expression (B.1a) can be written as:

$$\mathcal{P}\int_{-\infty}^{+\infty}\frac{1}{(x-\omega)\Big((x-\omega_0)^2+(\frac{\Gamma}{2})^2(1+W)^2\Big)}dx$$
$$\equiv\lim_{\varepsilon\to 0}\left[\int_{-\infty}^{-\varepsilon}dx+\int_{+\varepsilon}^{+\infty}dx\right]\frac{1}{(x-\omega)\Big((x-\omega_0)^2+(\frac{\Gamma}{2})^2(1+W)^2\Big)}, \tag{B.3}$$

where we omitted trivial prefactors. Elementary complex integration shows that

$$\left[\mathcal{P}\int_{-\infty}^{+\infty}dx+\lim_{\varepsilon\to 0}\int_{-\varepsilon}^{+\varepsilon}dx\right]\frac{1}{(x-\omega)\Big((x-\omega_0)^2+(\frac{\Gamma}{2})^2(1+W)^2\Big)}$$
$$=2\pi i\mathrm{Res}\left[\frac{1}{(x-\omega)\Big((x-\omega_0)^2+(\frac{\Gamma}{2})^2(1+W)^2\Big)}\right]_{x=\omega_0+i\frac{\Gamma}{2}(1+W)}. \tag{B.4}$$

The ε-integral instantly yields

$$\lim_{\varepsilon\to 0}\int_{-\varepsilon}^{+\varepsilon}dx\frac{1}{(x-\omega)\Big((x-\omega_0)^2+(\frac{\Gamma}{2})^2(1+W)^2\Big)}$$
$$=-i\pi\frac{1}{\Big((\omega-\omega_0)^2+(\frac{\Gamma}{2})^2(1+W)^2\Big)}. \tag{B.5}$$

The Residue Theorem states that

$$\mathrm{Res}\left[\frac{1}{(x-\omega)\Big((x-\omega_0)^2+(\frac{\Gamma}{2})^2(1+W)^2\Big)}\right]_{x=\omega_0+i\frac{\Gamma}{2}(1+W)}$$
$$=-\frac{i}{\Big(\Gamma(1+W)\Big)\Big(\omega_0-\omega+i\frac{\Gamma}{2}(1+W)\Big)}. \tag{B.6}$$

Combining (B.4), (B.5) and (B.6) proves relation (B.1a). The proof of relation (B.1b) is similar to the calculation sketched above.

APPENDIX C

The Poynting vector

The instantaneous Poynting vector is defined as [15, 59, 79]

$$\boldsymbol{P}(t,\boldsymbol{r}) = \mathrm{Re}\Big[\boldsymbol{E}(t,\boldsymbol{r})\Big] \times \mathrm{Re}\Big[\boldsymbol{H}(t,\boldsymbol{r})\Big], \tag{C.1}$$

expressed in units of $\mathrm{W/m^2}$ (stands for Watt, not to be mistaken with the pump parameter W used throughout this thesis). This above definition holds, whether the fields are complex-valued or not. Since the following holds for any (complex-valued or real) quantities $\boldsymbol{A}$ and $\boldsymbol{B}$,

$$\mathrm{Re}(\boldsymbol{A}) \times \mathrm{Re}(\boldsymbol{B}) = \frac{1}{2}\mathrm{Re}(\boldsymbol{A} \times \boldsymbol{B}^* + \boldsymbol{A} \times \boldsymbol{B}), \tag{C.2}$$

we find for the Poynting vector:

$$\begin{aligned}\boldsymbol{P}(t,\boldsymbol{r}) &= \mathrm{Re}\Big[\int_{-\infty}^{+\infty} d\omega \boldsymbol{E}(\omega,\boldsymbol{r})e^{i\omega t}\Big] \times \mathrm{Re}\Big[\int_{-\infty}^{+\infty} d\omega' \boldsymbol{H}(\omega',\boldsymbol{r})e^{i\omega' t}\Big] \\ &= \frac{1}{2}\mathrm{Re}\Big[\int_{-\infty}^{+\infty} d\omega \int_{-\infty}^{+\infty} d\omega' \\ &\qquad \boldsymbol{E}(\omega,\boldsymbol{r}) \times (\boldsymbol{H}(\omega,\boldsymbol{r'}))^* e^{-i\omega' t} e^{i\omega t} + \boldsymbol{E}(\omega,\boldsymbol{r}) \times \boldsymbol{H}(\omega',\boldsymbol{r}) e^{i\omega' t} e^{i\omega t}\Big].\end{aligned} \tag{C.3}$$

Time-averaging the Poynting vector yields

$$\begin{aligned}\langle \boldsymbol{P}(t,\boldsymbol{r})\rangle &= \lim_{T\to+\infty}\frac{1}{2T}\int_{-T}^{+T} dt\boldsymbol{P}(t,\boldsymbol{r}) \\ &= \lim_{T\to+\infty}\frac{1}{2}\mathrm{Re}\Bigg[\int_{-\infty}^{+\infty}d\omega\int_{-\infty}^{+\infty}d\omega'\Big(\boldsymbol{E}(\omega,\boldsymbol{r})\times(\boldsymbol{H}(\omega',\boldsymbol{r}))^*\frac{\sin((\omega-\omega')T)}{(\omega-\omega')T} \\ &\qquad + \boldsymbol{E}(\omega,\boldsymbol{r})\times\boldsymbol{H}(\omega',\boldsymbol{r})\frac{\sin((\omega+\omega')T)}{(\omega+\omega')T}\Big)\Bigg]. \qquad \text{(C.4)}\end{aligned}$$

If we consider complex-valued electromagnetic fields, only positive frequencies need to be taken into account; the second term of (C.4) can be then discarded and we obtain from (C.3)

$$\langle \boldsymbol{P}(t,\boldsymbol{r})\rangle = \frac{1}{2}\left\langle \mathrm{Re}\Big[\boldsymbol{E}(t,\boldsymbol{r})\times\boldsymbol{H}^*(t,\boldsymbol{r})\Big]\right\rangle. \qquad \text{(C.5)}$$

which is the expression used in (4.49). The Poynting vector is related to the electromagnetic energy density. This relation can be easily deduced from the Maxwell equations; in free space, we have

$$\begin{aligned}&-\boldsymbol{\nabla}\cdot(\boldsymbol{E}(t,\boldsymbol{r})\times\boldsymbol{H}^*(t,\boldsymbol{r}))+\text{H.c.} \\ &=2\frac{\partial}{\partial t}\left(\varepsilon_0\boldsymbol{E}^*(t,\boldsymbol{r})\cdot\boldsymbol{E}(t,\boldsymbol{r})+\mu_0\boldsymbol{H}^*(t,\boldsymbol{r})\cdot\boldsymbol{H}(t,\boldsymbol{r})\right), \qquad \text{(C.6)}\end{aligned}$$

where H.c. stands for "Hermitian conjugate". Expression (C.6) can be rewritten in terms of the Poynting vector as

$$-\boldsymbol{\nabla}\cdot\boldsymbol{P}(t,\boldsymbol{r}) = \frac{\partial}{\partial t}\left(\varepsilon_0\boldsymbol{E}^*(t,\boldsymbol{r})\cdot\boldsymbol{E}(t,\boldsymbol{r})+\mu_0\boldsymbol{H}^*(t,\boldsymbol{r})\cdot\boldsymbol{H}(t,\boldsymbol{r})\right). \qquad \text{(C.7)}$$

Since the electromagnetic energy density $u(t,\boldsymbol{r})$ is given by

$$u(t,\boldsymbol{r}) = \varepsilon_0\boldsymbol{E}^*(t,\boldsymbol{r})\cdot\boldsymbol{E}(t,\boldsymbol{r})+\mu_0\boldsymbol{H}^*(t,\boldsymbol{r})\cdot\boldsymbol{H}(t,\boldsymbol{r}). \qquad \text{(C.8)}$$

we find that the Poynting vector and the electromagnetic energy density are related by

$$\boldsymbol{\nabla}\cdot\boldsymbol{P}(t,\boldsymbol{r})+\frac{\partial}{\partial t}u(t,\boldsymbol{r}) = 0. \qquad \text{(C.9)}$$

APPENDIX D

Computational convergence of an atom-oscillator system

The goal of this Appendix is to elaborate on the computational convergence of the atom-oscillator systems considered in chapter 6. The spectral properties and statistics of the photons emitted by an atom-oscillator system vary with the number of oscillator levels. Since we are interested in the unsaturated $N \to \infty$ limit, in a typical calculation we computationally increase N until the property of interest (such as the spectrum) converges to a limiting value. The computational effort needed to attain convergence depends on the system parameters. For example, the excitation level of the oscillator, and hence the minimum value of N required to be unsaturated, depends on the atom-oscillator separation. Since for a given pump intensity the oscillator is more excited at smaller separations we expect convergence to be slower in that case. To illustrate how the separation affects the computational convergence, we determine the far-field angle-integrated spectrum $\langle\phi(\omega)\rangle$ for different atom-oscillator separations. The system's spectral width $\Delta\omega$ and maximum photon flux $\max[\langle\phi(\omega)\rangle]$ then vary with the pump intensity and the number of oscillator levels. By altering the pump intensity, we determine the system's minimal spectral width $\Delta\omega^* \equiv \min_{\{W\}}[\Delta\omega]$ and maximum photon flux $\langle\phi^*(\omega)\rangle \equiv \max_{\{W\}}[\max[\langle\phi(\omega)\rangle]]$; both vary with the resonator capacity N. Figure D.1 shows how both spectral properties change with N for different atom-oscillator separations. We observe that at $|\boldsymbol{r}_A - \boldsymbol{r}_S| = 0.62c/\omega_{ca}$ the spectrum attains its asymptotic limit around $N = 12$; at smaller separations a much larger N is required to attain convergence, illustrating that convergence is slower as the system's feedback increases.

As a closing comment, we note that the minimum number of oscillator levels

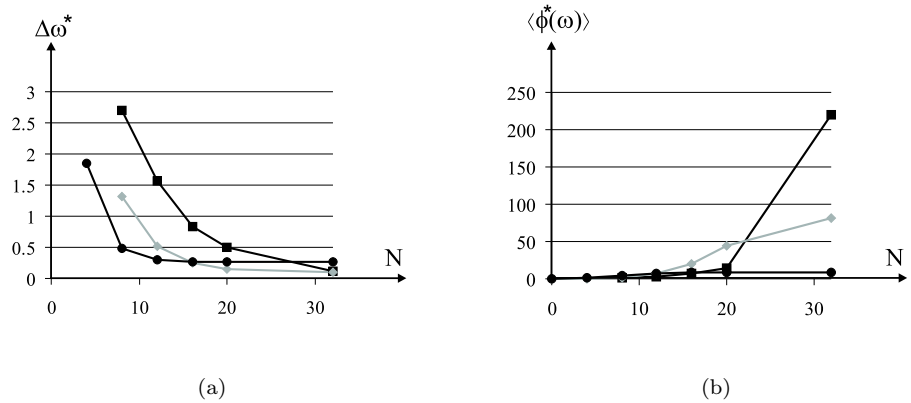

(a) (b)

Figure D.1: (a) The minimum spectral width $\Delta\omega^*$ (in units of Γ) and (b) the maximum photon flux $\langle\phi^*(\omega)\rangle$ of the angle-averaged far-field spectrum versus the resonator capacity N. The same configuration as in Figure 6.2 is considered, with as atom-oscillator separation $|\boldsymbol{r}_A - \boldsymbol{r}_S|$ equal to $0.62c/\omega_{ca}$ (black circles), $0.52c/\omega_{ca}$ (grey diamonds) and $0.42c/\omega_{ca}$ (black squares).

required to eliminate saturation effects by far exceeds the average number of excitations $\left\langle \hat{b}_N^\dagger \hat{b}_N \right\rangle$, as illustrated by expression (6.12). For example, if the average excitation number of the oscillator is of the order 1, considering only a few oscillator levels will cause significant saturation. This observation may seem physically counterintuitive, but can be easily understood by taking into account the distribution of the oscillator excitations: while the average excitation number of the oscillator may be small compared to N, the oscillator excitations are distributed over *all* the oscillator's levels, including the highest level (if the number of levels if finite). Hence, saturation effects are negligible only if the excitation number of the highest oscillator level is negligible.

Summary

What is a laser?

What is a laser? Quite extraordinarily, despite the abundance of excellent textbooks on laser dynamics, it is rather challenging to find an actual definition of the word "laser". Defining a laser is no easy feat, given that different scientific communities focus on laser operation in different systems and regimes. Strictly speaking, the extension of the laser acronym is the only aspect of lasers which everyone agrees on: "laser" stands for *Light Amplification by Stimulated Emission of Radiation*. The problem which arises when considering this extension is that it is not defining in itself: it is, after all, not possible to determine whether the light emitted by a given light source is produced through stimulated emission or through some other process. Consequently, light sources without transparent internal dynamics are difficult to classify as lasers, if a laser definition is based solely on the above acronym.

In practice, semantic issues are not dwelled upon too extensively and one focusses (as is done in most textbooks) on a description of lasers as ideal systems. Such an ideal laser typically consists of a gain medium in between two mirrors, as illustrated by Figure E-I. Laser oscillation occurs when a spontaneous emission event leads to light oscillating between the laser mirrors; leakage of light (due to the finite temporal storage capacity of the cavity) is compensated for by amplification through the gain medium.

Lasers: sorts and tastes

Despite the lack of a generally accepted laser definition, a wide range of amplifying systems which are generally accepted as lasers exists. As we described above, a laser typically consists of two essential ingredients: optical amplification and optical feedback. In the laser type depicted in Figure E-I, for example, amplification is incorporated through the pumping mechanism while the mirrors provide optical feedback. In practice, both the gain medium and the feedback come in many vari-

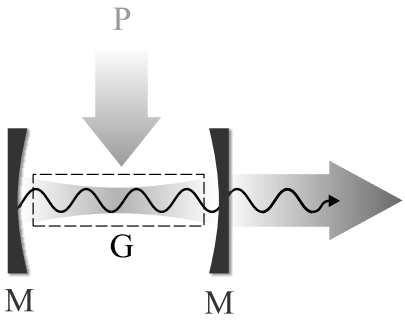

Figure E-I: A standard laser consists of a gain medium (G) between two mirrors (M). The gain medium is pumped by an external pump (P). The mirrors confine the intracavity light, which is amplified by interaction with the gain medium. One of the cavity mirrors (the right mirror in the figure) is partially reflecting, thereby allowing for the emission of laser light.

eties: the gain medium can be a solid state (as is the case in compact disc players, for example) or a gas (such as CO_2, used in medical applications); the feedback can be implemented in a Fabry-Pérot fashion (as in Figure E-I), as a ring cavity or chaotic cavity or through photonic crystals. The optical properties of the emitted laser light depend strongly on the implementation of gain and feedback, which sometimes leads to the question as to whether a given amplifying system can be considered to be a laser or not.

In this thesis, we present a study of the fundamental building blocks of laser systems. In this respect, we face the question of presenting a workable definition of a laser. It is rewarding to formulate such a definition since this clarifies semantic issues right from the beginning and allows us to focus on the physics of the systems we present. In this thesis, we adopt the following definition:

> *A single-mode laser is a system which combines gain and feedback, such that one field mode (the laser mode) is characterized by a gain-induced increase of its spectral weight at the cost of all other system modes. The amplitudes of all system modes decay in time to an external bath and are replenished by the gain source.*

Our definition of a single-mode laser is, although debatable, a workable definition in terms of experimentally observable quantities; its usage allows us to disregard laser-related semantic issues and concentrate on the physics of the systems at hand.

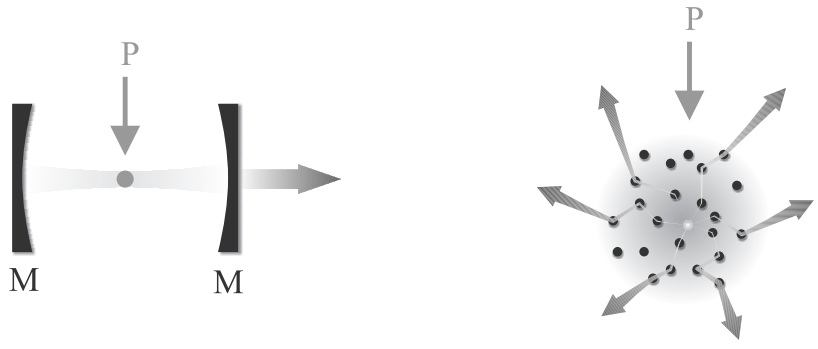

Figure E-II: (a) A one-atom (single-ion) laser consists of single atom (ion) inside a cavity. The atom (ion) is pumped while the cavity provides feedback. (b) A random laser consists of a gain medium containing random scatterers. The gain medium is pumped by an external pumping mechanism (P), while the optical feedback is provided by multiple scattering of light.

Lasers: from macro to micro

We now focus on the content of this thesis and the recent scientific discoveries which led to the questions we address. This thesis describes laser processes on a microscopic scale. In order to study the basic physics of the processes involved in laser oscillation, there has been an intensive search for laser operation in fundamental systems. The resulting drive toward miniaturization has led to, among others, the realization of vertical-cavity semiconductor lasers, dye-microsphere lasers, microring and microdisc semiconductor lasers, microsphere lasers and photonic-bandgap lasers. As laser systems are made smaller, a purely macroscopic description becomes inadequate and microscopic considerations should be taken into account. An interesting example of lasers which require a (partially) microscopic treatment is the class of one-atom lasers, schematically depicted in Figure E-II (a). In one-atom (or single-ion) lasers, the gain medium is reduced to a fundamental level, while macroscopic mirrors provide feedback. Another, contrasting example is the class of random lasers, shown in Figure E-II (b). In random lasers, the optical feedback is provided by scattering from microscopic particles, while the gain medium remains macroscopic. Obviously, neither the feedback mechanism nor the gain medium can be reduced to the dimensions smaller than those of one atom.

About this thesis

In this thesis, we explore the most fundamental system displaying both gain and feedback: a single pumped atom, surrounded by one or more passive atoms providing optical feedback by scattering. The atoms are positioned in free space in the

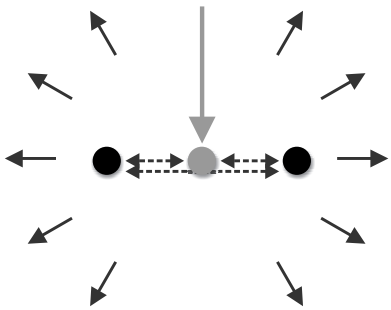

Figure E-III: The "scattering lasers" introduced and studied in this thesis, consisting of a small number of atoms (three in the figure) in free space. One of the atoms (grey) is pumped, while the others (black) are not. The dashed arrows depict light which is scattered back and forth between the atoms. A large fraction of the light in the system is emitted omnidirectionally and detected (solid black arrows). If the atoms are positioned closely enough, this few-atom system exhibits pronounced laser-like behavior.

absence of a cavity. The absence of a cavity ensures that the presented results are based solely on the scattering properties of the atomic building blocks and their description. We show that these systems, although very simple, show surprisingly strong spectral gain narrowing and mode redistribution. In addition, the observed gain-induced phenomena are more pronounced as the number of atoms increases, in correspondence with the intuitive macroscopic limit. Due to their remarkable behavior, we refer to few-atom systems with gain as "scattering lasers".

Overview of this thesis

To conclude this summary, we provide a technical overview of the contents of this thesis. The atomic systems we present are studied in several distinct phases. The first chapter serves an introductory purpose and provides the same overview as this summary. We start in chapter 2 with a description of the optical scattering properties of a single pumped atom. We show how to characterize the influence of the pump field through a single dimensionless parameter, expressing both a broadening of the atomic transition and a decrease of the atom's polarizability. In addition, the presence of gain causes the atom to scatter partially inelastically and changes its dispersion and dissipation. In chapter 3 we describe N atoms with gain in the framework of multiple scattering of light. We demonstrate that, remarkably, a two-atom system with gain exhibits threshold behavior within a semiclassical multiple-scattering formalism. In chapter 4 we calculate a first-order estimation of the atomic saturation induced by off-resonant light. We demonstrate such saturation to be significant and to suppress the manifestation of a threshold as predicted in a semiclassical formalism. In chapter 5, we proceed beyond the above first-order approximation and present a quantum-mechanical study of N-atom systems with gain. We show that few-atoms with gain exhibit pronounced gain narrowing, pro-

viding the atoms are in each other's near-field. Finally, in chapter 6 we demonstrate that eliminating the saturation of the passive atoms leads to even more pronounced mode competition effects. As the applied pump intensity increases, the microscopic systems under consideration exhibit a smooth crossover from a regime governed by spontaneous emission to a regime where pronounced laser effects dominate.

Samenvatting

Wat is een laser?

Wat is een laser? Merkwaardig genoeg is er in de wetenschappelijke wereld geen consensus over het antwoord op deze vraag. Dat is op zich niet zo erg: verschillende wetenschappelijke disciplines stellen immers een ander eisenpakket voorop bij het definiëren van het "laser"-concept, met als gevolg dat verschillende definities van een "laser" de ronde doen. In strikte zin is het enige aspect van lasers waar iedereen het over eens is, dat "laser" staat voor *Light Amplification by Stimulated Emission of Radiaton*, ofwel *lichtversterking door gestimuleerde emissie*. Het probleem dat deze betekenis met zich meebrengt, is dat ze niet definiërend is: het is immers niet mogelijk om van een willekeurige lichtbron te bepalen of het licht al dan niet via gestimuleerde emissie wordt uitgezonden. Dit heeft als gevolg dat lichtbronnen zonder transparante interne dynamica moeilijk te classificeren zijn als wel of geen laser.

In de praktijk maakt men zich echter zelden zorgen om semantische kwesties, en kiest men (zoals in veel tekstboeken) voor een beschrijving van lasers als geïdealiseerde systemen. Een dergelijke ideale laser bestaat in essentie uit een versterkend medium dat zich bevindt tussen een aantal (meestal twee) spiegels, zoals aangegeven in Figuur N-I. Vanuit een conceptueel standpunt is de werking van een laser heel eenvoudig. Om een laser vanuit zijn "uit" toestand "aan" te kunnen zetten, moet op een willekeurige plaats tussen de spiegels spontaan een "kiem" van licht ontstaan. Deze lichtkiem plant zich voort en kaatst heen en weer tussen de laserspiegels; door het pompen wordt het licht bij elke doorgang door het versterkende medium intenser (uiteraard is het zo dat een deel van het licht helemaal niet heen en weer kaatst maar gewoon weglekt door de eindige afmetingen van de spiegels — dit lekkende deel van het licht draagt niet bij tot de laserwerking maar is verlies, inherent aan het laserproces). Omdat men geïnteresseerd is in laserlicht dat uit de laser komt zorgt men ervoor dat één van de spiegels in het systeem niet al het licht reflecteert maar een kleine fractie doorlaat; het licht dat zo ontsnapt is laserlicht.

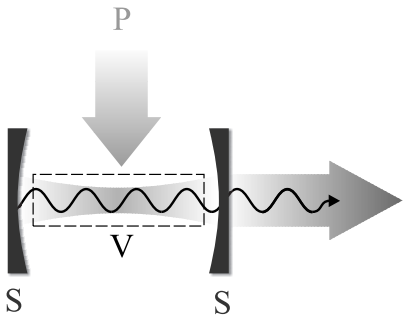

Figuur N-I: Een standaard laser bestaat uit een versterkend medium (V) tussen twee spiegels (S). Het versterkend medium wordt aangedreven door een pomp (P). De spiegels sluiten het licht grotendeels in; doordat het licht vele malen tussen de spiegels heen en weer kaatst en daarbij door het versterkend medium reist wordt het geïntensifieerd. Eén van de spiegels (de rechter spiegel in de figuur) laat een fractie van het licht door; het laserlicht kan zo het systeem verlaten.

Lasers: soorten en smaken

Niettegenstaande het gebrek aan een algemeen aanvaarde definitie van een laser, bestaat er een groot scala aan systemen die door de wetenschappelijke wereld als lasers worden beschouwd. Zoals hierboven beschreven, bevat een laser twee essentiële ingrediënten: optische versterking en optische feedback. In het type laser dat bijvoorbeeld in Figuur N-I wordt getoond, gebeurt de versterking via het pompmechanisme en zorgen de spiegels voor de feedback. In de praktijk is het zo dat zowel het versterkende medium als de feedback op veel verschillende manieren geïmplementeerd kunnen worden. Het medium kan bijvoorbeeld een vaste stof zijn (zoals in een cd-speler, waar het medium een halfgeleider is) of een gas (zoals in medische toepassingen waar gasvormig CO_2 wordt gebruikt als versterkend medium); de feedback kan worden geïmplementeerd via planparallelle spiegels (zoals de spiegels in Figuur N-I), aan de hand van ringvormige of chaotische trilholtes of aan de hand van (fotonische) kristallen, om maar enkele voorbeelden te noemen. Al naargelang de gekozen implementatie van versterking en feedback kunnen de eigenschappen van lasers drastisch verschillen; de mogelijkheid bestaat dat discussie ontstaat over de vraag of een versterkend systeem als laser kan worden beschouwd of niet.

In dit proefschrift worden bijzondere versterkende systemen bestudeerd, waar we later in detail op ingaan. Om onze systemen te classificeren tussen andere versterkende systemen — zowel lasers al niet-lasers — is het noodzakelijk om een gefundeerde eenduidige definitie van een laser te formuleren. We stellen daarbij twee eisen voorop: onze definitie moet experimenteel toetsbaar zijn, en alle systemen die algemeen erkend worden als lasers, moeten onder onze laser definitie vallen (en

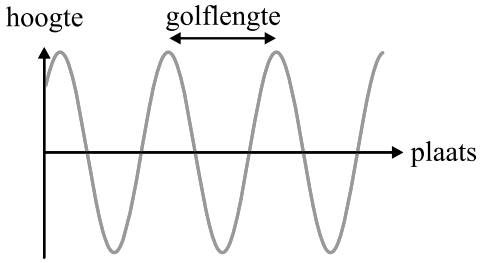

Figuur N-II: Een illustratie van het concept golflengte. De golflengte in de figuur is gedefinieerd als de afstand tussen twee opeenvolgende golfpieken.

omgekeerd, uiteraard, mogen alle systemen die duidelijk geen lasers zijn, niet onder onze definitie vallen). We zijn op zoek gegaan naar een unificerende eigenschap van een breed scala lasers en kwamen tot de vaststelling dat lasers één eigenschap gemeen hebben: naarmate de pompintensiteit toeneemt, stijgt de intensiteit van het laserlicht terwijl het bereik van golflengtes waarin de laser licht uitzendt kleiner wordt (om in het ideale geval licht te emitteren op één enkele golflengte). Deze eigenschap zal de basis zijn van onze laserdefinitie. Om deze bijzondere eigenschap nader toe te lichten, maken we een korte zijsprong om wat dieper in te gaan op het concept *golflengte*.

De golflengte van licht

Licht kan zich gedragen als een golf, net zoals geluid, seismische trillingen of golven op zee. Met een golf kan men een golflengte associëren. Om het golflengteconcept te visualiseren beschouwen we even het voorbeeld van zeegolven aan het zeeoppervlak. Als een waarnemer zich op een vaste plaats bevindt en een zeegolf ziet langskomen, dan observeert hij/zij een alternerend stijgende en dalende beweging, zoals geïllustreerd in Figuur N-II; de golflengte van de golf is gedefinieerd als de afstand tussen twee opeenvolgende golfpieken.

In het geval van zichtbare lichtgolven is het zo dat de golflengte bepaalt welke *kleur* we associëren met dat licht; rood licht heeft dus een andere golflengte dan blauw licht. Om de grote reikwijdte van lichtgolflengtes in de natuur te illustreren, tonen we in Figuur N-III een aantal algemeen bekende (elektromagnetische) golven en de ermee geassocieerde golflengte.

Naast een variatie qua golflengte, kan ook het *aantal* golflengtes in een lichtbron variëren. Zo bevatten zowel rood als blauw licht maar één golflengte, maar bevat wit licht juist heel veel golflengtes (namelijk alle kleuren van het zichtbare spectrum).

Lasers en golflengteselectiviteit

Zoals eerder vermeld hebben lasers de opmerkelijke eigenschap dat, naarmate de pompintensiteit toeneemt, het aantal golflengtes waarin ze emitteren vermindert

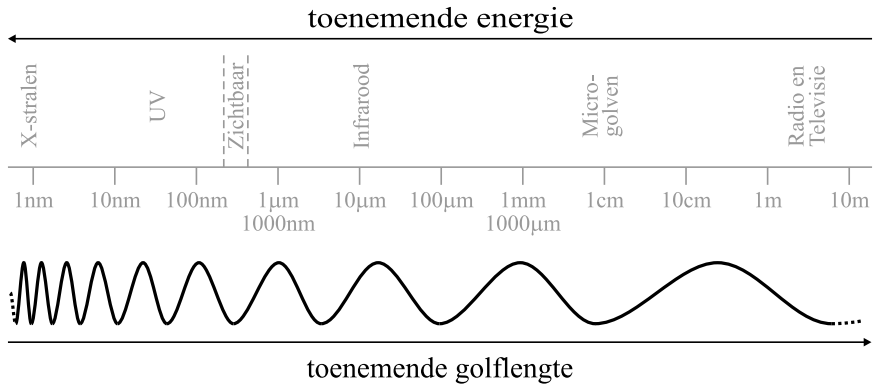

Figuur N-III: Selectie uit het elektromagnetische spectrum. Van links naar rechts op de figuur neemt de golflengte van het licht toe; van rechts naar links neemt de energie van de golven toe (energie en golflengte zijn omgekeerd evenredig met elkaar).

terwijl de intensiteit van het uitgezonden licht toeneemt. Met andere woorden: terwijl een laser bij lage pompintensiteit in veel golflengtes uitzendt, wordt het laserlicht bij hoge pompintensiteit intenser en gedomineerd door één kleur. De zuiverheid qua kleur bij hoge pompintensiteit is wat laserlicht zo bijzonder maakt en geschikt voor een breed scala aan toepassingen.

Zowel de golflengte(s) als de hoeveelheid licht die een systeem uitzendt zijn experimenteel vast te stellen; in dit proefschrift maken we daar handig gebruik van en definiëren een laser als volgt:

> *Een (monomodale) laser is een systeem waarin optische versterking en feedback worden gecombineerd, zodanig dat als de versterking intensifieert, de reikwijdte van golflengtes waarin de laser emitteert afneemt terwijl de intensiteit van het laserlicht toeneemt.*

Niettegenstaande het feit dat de bovenstaande definitie aanvechtbaar is, biedt ze een eenvoudig te verifiëren criterium in termen van experimenteel meetbare grootheden; het gebruik van deze definitie als toetssteen laat ons toe ons te distantiëren van semantische discussies en ons te richten op de onderliggende natuurkunde.

Lasers: van macro naar micro

Nu we het laserconcept geïntroduceerd hebben, kunnen we ons richten we op de inhoud van dit proefschrift en de recente historische ontwikkelingen die tot de vraagstelling in dit proefschrift hebben geleid. Dit proefschrift beschrijft laserprocessen op microscopische schaal. Om de microscopische processen te begrijpen die de laserdynamica beheersen, is men al enige tijd op zoek naar laserwerking op fundamenteel niveau. Het creëren van steeds kleinere lasers gebeurt in de praktijk

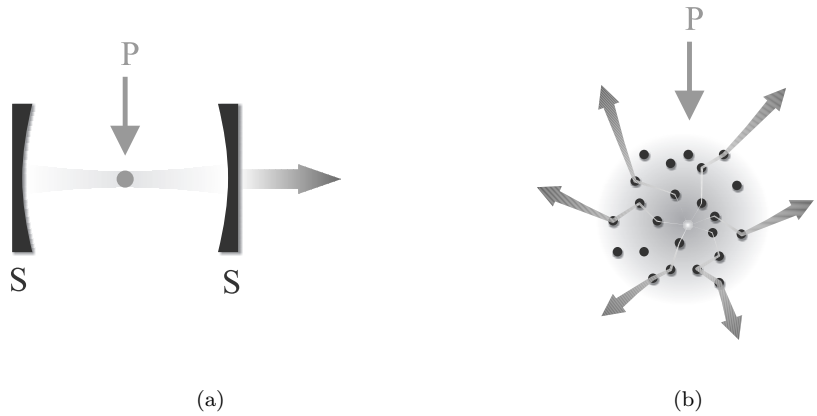

(a) (b)

Figuur N-IV: (a) Een één-atoom laser bestaat uit één atoom dat gevangen wordt tussen twee spiegels. Het atoom wordt gepompt; het licht dat het atoom zo uitzendt wordt gevangen door de spiegels. Eén van de spiegels (de rechter spiegel in de figuur) laat een fractie van het licht door; het laserlicht kan zo het systeem verlaten. (b) Een random laser bestaat uit een versterkend medium (grijze achtergrond) dat verstrooiende deeltjes bevat (zwarte cirkels). Het versterkend medium wordt aangedreven door een externe pomp (P). Licht wordt verstrooid aan de verstrooiende deeltjes en tegelijk geïntensifieerd door het aanwezige versterkend medium. Het zo ontstane laserlicht wordt omnidirectioneel uitgezonden.

door ofwel de feedback, ofwel het versterkend medium te verkleinen (of allebei, uiteraard). Een recent voorbeeld van een laser waarin het versterkend medium tot de ultieme limiet is verkleind is een "één-atoom laser", geïllustreerd in Figuur N-IV(a). Een één-atoom laser bestaat uit twee spiegels met ertussen één enkel atoom dat gepompt wordt. In een één-atoom laser is de versterking dus gereduceerd tot een fundamenteel (atomair) niveau, terwijl de feedback macroscopisch is gebleven. Een ander — contrasterend — voorbeeld van een gedeeltelijk microscopische laser is een "random laser", geïllustreerd in Figuur N-IV(b). Een random laser bestaat uit een versterkend medium waarin microscopische verstrooiers zijn ingebed. Wanneer in een random laser een kiem van licht spontaan ontstaat, zorgen de verstrooiers ervoor dat het licht zich voortplant langs een onregelmatig pad terwijl het geïntensifieerd wordt door het versterkende medium. Het laserlicht dat een random laser emitteert is omnidirectioneel, dit in tegenstelling tot de directionele emissie van de lasers in Figuur N-I en N-IV(a). Uiteraard kunnen noch het versterkend medium noch de feedback worden verkleind tot dimensies kleiner dan die van één atoom.

Over dit proefschrift

In dit proefschrift beschrijven we de meest fundamentele systemen die optische versterking en feedback combineren: één gepompt atoom, omgeven door een klein aantal passieve atomen die samen voor de feedback zorgen, zoals geïllustreerd in

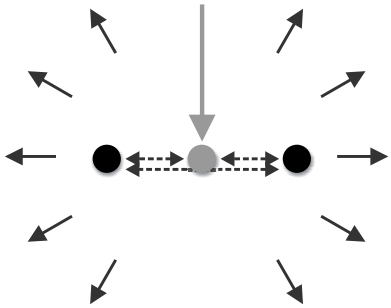

Figuur N-V: De "scattering lasers" die in dit proefschrift worden bestudeerd bestaan uit een klein aantal atomen (drie in de figuur) in de vrije ruimte. Eén van de atomen (grijs) wordt gepompt, de anderen (zwart) niet. De dubbele stippellijn illustreert licht dat door verstrooiing heen en weer kaatst tussen de atomen. Een deel van het licht wordt naar buiten uitgezonden en gedetecteerd (enkele zwarte pijlen). Indien de atomen dicht genoeg bij elkaar zijn gepositioneerd, vertoont dit systeem gedrag dat analoog is aan macroscopische lasers.

Figuur N-V. De atomen zijn gepositioneerd in de vrije ruimte. De optische versterking in onze systemen wordt verzorgd door het gepompte atoom; het licht dat dit atoom uitzendt wordt verstrooid door de passieve atomen die zo voor feedback zorgen. Omdat we kunnen aantonen dat deze systemen duidelijk laserkarakter vertonen, refereren we naar onze atomaire systemen als "scattering lasers"[1]. Het fundamenteel karakter van scattering lasers uit zich in het feit dat ze volledig kunnen worden gekarakteriseerd in termen van de atomen waaruit ze bestaan; in die zin zijn scattering lasers de enige lasers die op atomair niveau exact kunnen worden beschreven. Het verband met de lasers uit Figuur N-IV is intuïtief duidelijk: scattering lasers kunnen worden beschouwd als een één-atoom laser waarbij de spiegels worden vervangen door slechts enkele passieve atomen, of als een random laser waarbij het versterkend medium is verkleind tot één enkel gepompt atoom.

Overzicht van dit proefschrift

Ter afronding van deze samenvatting geven we in wat volgt een technisch overzicht van de verschillende hoofdstukken van dit proefschrift. De atomaire systemen die we bestudeerd hebben worden in een aantal opeenvolgende fasen beschreven. Het eerste hoofdstuk heeft een inleidende functie en geeft hetzelfde overzicht als deze samenvatting. Het tweede hoofdstuk beschrijft de eigenschappen van één enkel gepompt atoom. De lichtverstrooiing van een atoom wordt beschreven door de *polariseerbaarheid* van dat atoom; we tonen in hoofdstuk 2 aan dat de aanwezigheid van een pomp zich vertaalt in een afname van de polariseerbaarheid en een verandering van

[1] "To scatter" betekent "verstrooien". De feedback in onze atomaire systemen wordt verzorgt door de passieve atomen die het licht verstrooien — vandaar de naam "scattering lasers".

het teken ervan (een negatieve polariseerbaarheid impliceert dat licht niet uitdooft maar wordt versterkt, wat te verwachten is in de aanwezigheid van een pomp). We tonen verder aan dat de keuze van pompimplementatie belangrijke gevolgen heeft voor de verstrooiingseigenschappen van het atoom. Het derde hoofdstuk beschouwt systemen met meerdere atomen en beschrijft ze op een semi-klassieke manier. We tonen aan dat een dergelijke aanpak leidt tot duidelijk lasergedrag en het verschijnen van een laserdrempel, zelfs indien slechts twee atomen worden beschouwd. In hoofdstuk 4 gaan we verder in op de benaderingen die inherent zijn aan een semi-klassieke theorie en behandelen een eerste-orde correctie op deze beschrijving; deze correctie leidt tot het verdwijnen van bovenstaande laserdrempel. Omdat het gestructureerd uitbreiden van een semi-klassieke theorie naar hogere-orde correcties moeilijk blijkt, gaan we in hoofdstuk 5 over op een volledig kwantummechanische beschrijving van scattering lasers; het blijkt dat deze systemen ook in een kwantumbeschrijving duidelijk lasergedrag vertonen, wat hun naam rechtvaardigt. Verder tonen we aan dat de mate waarmee het lasergedrag zich in deze systemen manifesteert toeneemt met het aantal atomen. Meer precies is het zo dat lasergedrag meer prominent aanwezig is naarmate meer licht kan worden opgesloten in het systeem; de aanwezigheid van meer atomen leidt tot een grotere capaciteit voor het opvangen van licht en dus tot een duidelijker lasergedrag. Omdat we computationeel beperkt zijn tot het uitrekenen van systemen met slechts enkele atomen, gaan we in hoofdstuk 6 over op systemen waar veel meer licht in kan opgesloten worden: één enkel gepompt atoom dat gekoppeld wordt aan een microtrilholte. Daar deze laatste systemen een veel grotere capaciteit hebben wat lichtopslag betreft, vertonen ze meer uitgesproken lasergedrag.

Bibliography

[1] G. Agarwal, A. Brown, L. Narducci, and G. Vetri, *Collective Atomic Effects in Resonance Fluorescence*, Phys. Rev. A **15**, 1613 (1977) — p.20, 57, and 93.

[2] P. Agostini, A. Georges, S. Wheatley, P. Lambropoulos, and M. Levenson, *Saturation effects in resonant three-photon ionization of sodium with a non-monochromatic field*, J. Phys. B **11**, 1733 (1978) — p.58.

[3] U. Akram, Z. Ficek, and S. Swain, *Decoherence and coherent population transfer between two coupled systems*, Phys. Rev. A **62**, 013413 (2000) — p.80.

[4] L. Allen and J. Eberly, *Optical Resonance and Two-level Atoms* (Dover Publications, New York, 1987) — p.23.

[5] L. Allen and G. Peters, *Superradiance, coherence brightening and amplified spontaneous emission*, Phys. Lett. A **31**, 95 (1970) — p.20, 57, and 93.

[6] L. Allen and G. Peters, *Amplified spontaneous emission II. The connection with laser theory*, J. Phys. A **4**, 377 (1971) — p.20.

[7] L. Allen and G. Peters, *Amplified spontaneous emission III. Intensity and saturation*, J. Phys. A **4**, 564 (1971) — p.20.

[8] L. Allen and G. Peters, *Spectral distribution of amplified spontaneous emission*, J. Phys. A **5**, 695 (1972) — p.20.

[9] K. An, J. Childs, R. Dasari, and M. Feld, *Microlaser: A laser with One Atom in an Optical Resonator*, Phys. Rev. Lett. **73**, 3375 (1994) — p.20 and 24.

[10] N. Ashcroft and N. Mermin, *Solid State Physics* (Saunders College, Philadelphia, 1976) — p.32 and 129.

[11] A. Badolato, K. Hennessy, M. Atatüre, J. Dreiser, E. Hu, P. Petroff, and A. İmamoğlu, *Deterministic coupling of single quantum dots to single nanocavity modes*, Science **308**, 1158 (2005) — p.105.

[12] J.-L. Basdevant and J. Dalibard, *The Quantum Mechanics Solver* (Springer-Verlag, Berlin Heidelberg New York, 2000) — p.57.

[13] O. Benson and Y. Yamamoto, *Master-Equation Model of a Single Quantum Dot Microsphere Laser*, Phys. Rev. A **59**, 4756 (1999) — p.103 and 106.
[14] B. Blind, P. Fontana, and P. Thomann, *Resonance fluorescence spectrum of intense amplitude modulated laser light*, J. Phys. B **13**, 2717 (1980) — p.58.
[15] C. Bohren and D. Huffman, *Absorption and scattering of light by small particles* (Wiley Science Paper Series, New York, 1998) — p.131.
[16] R. Bonifacio and L. Lugiato, *Cooperative radiation processes in two-level systems: Superfluorescence*, Phys. Rev. A **11**, 1507 (1975) — p.20 and 93.
[17] A. Boozer, A. Boca, J. Buck, J. McKeever, and H. Kimble, *Comparison of Theory and Experiment for a One-Atom Laser in a Regime of Strong Coupling*, Phys. Rev. A **70**, 023814 (2004) — p.103.
[18] P. Bushev, D. Rotter, A. Wilson, F. Dubin, C. Becher, J. Eschner, R. Blatt, V. Steixner, P. Rabl, and P. Zoller, *Feedback Cooling of a Single Trapped Ion*, Phys. Rev. Lett. **96**, 43003 (2006) — p.24.
[19] V. Bužek, A. Wilson-Gordon, P. Knight, and W. Lai, *Coherent states in a finite-dimensional basis: Their phase properties and relationship to coherent states of light*, Phys. Rev. A **45**, 8079 (1992) — p.109.
[20] A. Caldera and A. Leggett, *Quantum Tunneling in a Dissipative System*, Ann. Phys. **149**, 374 (1983) — p.78.
[21] H. Cao, Y. Ling, J. Xu, C. Cao, and P. Kumar, *Photon Statistics of Random Lasers with Resonant Feedback*, Phys. Rev. Lett. **86**, 4524 (2001) — p.20.
[22] H. Carmichael, *An Open Systems Approach to Quantum Optics* (Springer-Verlag, Berlin, 1993) — p.88.
[23] H. Carmichael, *Statistical Methods in Quantum Optics 1* (Springer-Verlag, Berlin Heidelberg New York, 2002) — p.26 and 109.
[24] H. Carmichael and D. Walls, *Master Equation for Strongly Interacting Systems*, J. Phys. A **6**, 1552 (1973) — p.82.
[25] L. Casperson, *Threshold characteristics of mirrorless lasers*, J. Appl. Phys. **48**, 256 (1977) — p.20.
[26] V. Chaltykyan, G. Grigoryan, and Y. Pashayan, *Interaction of non-monochromatic laser field with two-level atom*, J. Mod. Opt. **47**, 11 (2000) — p.58.
[27] T. Chanelière, D. Wilkowski, Y. Bidel, R. Kaiser, and C. Miniatura, *Saturation-induced coherence loss in coherent backscattering of light*, Phys. Rev. E **70**, 036602 (2004) — p.34.
[28] C. Chang-Hasnain, *VCSELs: Advances and Prospects*, Optics & Photonics News **9**, 35 (1998) — p.19.
[29] J. Cirac, M. Lewenstein, and P. Zoller, *Laser cooling a trapped ion in a cavity: Bad-cavity limit*, Phys. Rev. A **51**, 1650 (1995) — p.19 and 118.
[30] C. Cohen-Tannoudji, J. Dupont-Roc, and G. Grynberg, *Atom-Photon Interactions* (Wiley Science Paper Series, New York, 1998) — p.25, 26, 27, 34, 60, 64, 71, 77, 82, and 109.
[31] P. de Vries, D. van Coevorden, and A. Lagendijk, *Point scatterers for classical waves*, Rev. Mod. Phys. **70**, 447 (1998) — p.23, 46, and 53.
[32] D. Dialetis, *Spontaneous Emission by a System of Identical Atoms*, Phys.

Rev. A **2**, 599 (1970) — p.20 and 93.
[33] R. Dicke, *Coherence in Spontaneous Radiation Processes*, Phys. Rev. **93**, 99 (1954) — p.20, 57, and 93.
[34] R. Dicke, *Coherence Brightened Laser* in *Quantum electronics*, P. Grivet and N. Bloembergen (eds.) (Columbia University Press, New York, 1964) — p.20 and 93.
[35] J. Eberly, *Superradiance Revisited*, Am. J. Phys. **40**, 1374 (1972) — p.20, 57, and 93.
[36] E. Economou, *Green's Functions in Quantum Physics* (Springer-Verlag, Berlin Heidelberg, 1979) — p.50.
[37] U. Eichmann, J. Bergquist, J. Bollinger, J. Gilligan, W. Itano, D. Wineland, and M. Raizen, *Youngs interference experiment with light scattered from two atoms*, Phys. Rev. Lett. **70**, 2359 (1993) — p.125.
[38] P. Elyutin, *Linear Susceptibility of a Three-Level System in a Strong Non-monochromatic Radiation Field*, Opt. Spektrosc. **43**, 542 (1977) — p.58.
[39] J. Eschner, C. Raab, F. Schmidt-Kaler, and R. Blatt, *Light interference from single atoms and their mirror images*, Nature **413**, 495 (2001) — p.24 and 125.
[40] X. Fan, P. Palinginis, S. Lacey, H. Wang, and M. C. Lonergan, *Coupling semiconductor nanocrystals to a fused-silica microsphere:a quantum-dot microcavity with extremely high Q factors*, Opt. Lett. **25**, 1600 (2000) — p.105.
[41] Z. Ficek, J. Seke, A. Soldatov, and G. Adam, *Saturation of a two-level atom in polychromatic fields*, J. Opt. B **2**, 780 (2000) — p.58.
[42] H. Freedhoff, *Master equation for electric quadrupole transitions*, J. Phys. B **22**, 435 (1989) — p.107 and 126.
[43] H. Freedhoff and Z. Chen, *Resonance fluorescence of a two-level atom in a strong bichromatic field*, Phys. Rev. A **41**, 6013 (1990) — p.58.
[44] A. Fu, C. Micheel, J. Cha, H. Chang, H. Yang, and A. Alivisatos, *Discrete Nanostructures of Quantum Dots/Au with DNA*, J. Am. Chem. Soc. **126**, 10832 (2004) — p.125.
[45] D. Gammon and D. Steel, *Optical Studies of Single Quantum Dots*, Phys. Today **55**, 36 (2002) — p.24.
[46] C. Garrett, W. Kaiser, and W. Bond, *Stimulated Emission into Optical Whispering Modes of Spheres*, Phys. Rev. **124**, 1807 (1961) — p.19.
[47] B. Gerardot, S. Strauf, M. de Dood, A. Bychkov, A. Badolato, K. Hennessy, E. Hu, D. Bouwmeester, and P. Petroff, *Photon Statistics from Coupled Quantum Dots*, Phys. Rev. Lett. **95**, 137403 (2005) — p.24 and 125.
[48] C. Ginzel, H.-J. Briegel, U. Martini, B. Englert, and A. Schenzle, *Quantum optical master equations: The one-atom laser*, Phys. Rev. A **48**, 732 (1993) — p.24.
[49] S. Gnutzmann, *Photon statistics of a bad-cavity laser near threshold*, Eur. Phys. J. D **4**, 109 (1998) — p.19 and 118.
[50] M. Gross and S. Haroche, *Superradiance: an essay on the theory of collective spontaneous emission*, Phys. Rep. **93**, 301 (1982) — p.20, 57, and 93.
[51] F. Haake, H. King, G. Schröder, J. Haus, R. Glauber, and F. Hopf, *Macro-*

scopic Quantum Fluctuations in Superfluorescence, Phys. Rev. Lett. **42**, 1740 (1979) — p.20 and 93.

[52] F. Haake, H. King, G. Schröder, J. Haus, R. Glauber, and F. Hopf, *Delay-Time Statistics and Inhomogeneous Line Broadening in Superfluorescence*, Phys. Rev. Lett. **45**, 558 (1980) — p.20 and 93.

[53] F. Haake, M. Kolobov, C. Fabre, E. Giacobino, and S. Reynaud, *Superradiant laser*, Phys. Rev. Lett. **71**, 995 (1993) — p.20 and 93.

[54] H. Haken, *Laser Theory* (Springer, Berlin, 1984) — p.17.

[55] S. Harris, *Lasers without inversion: Interference of lifetime-broadened resonances.*, Phys. Rev. Lett. **62**, 1033 (1989) — p.24 and 37.

[56] S. Harris, J. Field, and A. İmamoğlu, *Nonlinear optical processes using electromagnetically induced transparency*, Phys. Rev. Lett. **64**, 1107 (1990) — p.34.

[57] C. Hood, M. Chapman, T. Lynn, and H. Kimble, *Real-Time Cavity QED with Single Atoms*, Phys. Rev. Lett. **80**, 4157 (1998) — p.105.

[58] M. Imada, S. Noda, C. Alongkarn, T. Tokuda, M. Murata, and G. Sasaki, *Coherent two-dimensional lasing action in surface-emitting laser with triangular-lattice photonic crystal structure*, Appl. Phys. Lett. **75**, 316 (1995) — p.19.

[59] J. Jackson, *Classical electrodynamics* (John Wiley & Sons, New York, 1999) — p.131.

[60] E. Jaynes and F. Cummings, *Comparison of quantum and semiclassical radiation theories with application to the beam maser*, Proc. IEEE **51**, 89 (1963) — p.120.

[61] A. Kaplan, *Exact theory of relaxation of two-level systems in a strong non-monochromatic field*, Sov.Phys.-JETP **38**, 705 (1974) — p.58.

[62] V. Klimov, M. Ducloy, and V. Letokhov, *Strong interaction between a two-level atom and the whispering-gallery modes of a dielectric microsphere: Quantum-mechanical consideration*, Phys. Rev. A **59**, 2996 (1999) — p.105 and 126.

[63] S. Kuppens, M. van Exter, and J. Woerdman, *Quantum-Limited Linewidth of a Bad-Cavity Laser*, Phys. Rev. Lett. **72**, 3815 (1994) — p.95.

[64] D. Kupriyanov, I. Sokolov, P. Kulatunga, C. Sukenik, and M. Havey, *Coherent backscattering of light in atomic systems: Application to weak localization in an ensemble of cold alkali-metal atoms*, Phys. Rev. A **67**, 013814 (2003) — p.39 and 125.

[65] A. Lagendijk, *Spectral density in time-dependent perturbation theory*, Am. J. Phys. **44**, 1098 (1976) — p.58 and 60.

[66] A. Lagendijk and B. van Tiggelen, *Resonant Multiple Scattering of Light*, Phys. Rep. **270**, 145 (1996) — p.23, 31, 49, and 50.

[67] W. Lamb, W. Schleich, M. Scully, and C. Townes, *Laser physics: Quantum controversy in action*, Rev. Mod. Phys. **71**, S263 (1999) — p.19.

[68] N. Lawandy, R. Balachandran, A. Gomes, and E. Sauvain, *Laser action in strongly scattering media*, Nature **368**, 436 (1994) — p.20.

[69] J. Lee, A. O. Govorov, and N. Kotov, *Bioconjugated Superstructures of CdTe Nanowires and Nanoparticles: Multistep Cascade Förster Resonance Energy Transfer and Energy Channeling*, Nano Lett. **5**, 2063 (2005) — p.125.

[70] R. Lee, O. Painter, B. Kitzke, A. Scherer, and A. Yariv, *Photonic Bandgap Disk Laser*, Electron. Lett. **35**, 569 (1999) — p.17.
[71] R. Lehmberg, *Radiation from an N-Atom System: I. General Formalism*, Phys. Rev. A **2**, 883 (1970) — p.74 and 109.
[72] D. Leibfried, R. Blatt, C. Monroe, and D. Wineland, *Quantum Dynamics of Single Trapped Ions*, Rev. Mod. Phys. **75**, 281 (2003) — p.24.
[73] V. Letokhov, *Generation of Light by a Scattering Medium with Negative Resonance Absorption*, Sov. Phys.-JETP **26**, 835 (1968) — p.20.
[74] G. Lindblad, *On the Generators of Quantum Dynamical Semigroups*, Commun. Math. Phys. **48**, 119 (1976) — p.28.
[75] R. Loudon, *The Quantum Theory of Light* (Oxford University Press, New York, 2000), third ed. — p.24, 30, 48, and 66.
[76] O. Luiten, H. Werij, I. Setija, M. Reynolds, T. Hijmans, and J. Walraven, *Lyman-α spectroscopy of magnetically trapped atomic hydrogen*, Phys. Rev. Lett. **70**, 544 (1993) — p.36.
[77] H. Maeda and A. Yariv, *Narrowing and rebroadening of amplified spontaneous emission in high-gain laser media*, Phys. Lett. A **43**, 383 (1973) — p.20.
[78] T. Maiman, *Stimulated Optical Radiation in Ruby*, Nature **187**, 493 (1960) — p.17.
[79] L. Mandel and E. Wolf, *Optical Coherence and Quantum Optics* (Cambridge University Press, Cambridge, 1995) — p.17, 29, 60, 70, 78, and 131.
[80] J. McKeever, A. Boca, A. Boozer, J. Buck, and H. Kimble, *Experimental realization of a one-atom laser in the regime of strong coupling*, Nature **425**, 268 (2003) — p.20, 24, and 103.
[81] J. McKeever, J. Buck, A. Boozer, and H. Kimble, *Cavity QED "By The Numbers"*, arXiv: quant-ph/0403121 (2004) — p.105.
[82] K. Meduri, P. Sellin, G. Wilson, and T. Mossberg, *Coherently Driven Three-level Atoms: Unexpected Inversions, Pump Bandwidth Effects and Observation of Continuous Lasing*, Quant. Opt. **6**, 287 (1994) — p.24 and 37.
[83] D. Meschede, H. Walther, and G. Müller, *One-Atom Maser*, Phys. Rev. Lett. **54**, 551 (1985) — p.20 and 24.
[84] U. Mohideen, W. Hobson, S. Pearton, F. Ren, and R. Slusher, *GaAs/AlGaAs microdisk lasers*, Appl. Phys. Lett. **64**, 1911 (1994) — p.19.
[85] B. Mollow, *Power Spectrum of Light Scattered by Two-Level Systems*, Phys. Rev. **188**, 1969 (1969) — p.34 and 57.
[86] Y. Mu and C. Savage, *One-atom lasers*, Phys. Rev. A **46**, 5944 (1992) — p.103.
[87] R. Newton, *Scattering Theory of Particles and Waves* (Dover, New York, 2002) — p.31.
[88] T. Nieuwenhuizen, A. Burin, Y. Kagan, and G. Shlyapnikov, *Light propagation in a solid with resonant atoms at random positions*, Phys. Lett. A **184**, 360 (1994) — p.48.
[89] J. Nöckel and A. Stone, *Ray and wave chaos in asymmetric resonant optical cavities*, Nature **385**, 45 (1997) — p.17.
[90] A. Oraevskii, M. Scully, and V. Velichanskii, *Quantum dot laser*, Quantum

electronics **28**, 203 (1998) — p.103 and 106.
[91] Y. Oseledchik, *Relaxation Kinetics in a Gaussian Noise Field*, J. Appl. Spectrosc. **25**, 1036 (1977) — p.58.
[92] M. Pelton and Y. Yamamoto, *Ultralow threshold laser using a single quantum dot and a microsphere cavity*, Phys. Rev. A **59**, 2418 (1999) — p.103 and 106.
[93] G. Peters and L. Allen, *Amplified spontaneous emission I. The threshold condition*, J. Phys. A **4**, 238 (1971) — p.20.
[94] G. Peters and L. Allen, *Amplified spontaneous emission IV. Beam divergence and spatial coherence*, J. Phys. A **5**, 546 (1972) — p.20.
[95] P. Pinkse, T. Fisher, P. Maunz, and G. Rempe, *Trapping an atom with single photons*, Nature **404**, 365 (2000) — p.105.
[96] A. Popov, S. Myslivets, G. Jin-Ye, Z. Han-Zhuang, and B. Wellegehausen, *Inversionless gain in a three-level system driven by a strong field and collisions*, Chinese Physics **9**, 124 (2000) — p.24 and 37.
[97] A. Rau and R. Wendell, *Embedding Dissipation and Decoherence in Unitary Evolution Schemes*, Phys. Rev. Lett. **89**, 220405 (2002) — p.28.
[98] E. Ressayre and A. Tallet, *Quantum theory for superradiance*, Phys. Rev. A **15**, 2410 (1977) — p.20, 57, and 93.
[99] P. Rice and H. Carmichael, *Photon statistics of a cavity-QED laser: A comment on the laser phase transition analogy*, Phys. Rev. A **50**, 4318 (1994) — p.19 and 101.
[100] T. Richter, *Photon Correlations in the cooperative radiation from a continuously and incoherently pumped three-atom basis*, J. Phys. B **15**, 1293 (1982) — p.84.
[101] M. Rosenblit, P. Horak, S. Helsby, and R. Folman, *Single-atom detection using whispering-gallery modes of microdisk resonators*, Phys. Rev. A **70**, 053808 (2004) — p.105.
[102] R. Roy and L. Mandel, *Optical bistability and first order phase transition in a ring dye laser*, Opt. Comm. **34**, 133 (1980) — p.17.
[103] D. Sadot and E. Boimovich, *Tunable Optical Filters for Dense WDM Networks*, IEEE Comm. Magazine **36**, 50 (1998) — p.105.
[104] T. Savels, A. Mosk, and A. Lagendijk, *Light scattering from three-level systems: The T-matrix of a point-dipole with gain*, Phys. Rev. A **71**, 043814 (2005) — p.21.
[105] A. Schawlow and C. Townes, *Infrared and Optical Masers*, Phys. Rev. **112**, 1940 (1958) — p.93.
[106] M. Scully, S.-Y. Zhu, and A. Gavrielides, *Degenerate Quantum-Beat Laser: Lasing without Inversion and Inversion without Lasing*, Phys. Rev. Lett. **62**, 2813 (1989) — p.24 and 37.
[107] M. Scully and M. Zubairy, *Quantum Optics* (Cambridge University Press, Cambridge, 1997) — p.28, 29, 57, and 109.
[108] M. Scully and M. Zubairy, *Quantum Optics,* chap. 10 (Cambridge University Press, Cambridge, 1997) — p.86.
[109] V. Shatokhin, C. A. Müller, and A. Buchleitner, *Coherent Inelastic Backscat-*

tering of Intense Laser Light by Cold Atoms, Phys. Rev. Lett. **94**, 043603 (2005) — p.125.

[110] B. Shore and P. Knight, *The Jaynes-Cummings model*, J. Mod. Opt. **40**, 1195 (1993) — p.120.

[111] A. Siegman, *Lasers* (University Science Books, Mill Valley, 1986) — p.17, 39, and 51.

[112] A. Siegman, *Lasers,* chap. 25 (University Science Books, Mill Valley, 1986) — p.18 and 100.

[113] O. Sigwarth, G. Labeyrie, T. Jonckheere, D. Delande, R. Kaiser, and C. Miniatura, *Magnetic Field Enhanced Coherence Length in Cold Atomic Gases*, Phys. Rev. Lett. **93**, 143906 (2004) — p.125.

[114] H. Steudel, *Radiation Rate and Spectrum of a Continuously Pumped Three-Atom System*, J. Phys. B **12**, 3309 (1979) — p.84 and 87.

[115] H. Steudel, *The Initial Process of Superfluorescence in Microscopic Description*, Ann. Phys. **37**, 57 (1980) — p.20 and 93.

[116] S. Strauf, K. Hennessy, M. Rakher, Y.-S. Choi, A. Badolato, L. Andreani, E. Hu, P. Petroff, and D. Bouwmeester, *Self-Tuned Quantum Dot Gain in Photonic Crystal Lasers*, Phys. Rev. Lett. **96**, 127404 (2006) — p.17 and 50.

[117] A. Szöke and A. Javan, *Effects of Collisions on Saturation Behavior of the 1.15-μ Transition of Ne Studied with He-Ne laser*, Phys. Rev. **145**, 137 (1966) — p.17.

[118] C. Tai, *Dyadic Green Functions in Electromagnetic Theory* (IEEE Press, New York, 1994) — p.43.

[119] H.-M. Tzeng, K. Wall, and M. Long, *Laser emission from individual droplets at wavelengths corresponding to morphology-dependent resonances*, Opt. Lett. **9**, 499 (1984) — p.19.

[120] K. Vahala, *Optical microcavities*, Nature **424**, 839 (2003) — p.105.

[121] M. van der Mark, M. van Albada, and A. Lagendijk, *Light scattering in strongly scattering media: Multiple scattering and weak localization*, Phys. Rev. B **37**, 3575 (1988) — p.39 and 125.

[122] K. van der Molen, A. Mosk, and A. Lagendijk, *Intrinsic fluctuations in random lasers,* Accepted by Phys. Rev. A — p.20.

[123] K. van der Molen, P. Zijlstra, A. Lagendijk, and A. Mosk, *Laser threshold of Mie resonances*, Opt. Lett. **31**, 1432 (2006) — p.19.

[124] W. van der Veer, R. van Diest, A. Dönszelmann, and H. van Linden van den Heuvell, *Experimental Demonstration of Light Amplification without Population Inversion*, Phys. Rev. Lett. **70**, 3243 (1993) — p.24 and 37.

[125] S. van Enk, J. Cirac, and P. Zoller, *Photon channels for quantum communication*, Science **279**, 205 (1998) — p.105.

[126] F. Vollmer, D. Braun, A. Libchaber, M. Khoshsima, I. Teraoka, and S. Arnold, *Protein detection by optical shift of a resonant microcavity*, Appl. Phys. Lett. **80**, 4057 (2002) — p.105.

[127] T. Wellens, B. Grémaud, D. Delande, and C. Miniatura, *Coherent backscattering of light by two atoms in the saturated regime*, Phys. Rev. A **70**, 023817 (2004) — p.39.

[128] H. Wiseman, *Defining the (atom) laser*, Phys. Rev. A **56**, 2068 (1997) — p.17.

[129] H. Wiseman, *Light amplification without stimulated emission: Beyond the standard quantum limit to the laser linewidth*, Phys. Rev. A **60**, 4083 (1999) — p.95.

[130] J. Woerdman, M. van Exter, and N. van Druten, *Quantum Noise of Small Lasers*, Advances in Atomic, Molecular and Optical Physics **47**, 205 (2001) — p.19, 101, 103, and 118.

[131] T. Yoon, S. Pulkin, J. Park, M. Chung, and H.-W. Lee, *Theoretical analysis of resonances in the polarization spectrum of a two-level atom driven by a polychromatic field*, Phys. Rev. A **60**, 605 (1999) — p.58.

[132] P. Zhou and S. Swain, *Resonance fluorescence and absorption spectra from a two-level atom driven by coherent and stochastic fields*, Phys. Rev. A **58**, 4705 (1998) — p.58.

[133] P. Zoller, *Resonant Multi-Photon Ionization by Finite-Bandwidth Chaotic Fields*, Phys. Rev. A **19**, 1151 (1979) — p.58.

[134] P. Zoller, *Saturation of two-level atoms in chaotic fields*, Phys. Rev. A **20**, 2420 (1979) — p.58 and 63.

Index